MASTER

Design and manufacturing of watch components by femtosecond laser irradiation and etching techniques

Dielissen, F.F.A.

Award date:
2012

Design and manufacturing of watch components by femtosecond laser irradiation and etching techniques

Document number: 2012_MNSE_01

May 1, 2012

Master Thesis
F.F.A. Dielissen (0569114)

Committee:
Prof.dr.ir. A.A. van Steenhoven
Dr. Y.J. Bellouard
Dr.ir. J.P.M. Hoefnagels

Supervisor: Dr. Y.J. Bellouard
Micro- & Nano- Scale Engineering Group
Department of Mechanical Engineering
Eindhoven University of Technology

Associate Company:

Support: Dr. Thierry Hessler
         Nicolas Rebeaud
Division Asulab
The Swatch Group Research and Development
Switzerland

Preface

With this thesis, I conclude my graduation project and finish my master's degree in Mechanical Engineering at the Eindhoven University of Technology. I have been working on this project at the division Asulab at the Swatch Group Research and Development in Marin, Switzerland. During this project, I have been supported by several people whom I would like to thank here.

First of all, I would like to thank the people at Asulab for making me feel comfortable while working there and their support. Special thanks go to my coach Thierry Hessler for his guidance, overall support and his shared knowledge and to Nicolas Rebeaud who supported me during the designing part of my project. Furthermore, I thank my supervisor Yves Bellouard, for his advice, coaching and support during the whole project. Next to this, I would like to thank my family, friends and fellow students for supporting me.

This master's thesis also marks the end of my time as a student in Eindhoven. I am looking back on seven and a half fantastic years. I wish to thank my friends and my girlfriend Lea for all the good times and memories.

Freek Dielissen

Eindhoven, May 1, 2012

Summary

The balance wheel is the beating heart of a mechanical watch. It is a weighted wheel that rotates back and forth, brought back toward its center position by a balance spring. The combination of the mass of the balance wheel and the elasticity of the spring keeps the time between each oscillation constant and determines the accuracy of the watch. To keep this balance wheel in its pivot, shock-absorbers are needed on each end of the axis of the balance wheel.

The current shock-absorber that is used in watches does not meet the desired requirements Asulab would like to reach. Hysteresis occurs while using this part and it does not pass qualifying shock tests. Finally, the assembly of this part is difficult due to the many small parts. Therefore, a prototype shock-absorber made out of Nickel (called Ni-prototype) is being designed by Asulab. In the future, the manufacturer would like to redesign this Ni-prototype part out of a gemstone. This new prototype would be just one mechanical piece that will replace other pieces in the current shock-absorber assembly. This mechanical piece will be easier to assemble but will have to meet the same requirements during normal used of a watch and pass the qualifying shock tests. The main goal of this project is to redesign and manufacture the existing Ni-prototype shock-absorber for different materials while keeping similar mechanical specifications.

First different materials are tested with a new fabrication method because conventional drilling techniques, such as laser ablation or mechanical drilling are not suitable to achieve the desired shape, design or tolerances. The used fabrication method is a laser technique with a femtosecond laser followed by an etching technique. Quartz and ruby are tested with this method. At first, the goal was to make the new prototype out of ruby. Unfortunately, these materials will not be used because the etching results were disappointing during the experiments. To machine the new prototype, fused silica is chosen because this material is a known material hence, the laser parameters and etching conditions are known.

Secondly, the new prototype is analytically derived and modeled with ANSYS. The analytical and finite element methods are used to calculate mechanical deformations due to lateral or vertical forces applied in the center of the component. The analytical method using compliances and stiffness matrices is very accurate to calculate the deformations but the finite element method is used to derive the final dimensions of the new prototype executed in fused silica. The new prototype was redesigned in order to meet the mechanical specifications, the requirements and pass the qualifying shock tests.

Finally, the new prototype is structured several times on a $250\,\mu$m thick fused silica substrate and is immersed in 2.5% HF. Unfortunately, the shock-absorber did not come out of the substrate. Mechanical testing was therefore not possible during the time of this diploma project but the substrate showed that the edges of the etched curves were sharp and the etched surface was smooth. The taped hole in the center of the substrate was successfully irradiated and etched out. These results are hopeful for further investigation. Replacing the current manufacturing setup will improve the results. New stages should replace the current two stages. These new stages need to have a writing domain of 10x10 cm and have to be very accurate (nanoscale). Irradiation will be more homogeneous over the curvatures of the shock-absorber and this improves a constant etching speed which may finally lead to a successful manufacturing approach and a working shock-absorber.
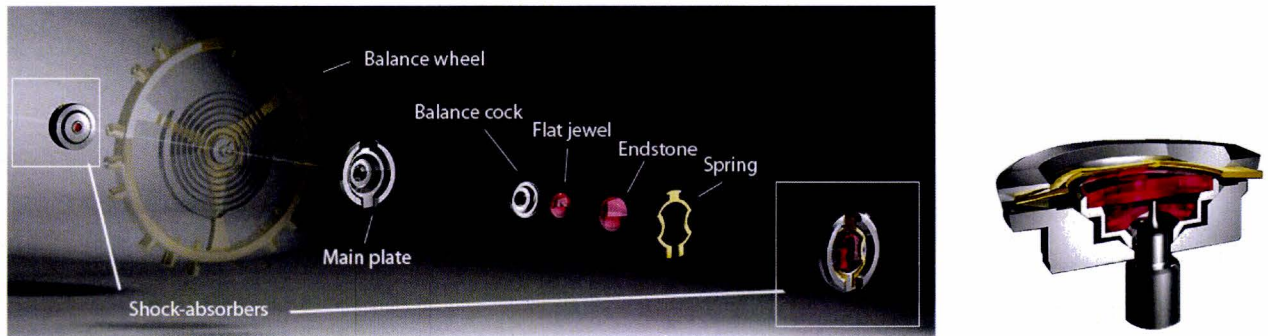
Contents

Chapter 1

Introduction

Watches evolved in the 17th century from spring powered clocks [1], which appeared in the 15th century. The first watches were strictly mechanical. As technology progressed, the mechanisms used to measure time have, in some cases, been replaced by use of quartz vibrations or electromagnetic pulses. The first digital electronic watch was developed in 1970. Expensive, collectible watches valued for their workmanship and esthetical appeal, have often purely mechanical movements and are powered by springs. A mechanical watch is powered by an internal spiral spring called mainspring. A schematic view of the main components of the watch movements is illustrated in figure 1.1.

Figure 1.1: Schematic view of the main components of the watch movements: The barrel(drum-shaped housing containing the mainspring) is the energy storage of a mechanical watch. This barrel is connected to a gain train. The escape wheel is the last wheel in this train. Together with the pallet fork, it forms the escapement. The pallet fork transfers the power to the balancewheel and controls the train. The balance wheel splits the time into equal portions. From the escape wheel to the barrel, the whole train consists of reduction gears.

A mechanical watch consists of hundreds of components. One of them is the balance wheel. This can be seen as the beating heart of a mechanical watch. It is a weighted wheel that rotates back and forth, brought back toward its center position by a balance spring. The combination of the mass of the balance wheel and the elasticity of the spring keeps the time between each oscillation constant and determines the accuracy of the watch. To keep this balance wheel in its pivot, shock-absorbers are needed on each end of the axis of the balance wheel. This can be seen in figure 1.2(a). The shock-absorber holds the balance wheel in place and maintains the balance wheel rotation while the watch is hold sideways or upside down. Furthermore, it protects the balance wheel against shocks during regular use of the watch. However, the current shock-absorber that is used in watches does not meet the desired requirements Asulab would like to reach. Hysteresis occurs while using this part and it does not pass qualifying shock tests. Finally, the assembly of this part is difficult due to the many small parts. Therefore, a prototype shock-absorber made out of Nickel (called Ni-prototype) is being

(a) Exploded view: the flat jewel and endstone are spring-loaded in, respectively, the main plate and balance cock. When the watch is subjected to a shock, these bearings "give" laterally and/or vertically.

(b) 3D view: the shock-absorber assembly including the axis of the balance wheel

Figure 1.2: Two different views of the current shock-absorber assembly.

designed by Asulab. In the future, the manufacturer would like to redesign this Ni-prototype part out of a gemstone. This new prototype would be just one mechanical piece that will replace other pieces in the current shock-absorber assembly. This mechanical piece will be easier to assemble but will have to meet the same requirements during normal used of a watch and pass the qualifying shock tests. The main goal of this project is to:

Redesign and manufacture the existing Ni-prototype shock-absorber for different materials while keeping similar mechanical specifications.

During this project, the existing Ni-prototype design is redimensioned for new materials while keeping the same specifications as the current shock-absorber. The ruby stones and the spring mechanism are replaced by just one component. To fabricate this component, conventional drilling techniques, such as laser ablation or mechanical drilling are not suitable to achieve the desired shape, design or tolerances. In this project, experiments with a femtosecond laser followed by etching techniques are performed to explore the possibilities of this process for machining.

First, laser and etching experiments are performed on quartz and ruby to find out if the technique and materials are suitable to machine this component. Simultaneously, analytical models of the new prototype shock-absorber are made followed by simulations with ANSYS to redesign this component. Finally, the fabrication method is used to machine this new prototype shock-absorber.

Chapter 2

Suitable laser techniques

2.1 Introduction: lasers

A laser is a device that emits light through a process of optical amplifications based on the stimulated emission of photons. A laser produces a monochromatic beam, meaning that the spectrum consists of only one single wavelength. Industrial lasers used for micromanufacturing, can be divided into three main categories: infra-red lasers, excimer lasers and femtosecond lasers. The main differences between these lasers is the pulse duration of a laser. This can vary from a continuous operation (for CO_2 laser) to a few femtoseconds. The shorter the pulse, the higher the light intensity during the pulse.

An important property of a laser beam is to be Gaussian. This means that the intensity distribution over the cross section of the beam can be approximated by a Gaussian function. Figure 2.1 shows the envelope profile of a focused Gaussian beam. The minimum beam width is called beam waist and is
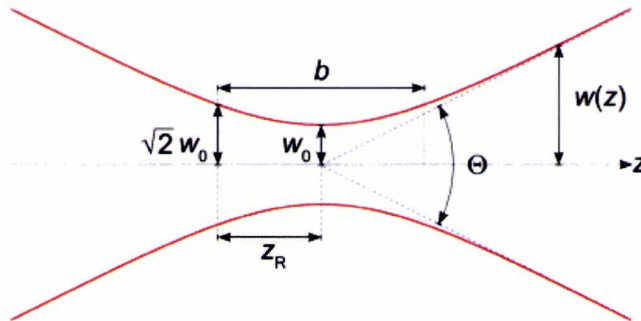

Figure 2.1: Cross section of a Gaussian beam with parameters that define the divergence of a Gaussian beam where W_0 is the beam waist, Φ the total angular spread and Z_r the Rayleigh distance.

governed by the wavelength and the focusing optics (numerical aperture in particular). As a rule of thumb, a laser beam cannot be focused to a diameter smaller than the laser wavelength. For ultrafast laser, non-linear absorption takes place which means that the laser affected zone can eventually be smaller than the laser wavelength and therefore, than the beam waist. For ultrafast laser, the energy deposition inside the material is determined by the w_{nla} (the non-linear absorption waist) but also by the repetition rate (f) of the laser pulse, the writing speed (v) and the energy per pulse. If we assume that the ratio v/f is much smaller than the non-linear beam waist, the deposited energy per unit surface (Φ_d) on the material can be approximated by [2]:

$$\Phi_d = \frac{4E_p}{\pi w_{nla}} \frac{f}{v} \tag{2.1}$$

where f is the laser repetition rate and v the writing speed.

3

2.2 Femtosecond laser

In materials microprocessing, femtosecond (fs) lasers are widely used when high accuracy and small-sized structures are required [3]. The advantage of femtosecond laser irradiation lies in the ability to produce very high peak power intensity and to deliver energy into a material before thermal diffusion has occurred. The molten phase is then practically absent and as a result this reduces shock and thermal stress, which lead to a minimized heat affected zone around the machined feature [4]. During irradiation, one of the possible effects is amorphization and/or defects creation. If the process of femtosecond laser irradiation is combined with chemical etching, this offers the possibility to remove material in the three dimensions with structure size within the micro-nano scale domain. This was first performed and reported in 1999 on a photosensitive glass [5]. Subsequently, similar 3D micro structuring was performed in other materials such as fused silica and sapphire. With this technique the first step is to irradiate a sample to a tightly focused femtosecond laser beam. Patterns are written in- or onto the sample. The combination of the pulse energy, repetition rate and the writing speeds is such, that no material is removed but structural modifications of the material will take place at the laser focal spot. Secondly, the sample is immersed in a chemical etchant. The irradiated areas will, depending on the material used, react faster with the etchant than the non-irradiated areas which gives the possibility to structure material. The difference in etching rate between non-irradiated and irradiated areas can be very large (for sapphire $1 : 10^4$ [6]).

The next section is focused on a literature study of femtosecond laser irradiation combined with wet chemical etching on fused silica and sapphire. In addition to the important parameters that affect the energy deposition, additional parameters are described which also influence the structuring of materials. The footnote in the description refers to the laser-used with the corresponding parameters such as repetition rate, pulse energy and pulse duration. At the end of this chapter a short summary is given and in appendix A, the laser parameters and the different etchants are summarized.

2.3 Literature study: Fs laser irradiation combined with etching techniques

Femtosecond laser irradiation combined with etching techniques offers the possibility to remove material in the three dimensions and with high accuracy. 3D structures can be removed even inside materials with nanoscale resolution. This section described this technique for fused silica and for sapphire. These materials are chosen having in mind that the technique used during this project will be applied on these materials (as well as on rubies).

2.3.1 Fused Silica

Applied to fused silica, femtosecond laser machining and wet chemical etching can be used to generate a variety of structures such as waveguides, nanogratings, diffractive elements, fluidic channels as well as mechanical components such as flexures.

Fabrication of micro-channels [7]: The fused silica sample is exposed to femtosecond laser pulses[1] to fabricate micro-channels. The affected regions are hit multiple times by the laser (500 to 2500) due to the fact that the repetition rate is significantly large with respect to a writing speed of $100\,\mu$m/s. Thanks to the non-linear absorption mechanism, channels inside the material can be fabricated. The channels are 5 mm long and are made with 10 adjacent lines, equally distributed. Two different sets of tunnel patterns are written. The first tunnel ("A") is written at a distance of $75\,\mu$m inside the

---

[1]Laser: Ti:Sapphire laser, Wavelength: 800 nm, Pulse Duration: 100 fs, Repetition Rate: 250 kHz, Pulse Energy: 55-1000 nJ

substrate. The second tunnel ("B"), is written at a distance of $420\,\mu$m from the same surface. For tunnel B, the pulse energy is slightly increased in order to compensate for optical aberration associated with the additional depth. The sample is after irradiation immersed in 5% HF for three hours. The modified etched region is shown in figure 2.2. In three hours, a depth of 1.2 mm is reached. This equals a etching rate of $6.6\,\mu$m/min. The etching rate of non-irradiated fused silica is typically around $3\,\mu$m/hour. This results in a etching ratio of about 130 between the irradiated and non-irradiated material.
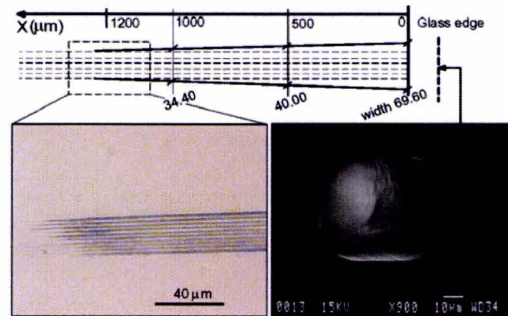

Figure 2.2: Micro-channel: optical and SEM observations of the length and entrance of the tunnel after femtosecond laser irradiation followed by etching in 5% HF for three hours.

In another reference [2], micro-channels are fabricated with only one single line[2]. The focus of this research is on the role of the deposited energy in Joule per squared area in the etching process of femtosecond laser exposed fused silica. Again, line patterns are written inside samples fused silica and the writing direction is perpendicular to the polarization. The writing speeds vary from 0.01 mm/s to 35 mm/s. The line pattern is performed four times with increasing repetition rates. First 100 KHz, followed by 250 KHz, 500 KHz and 860 KHz. Subsequently, the samples are immersed in a 2.5% HF etching bath for 4 hours to investigate etching rates. To couple energy deposition with the etching rates, equation 2.1 is used and a log-log plot can be derived shown in figure 2.3.
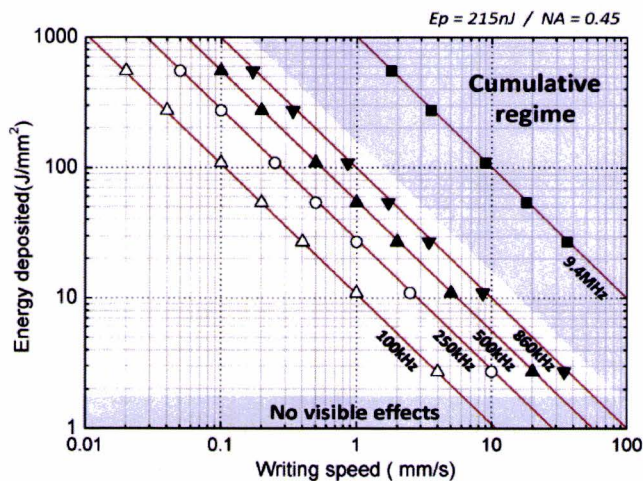

Figure 2.3: Log-log plot of the deposited energy versus writing speed. Each point indicated actual measurements for various repetition rates. The pulse energy and NA were kept the same for all experiments.

The points in the graph are experimental data for which visible patterns could be seen with an optical microscope. Figure 2.4 shows the etching lengths of the line patterns due to a varying energy

---

[2]Laser: Ytterbium-KGW, Wavelength: 1024 nm, Pulse Duration: 500 fs, Repetition Rate: 100, 250, 500, 860 kHz, Pulse Energy: 215 nJ, NA=0.45

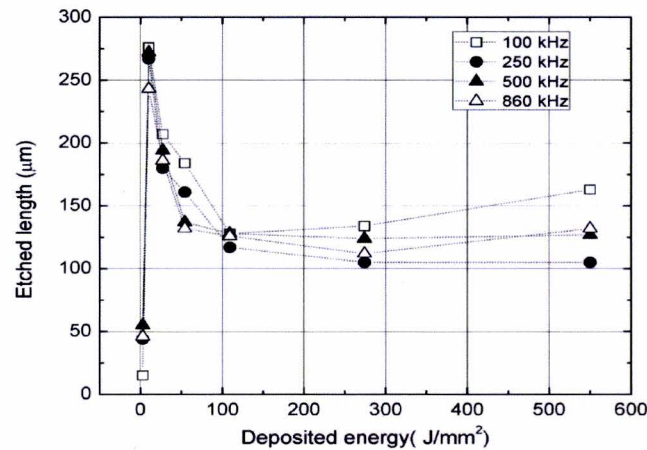deposition determined by the varying writing speed and repetition rates.

Figure 2.4: Deposited energy versus etching length for different repetition rates measured in an optical microscope. A pulse energy of 215 nJ is used and the samples are etched for 4 hours in a 2.5 % HF acid.

Similarly to the first literature reference mentioned above, channels at the surface were fabricated. A 30 μm wide and 675 μm deep surface channel is irradiated[3] on the surface of the fused silica substrate. This pattern is made with 15x90 lines with a mutual distance of 2 μm. Subsequently, the sample is immersed in 2.5% HF for two hours. Figure 2.5 shows the depth of the tunnel as function of the etching time. The measured etching speed is 1.2 μm/min. Further investigation to explore the influence of
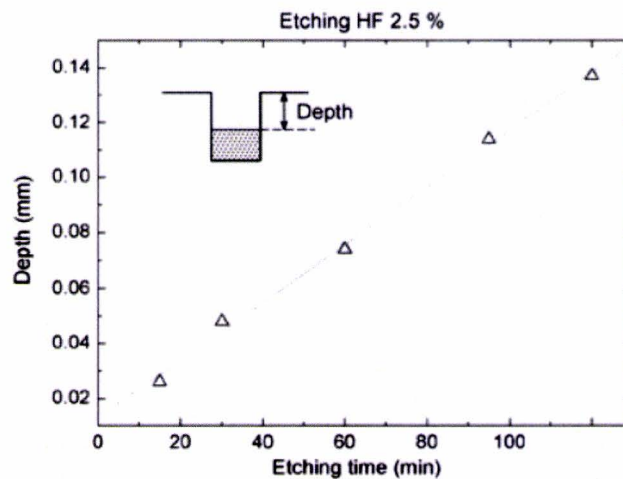

Figure 2.5: The depth of a channel, made with 15x90 parallel lines, as function of the etching time. After femtosecond laser irradiation, the sample is immersed in a 2.5% HF etching bath for two hours.

irradiation with different pulse energies is performed. Multiply channels at the surface are fabricated with a matrix of 60 tracks in horizontal direction and 11 tracks in vertical direction. Chemical etching is performed after irradiation. Figure 2.6 shows the different profiles and SEM images of the channels. The channels with the best shape quality are obtained with a pulse energy of 135 and 270 nJ. Below that energy fluence level the material is not influenced enough to etch the material properly. Moreover, increasing the pulse energy above 270 nJ does not lead to a better or faster etching procedure. In this case, the edges of these channels are fully etched but in the middle of the channels, a lot of material is still present.

---

[3]Laser: Ti:Sapphire laser, Wavelength: 800 nm, Pulse Duration: 100 fs, Repetition Rate: 250 kHz, Pulse Energy: 135-270 nJ
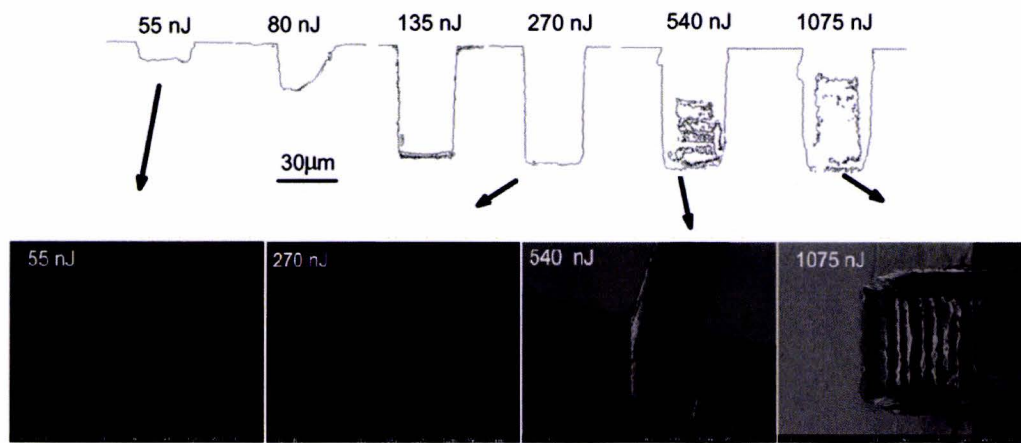
Figure 2.6: Etched channels with different pulse energies. Channels are made wih 60 by 11 laser tracks with a femtosecond laser. After irradiation, the samples are immersed in HF.

Beside surface profiles and depths, the surface structures of the microchannels for the different pulse energies are obtained. For the three highest pulse energies holes ranging in size from 10 to 100 nm in diameter are clearly visible at the surface. This is shown in figure 2.7 and suggests the presence of micro-explosion sites and/or plasma shock waves left behind micro-cavities which are exposed during the etching process.
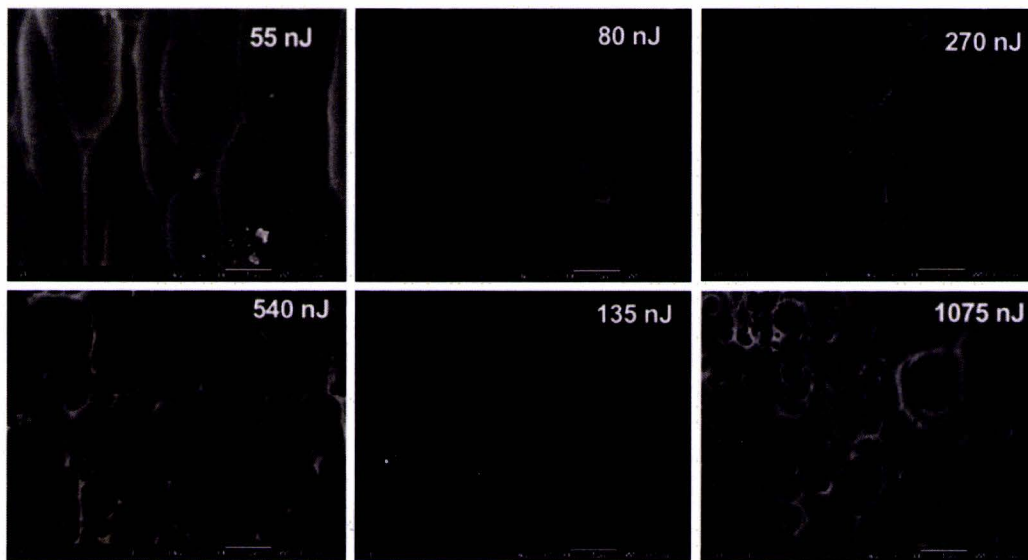

Figure 2.7: Surface structure of the etched channels as the different energy levels. For the three highest pulse energies holes ranging in size from 10 to 100 nm in diameter are clearly visible at the surface. This suggests the presence of micro-explosion sites and/or plasma shock waves left behind micro-cavities which are exposed during the etching process.

2.3.2   Sapphire

The most used etchant to etch sapphire is hydrofluoric (HF) acid. Besides HF, KOH is also known as etchant. Some different methods can be used to etch sapphire and as already mentioned different three dimensional structures can be fabricated. In this section more methods are discussed as well as different micro-structures.

Fabrication of micro-channels [6]: According to Wortmann *et al.* extremely high aspect ratios above 1000 can be achieved. Femtosecond laser irradiation[4] is carried out in sapphire substrates to fabricate micro-channels. For energies below $0.3\,\mu$J no modification is observed and energies above $1\,\mu$J induces crack formation in the irradiated volume. The writing speed used ranges from 0.1 to 1 mm/s. The pulse overlap is large due to the fact that the writing speed is significantly small compared to the repetition rate. The polarization is set perpendicular to the writing direction. With these parameters and conditions, long channels inside sapphire are exposed. After irradiation, the substrate of sapphire is immersed in a 40 % aqueous solution of HF for 24 hours in an ultrasonic bath. After the etching procedure, a significant change in refractive index is visible in the etched channel up to a certain depth. Figure 2.8 shows the through light microscopy images of the modified channel after irradiation and after etching.
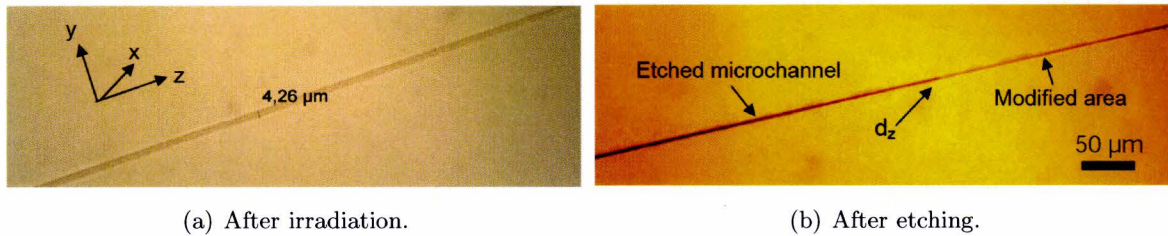

(a) After irradiation. (b) After etching.

Figure 2.8: Through light microscopy images of the modified channel after irradiation with a femtosecond laser followed by etching with 50% HF for 24 hours.

This experiment is also performed for different energy pulses, a varying writing speed and two different repetition rates. The etch depth ranges between 0.5 and 1 mm, depending on the machining parameters. Figure 2.9 shows the etching depth as function of the line energy. The line energy is calculated by multiplying the energy pulse with the repetition rate divided by the writing speed.
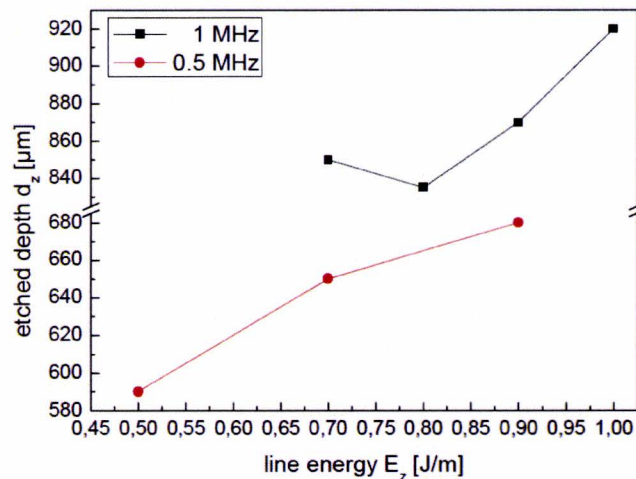

Figure 2.9: Etched depth as function of the line energy. The line energy is calculated by multiplying the energy pulse with the repetition rate divided by the writing speed.

When femtosecond lases-assisted etching techniques are understood well the possibilities to fabricated 3D-structures in materials are comprehensive. M. Hörstmann-Jungemann *et al.* [8] used this

---

[4]Laser: Fiber chirped amplifier (FCPA) IMRA μJuwel, Wavelength: 1045 nm, Pulse Duration: 400 fs, Repetition Rate: 0.5 and 1 MHz, Pulse Energies: 0.3 to $1\,\mu$J.

technique to cut material, to fabricate hollow channels and finally to create a hollow cube inside material.

Fabrication of cuts: By writing 50 tracks with a femtosecond laser[5] on top of each other in the volume of sapphire a cutting procedure can be started. The writing speeds for the setup is set at 1 mm/s and therefore the pulse to pulse overlap is large because the writing speeds is significantly small compared to the repetition rate. The writing direction is perpendicular to the polarization of the laser. After irradiation wet chemical etching is performed. To etch, the sample is immersed for 24 hours in 48% HF. The etching process is carried out in a ultrasonic bath to provide continuous movement of HF. The cutting method and results are shown in figure 2.10.

(a) Irradiation strategy to fabricate a cut.

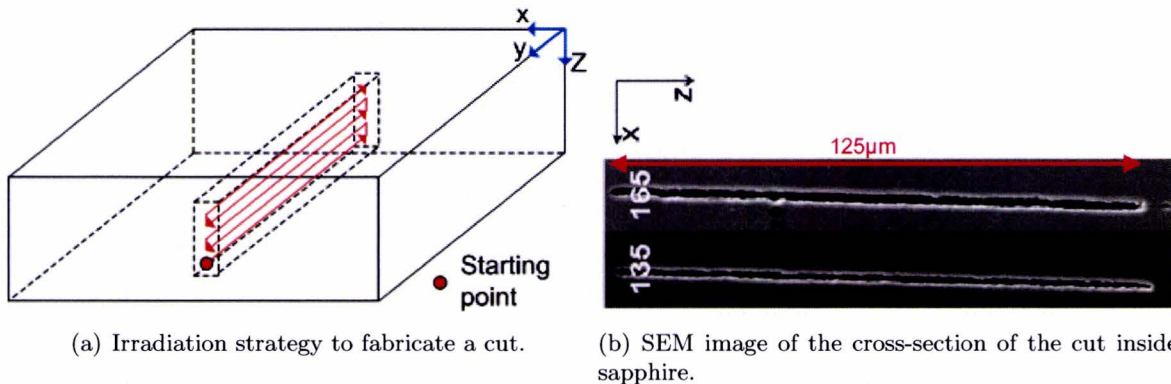(b) SEM image of the cross-section of the cut inside sapphire.

Figure 2.10: Cutting sapphire by writing 50 tracks on top of each other followed by etching for 24 hours in 48% HF.

This process strategy can also be used to cut out 3D micro parts or to fabricate micro-holes. The figure 2.11 shows a cylinder that is cut out of a $500\,\mu$m thick sample of sapphire right after irradiation with a pulse energy of 116 mW (around 232 nJ per pulse at a repetition rate of 500 kHz) and etching for 49 hours in 48% HF.
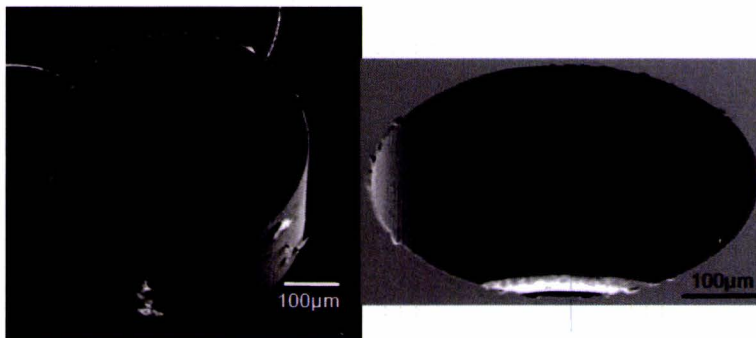

Figure 2.11: SEM micrograph of a cylinder with a diameter of $500\,\mu$m. The cylinder is after irradiation with a pulse energy of 232 nJ per pulse and a repetition rate of 500 kHz, immersed in a chemical bath of 48% HF for 49 hours.

Fabrication of micro-channels: Subsequently, micro-channels are produced by modifying single tracks in the volume of sapphire and adjacent etching. To write these micro-channels, a polarization

---

[5]Laser: Yb-glass fiber chirped pulse amplifier, Wavelength: 1045 nm, Pulse Duration: 450 fs, Repetition Rate: 500 kHz, NA: 0.6.

perpendicular to the writing direction is used. When several tracks are written next to each other, the length and width of these channels can be varied. When 6 tracks with an overlap of about $0.77\,\mu$m are written with a mean power of $91.3\,$mW (around $183\,$nJ per pulse) a nearly square shape cross section is the result. This can be explained due to the reflection and scattering of the laser beam from the second track at the lower refractive index area, the modified area, of the first track. The length of the channels can be varied by ranging the energy and the distance between the tracks. The tracks to make a micro-channel are written from the right to the left side. The longest channel is $1732\,\mu$m. This channel is made with 40 tracks with a mutual distance of $0.55\,\mu$m and a mean power of $92.4\,$mW (around $175\,$nJ per pulse). Figure 2.12 shows a light microscopy image of the different lengths of the micro-channels. To avoid cracks, a higher power cannot be used. An increase of tracks density will
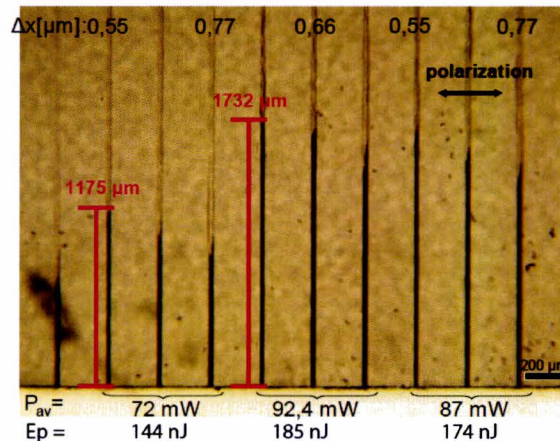

Figure 2.12: Light microscopy image of the microchannels produced with different powers and line distances (bottom illumination).

induce cracks since this produces more stress due to more amorphization of the material.

Fabrication of hollow volumes: When previous irradiation strategies are combined it is possible to fabricate hollow volumes. The strategy to create hollow volumes is to write several x-y planes on top each other. This strategy is shown for a hollow cube with dimensions 50x10x$10\,\mu$m in sapphire in figure 2.13(a). The procedure start at the lowest level and created several x-y planes until it reaches its desired shape. The mutual distance of the tracks in x direction is $0.55\,\mu$m and in z direction $3.5\,\mu$m. Subsequently, micro-channels are fabricated on the surface create an opening for the chemical acid for etching the modified areas. The cube is irradiated with a pulse energy of $120\,$mW (around $240\,$nJ per pulse). The result of this irradiation strategy is shown in figures 2.13(b) and 2.13(c). In figure 2.13(c), the residue of the nanoplanes are still visible. This shows that the roughness of surfaces with these strategies is limited by periodical nanostructures. The roughness is investigated with an atomic force microscopy(AFM) and compared to an optical polished surface. The difference between the average roughness of the optical polished surface and the cut surface is significant. The average roughness of the cut surface is $62.98\,$nm while the average roughness of the optical polished surface is $1.43\,$nm. The nanostructures seem to limit the smoothness of the surface. As shown, three-dimensional residue free volume removal inside sapphire is possible. This is confirmed by a research performed at the University of Tokushima [9]. They showed that, complete volume etching without residue with increasing etching temperatures is achievable, however, accompanied with undesirable phenomena. To achieve this, a femtosecond laser[6] is used to irradiate a cube with dimensions 10x10x$10\,\mu$m and four micro-channels which connect the cube with the surface of the sapphire sample. The distance between the laser tracks is in the x and y direction about $0.2\,\mu$m and in the z direction two different distances are used. These

---

[6]Laser, Wavelength: $800\,$nm, Pulse Duration: $130\,$fs. Pulse Energy: $40\,$nJ.

(a) Irradiation strategy for a hollow cub.   (b) Inlet channels.   (c) Hollow volume.
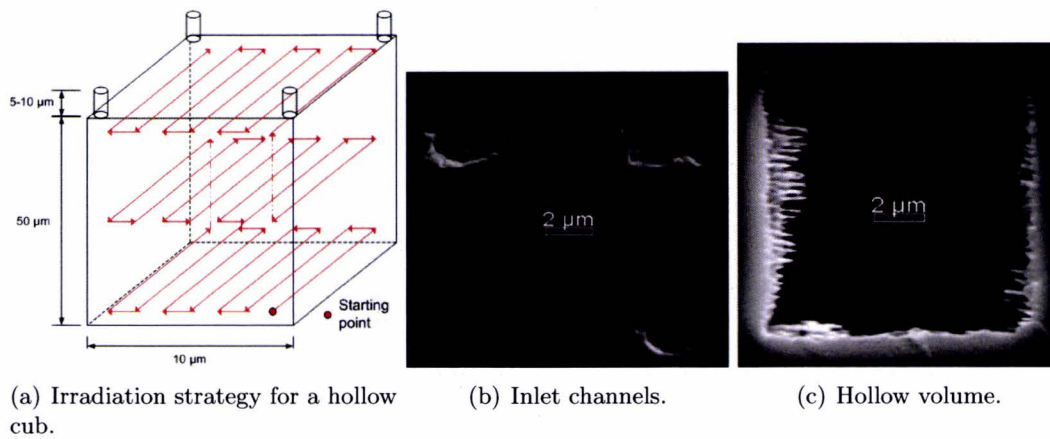
Figure 2.13: (a)Strategy and (b,c)SEM images of the top view of the inlet channels and the hollow volume.

distances are $1\,\mu$m and $2\,\mu$m, respectively. After irradiation, the samples are immersed in 10% aqueous solution of HF. The etching is carried out in a teflon-coated high-pressure cell. This cell, containing the etchant and the sample, is put in an electric oven. After etching, SEM observation are carried out. The SEM micrographs are shown in figure 2.14(a), 2.14(b) and 2.14(c). An optical micrograph of sapphire after etching at $120\,^\circ$C is also made and shown in figure 2.14(d). These inside-sapphire volumes are made with a vertical track distance of $2.0\,\mu$m. The different etching conditions make a

(a) Etching at $20\,^\circ$C for 72 hours.   (b) Etching at $100\,^\circ$C for 24 hours.   (c) Etching at $120\,^\circ$C for 24 hours.   (d) Etching at $120\,^\circ$C for 48 hours.
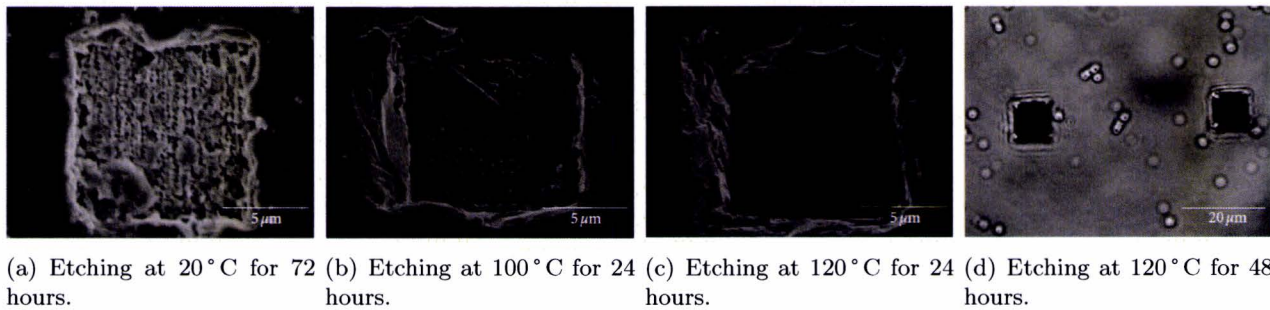
Figure 2.14: (a)-(c) SEM micrographs inside sapphire after etching with mentioned parameters. (d) Optical micrograph of sapphire after etching, both surface and subsurface are visible.

significant difference in the removal result. After etching for 72 hours at room temperature volume etching only slightly advanced. After 24 hours etching with a temperature of $100\,^\circ$C volume etching improved. A single layer was removed but a lot improvement in depth was hardly visible. When the etching temperature became $120\,^\circ$C much more removal took place. Complete removal was achieved, however a new problem appeared which can be seen in figure 2.14(d). Small surface pits appear. These pits were absent before etching but they appeared after etching for a long period with high temperature due to dislocations in the sapphire. Probably because of the crystalline structure of sapphire, the pits all have a hexagonal shape and are aligned along the same direction. In figure 2.14(d) the pits are clearly visible, that is because the pits on the surface scatter light in all directions making the surface useless for optical purposes. Using polishing, the surface pits can probably be removed but this is a time-consuming process. With a vertical distance between each track of $1.0\,\mu$m, etching works better. This can be seen in figure 2.15. However, with these parameters another problem appeared. At the corners of the cuboids cracks appear after irradiation and after etching, the cracks are more obvious because fluid penetrated into these cracks.
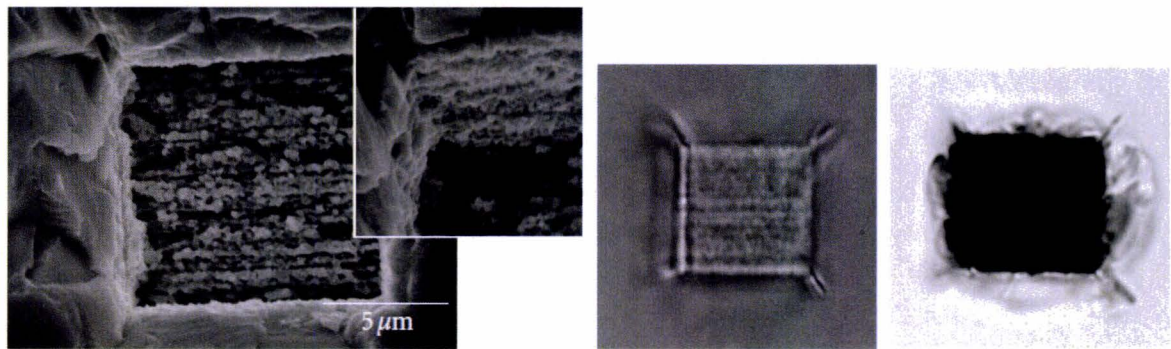
(a) Etching at 100 °C for 24 hours with a close up
oblique view tilted at 20 °.

(b) Optical micrograph
before etching.

(c) Optical micrograph af-
ter etching.

Figure 2.15: Graphs of inside removal of the cube with a vertical track distance of $1.0\,\mu$m.

These experiments are summarized in figure 2.16. In this figure all the variables are taken into account which gives a clear overview of the experiments. It is clear that both the laser parameters for irradiation and the etching condition can influence removal capability. The horizontal axis indicates the laser irradiation conditions and the vertical axis the etching conditions. The three lines indicates the border of the desirable situation and the arrow indicated the desirable direction. It is not clear if a overlapping region of the three lines exists. The three line cross at a point, but the relative positions of the three lines have not been determined yet and needs further research.
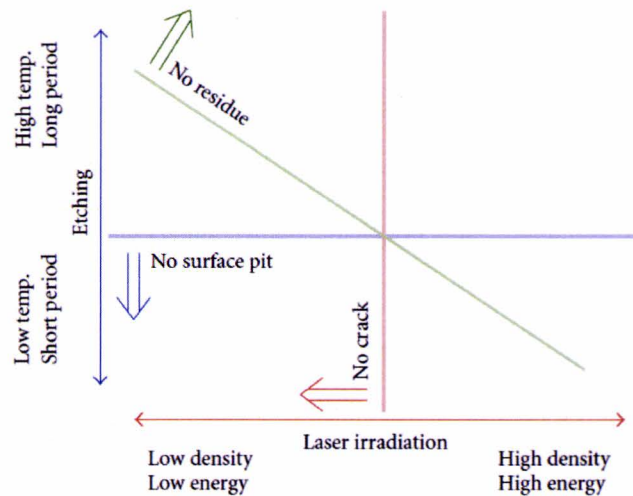

Figure 2.16: Schematic graph of removal properties of sapphire by fs laser-assisted etching. The three lines indicates the border of the desirable situation and the arrow indicated the desirable direction. It is not clear if a overlapping region of the three lines exists. The three line cross at a point, but the relative positions of the three lines have not been determined yet.

With femtosecond laser-assisted etching, more advanced microscale 3D objects can be fabricated that described before. Matsuo *et al.* [10] fabricated an optical rotator inside sapphire which can be seen in figure 2.17. Laser irradiation is performed followed by wet etching with 10 % HF for several days. The distance used between the tracks in the plane is $0.25\,\mu$m and in vertical direction the distance is $1\,\mu$m. Figure 2.18 shows the optical micrographs of the fabricated rotator before and after etching. The figure shows the shape of the rotator. After etching the region around the rotator is darkened (2.18(b)) and this suggest a successful fabrication. After testing the rotator, it turned out
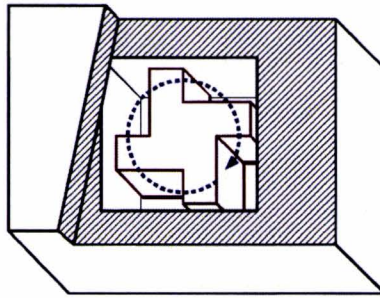
Figure 2.17: Design of the optical rotator inside sapphire. The arrow indicates the direction in which it will rotate.
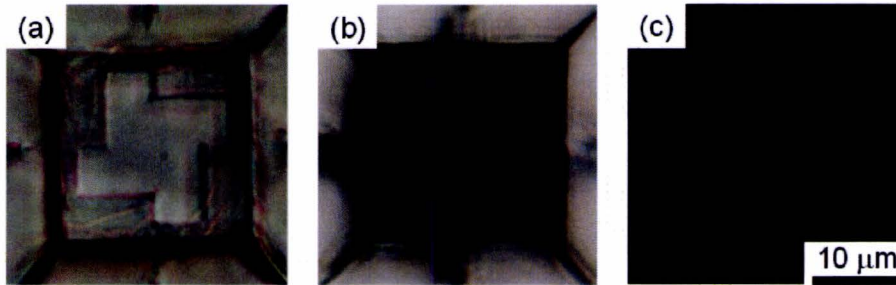

Figure 2.18: Top views of (a)Bright-field image after laser irradiation, (b)Bright-field image after etching and (c)Confocal image after etching.

that the rotator did not work. This is caused by a mesh-like un-etched surface at the region where the material should be removed. A solution maybe found in a combination of a different host material and a different etchant in which the etching rate of the unmodified host material is low but not zero.

The last method discussed to etch sapphire is by using KOH [11] as etchant. First void structures are fabricated followed by micro-channels:

Fabrication of void structures: With single femtosecond pulses[7] void structures are created in the sapphire. The energy pulses used varied between 90 to 150 nJ at the focus. This is schematically shown in figure 2.19. Subsequently, the sample is split along the plane of voids into two halves for
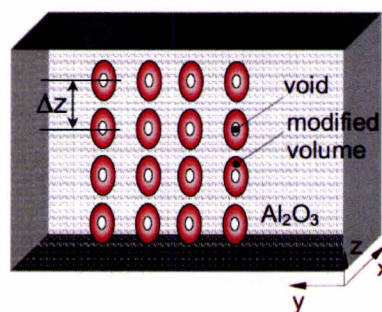
Figure 2.19: Schematics of the void structures created inside sapphire.

etching. The pieces where exposed to two different etching methods. One piece is just immersed in water to test if water alone can remove amorphous sapphire, however, no changes are observed after 1 hour of immersion. The second method is by using 1 M KOH solution. The sample sapphire is

---

[7]Laser, Wavelength: 800 nm, Pulse Duration: 150 fs, Repetition Rate: 20 Hz.

immersed for 1 hour and the amorphous regions were removed. Both results are shown in figure 2.20. The arrow marks the direction of irradiation and the ovals mark areas of amorphous sapphire which becomes elongated when the beam focus was placed at a larger depth.

(a) After irradiation.   (b) After immersion in water.   (c) After immersion in 1 M KOH.
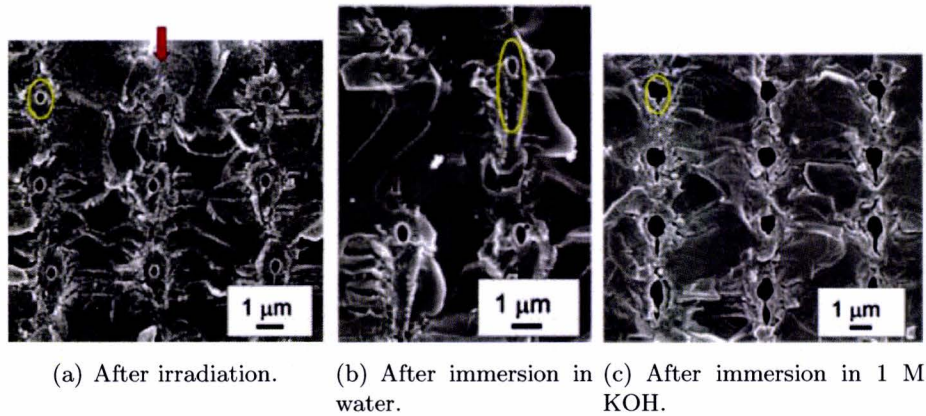
Figure 2.20: SEM micrographs of the void structures

Fabrication of micro-channels: After this result, fabrication of microchannels was performed with a pulse energy of about 140 nJ. The are made with overlapping axially voids. These overlapping distance is δz which is shown in figure 2.19 and is performed with different pulse energies. The same etching procedure is performed only in a more concentrated KOH solution. A 2 M KOH solution is used to etch the microchannels. Graph 2.21 shows the result of the experiment. After etching, it was found that a
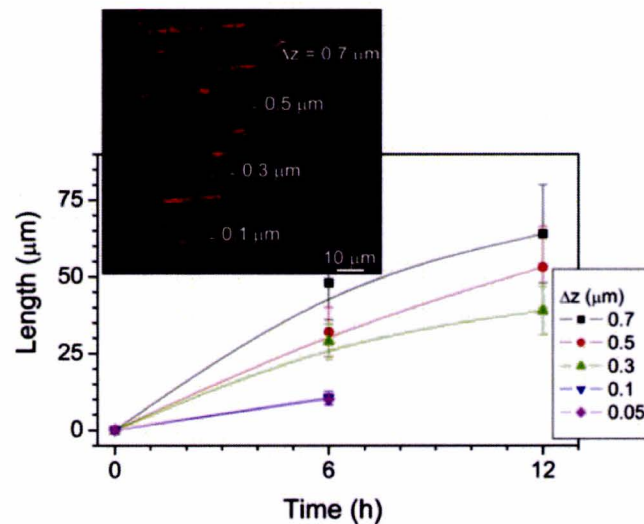
Figure 2.21: Length of the etched channel as function of the etching time

desirable channel was etched with a distance of δz between 0.5 and 1 μm. Above 1.5 μm, the channel was not etched out. The larger etching rate at larger pitch becomes stochastic at 1 to 1.2 μm distance. No permeable channel is formed by wet etching because probably fluctuation of the laser becomes critical and an overlap of amorphous regions disappear with these distance. Channels were reliably etched out when the pulse energy was larger than 100 nJ at the focus. When the energy at the focus was larger than 200 nJ, cracks appeared. Expecting is that etching in a heated solution will increase the development of the channels. In addition to the etching method with KOH, a combination of two

etchants is used. Again, channels was etched but now using a 2 M KOH solution with additionally 0.1 M HF. It is expected that the F⁻ ions facilitate wet etching and indeed an increase of etching rate up to four times was observed in the regions were the δz distance was between 0.05 and 1.9 μm. Unfortunately, unwanted tapering along the channels appeared.

2.4 Summary

This chapter described femtosecond laser irradiation with combined wet chemical etching techniques. The experiments that will be discussed in chapter 3 are based on this technique.

Femtosecond laser irradiation followed by etching techniques are performed in literature on sapphire and on fused silica. In appendix A all laser and etching parameters used in literature are mentioned. For the materials fused silica and sapphire the most promising laser and etchings conditions are summarized below.

Fused Silica: Because fused silica is amorphous, the writing direction is not important. The most important values can be derived with graph 2.3 and graph 2.4. For etching of an irradiated area does not hold that the more energy is deposited to fabricate this channel the better it will etch. Conversely, an optimum etching rate can be achieved with a lower energy deposition. According to graph 2.4, the optimal etching rate can be reached when the deposited energy is between 10 to 20 J/mm². The ratio between the writing speed and the repetition rate determines the deposited energy. The relation between these two parameters is schematically shown in graph 2.3. The writing direction used is perpendicular with respect to the polarization. For fused silica, HF will be used to etch. The used concentration is 2.5% and 5.0% and etching rates between 1.2 μm/min and 6.6 μm/min can be reached with these concentration.

Sapphire: Reported energy pulses are between 90 nJ up to 1000 nJ with writing speeds ranging from 100 and 1000 μm/s. The reported writing speeds are perpendicular to the polarization direction. Mutual distance are kept between 1 μm and 2 μm. Besides HF, KOH is also known as etchants but throughout literature, HF is mentioned as most promising etchant for sapphire. The concentrations used for sapphire are much higher than for fused silica. Concentrations of 10%, 40% and 48% are used. However, the etching speeds are also lower than on fused silica. The nominal etching speed of sapphire ranges between 3.3 μm/hour and 38 μm/hour. Moreover, most etching rate are achieved with special etching condition e.g. high temperatures.

Chapter 3

Structuring of Quartz and Ruby

This chapter will first briefly introduce three materials namely quartz, fused silica and ruby. Subsequently, the experiments with femtosecond laser irradiation followed by chemical etching on quartz and ruby are described. The chapter ends with a model to predict crack occurrence during laser machining.

3.1 Material properties

Here, some basic information about the mentioned materials is given but more detailed material properties such as Young's Modulus or refractive ratio are described in appendix B.

Quartz: One of the most known and second-most-abundant mineral on earth is quartz. It is also the mineral with the highest numbers of forms, habits and colors. Its chemical formula is SiO_2 and has a trigonal cristallographic structure. Pure quartz is needed for producing glass, ceramics and chemical apparatus. By rapid cooling of molten crystalline quartz, quartz glass also known as fused quartz can be produced. In fact, the name fused quartz can be confusing since it is not a quartz from a crystallographic definition but simply means a fused silica (see below) that was produced from a natural, molten quartz.

Fused Silica: In contrast to quartz, fused silica is a glass and therefore can be considered as amorphous (with the understanding that it does not have long range ordered crystalline structure). It is produced using high-purity silica sand as the feedstock, and is normally melted using an electric furnace, resulting in a material that is translucent or opaque. Fused silica glass combines a very low thermal expansion coefficient with excellent optical qualities and exceptional transmittance over a wide spectral range, especially in the ultraviolet. It is resistant to scratching and thermal shock. Fused silica is available in a number of grades for different applications.

Ruby: In essence, ruby is a red sapphire, since ruby and sapphire are identical in all properties except for color and chemical composition. Sapphire is a gemstone variety of the mineral corundum, an aluminum oxide given in chemical formula Al_2O_3. Together with emerald, diamond and ruby, sapphire is considered as one of the four precious stones. It is a desirable gemstone due to its hardness, durability, luster and rarity. Due to chromium impurities in corundum yield a red tint. Both sapphire and ruby have a hexagonal system and a hardness of 9(Mohl scale).

In the next sections the experimental results will be discussed. The experiments discussed here are only performed on quartz and ruby and not on fused silica. The effects of femtosecond laser irradiation on fused silica are already known and are used to identify some parameters for machining on quartz.

17

The information found in literature about sapphire is used to identify possible laser parameters for ruby.

3.2 Experimental results

3.2.1 Quartz

First experimental results: Some research are ongoing at the University in collaboration with Asulab on femtosecond drilling and wet chemical etching of quartz. These first results are comprehensive but a summary or conclusion has not yet been made. In these experiments, structures are machined. Figure 3.1 shows different writing parameters that can be varied within machining patterns (writing direction and the laser track density in x and z). Besides these parameters, the pulse energy, speed
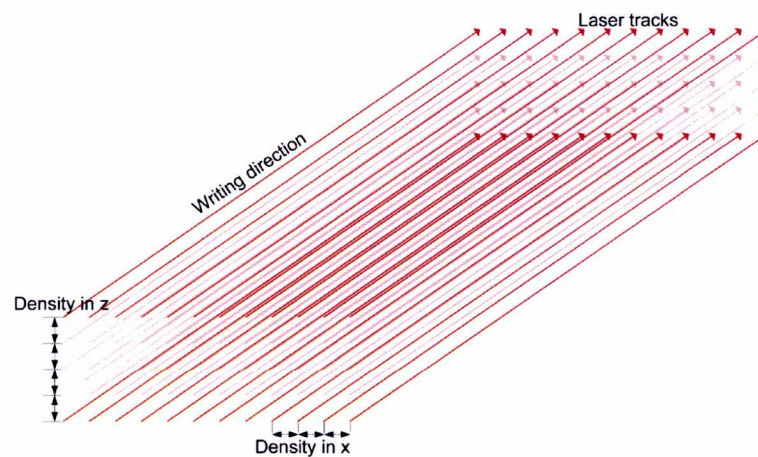

Figure 3.1: During machining, the density in x and y can be varied. The y direction is the writing direction.

and repetition rate of the laser can be varied. The polarization field was changed during experiments to parallel, perpendicular or circular with respect to the writing direction and finally, the orientation of the quartz substrate was changed. After examination of these quartz samples and the summaries of these experiments, some parameters can be determined as relevant parameters to machine quartz. The mutual distance between the laser tracks in x and z direction should be around 2 and 6 μm, respectively. The repetition can be set around 800 KHz with a writing speed between 15 to 20 mm/s. The writing direction should be perpendicular with respect to the polarization direction. These quartz substrates were subsequently etched in a pure HF bath (50%). Depths of about 15 to 20 μm were reached with only 2 to 4 minutes of etching.

Follow-up experiments: The first preliminary experiments were done in November 2010 and since some of the laser characteristics (like the pulse duration) have changed since then, the repetition of this experiment is a logical decision. These experiments were performed in a similar way. First the quartz substrate is irradiated with a femtosecond laser and subsequently immersed in a chemical bath of 50% HF. During these experiments the density of laser tracks in the z direction is varying and the energy deposition per area is changing due to a varying ratio between the writing speed and the repetition rate. The first formula written below represent the ratio (a) between the repetition rate and the writing speed. The second formula represent the ratio (n) in mutual distance in the z direction. The structures for different values of a, z, f and v are described in the appendices.

$$a = \frac{f \times h}{v \times z} \tag{3.1}$$

$$n = \frac{h}{z} \tag{3.2}$$

Where h is the height of the beam which is taken as $10\,\mu$m. f and v are the laser repetition rate and the writing speed, respectively.

The results of these experiments are described in detail in appendix C and D. Due to laser instabilities the results are not reliable. Therefore these results are only described in the appendices.

Last experiment: Once the issues of laser stability were solved, new experiments were executed. A square-like pattern (i.e. square with rounded edges) was developed by other people in the group to test birefringence effects in laser written structures and is illustrated in figure 3.2. By modifying
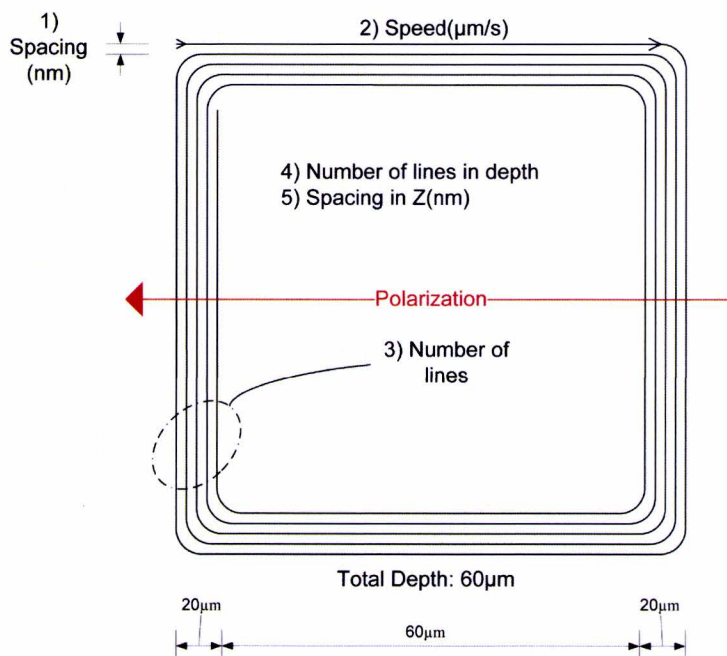

Figure 3.2: Shape of one square-like pattern. Possible parameters to vary are: spacing and number of lines in x and z direction, the writing speed and the repetition rate.

this square-like pattern and implementing it into a larger pattern it is possible to vary important laser parameter during one laser operation. This laser pattern is also used for the last experiment on ruby. The laser pattern is depicted in figure 3.3. It has dimensions of 2.85 mm by 2.35 mm and consist of 120 square-like structures and can be divided in several parts. Each part is divided into six columns where every two mutual columns are written with the same laser parameters. Looking at the bottom left part, three larger squares containing each 10 smaller squares can be seen. In the first larger square, the x-spacing is decreasing from 2000 nm at the bottom square to 1000 nm at the top square with steps of 250 nm. In the middle larger square, the z-spacing is increasing from $2\,\mu$m at the bottom square to $10\,\mu$m with steps of $2\,\mu$m. In the third larger square, the repetition rate and the writing speed are varying but the ratio between these two parameters is kept equal. The repetition rate decreases from 870 KHz at the bottom to 200 KHz at the top with a speed starting at 10 mm/s and finally ending with 2 mm/s. In the bottom left part, equal signs are shown. These signs indicate that the two squares are written with equal parameters. The last possible varying parameter is the pulse energy. Each part is written with a different energy level. The laser pattern described, is performed four times on two
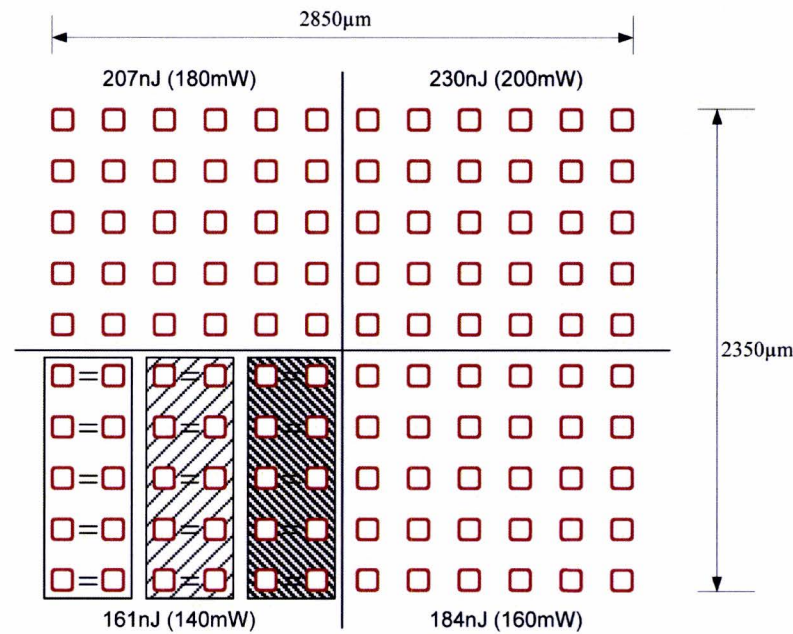
Figure 3.3: Laser pattern with dimensions of 2.85 mm by 2.35 mm consisting 120 square-like structures. It is divided into four parts which are irradiated with different pulse energies.

different substrates of quartz. The figures of these laser patterns are shown in appendix E. One can see clearly that there are some squares without any cracks or ablated areas but also some squares with a lot of cracks. Furthermore, there is a good repeatability between the four patterns and therefore reliable conclusions can be made. A pulse energy of 207 nJ is too high while a pulse energy of 161 nJ seems low. Furthermore, a x-spacing of $2\,\mu$m and a z-spacing of $4\,\mu$m is too small. The energy is then deposited in a small volume which will induce too much displacements inside the material and crack occurrence will be induced. The variation of the repetition rate and the speed while keeping the mutual ratio equal differs not much from each other. The results seems similar. According to these experimental results the following parameters are advised for further machining of quartz:

- Pulse energy = 184 nJ

- X-spacing = between 1.5 and $2\,\mu$m

- Z-spacing = between 6 and $8\,\mu$m

- Repetition rate = 870 KHz

- Writing speed = $5000\,\mu$m/s

After irradiation, the substrates are immersed in a 50% HF chemical bath. The results are described by Asulab and are attached in appendix E. Also the alpha-steps are shown in the appendix. According to the description given by Asulab, the depth of the structures without cracks is disappointing. Some of the "cracked" ones have been measured and some of them can be deep. The final depth is often difficult to measure due to a 60° tip of the alpha-step. According to the alpha-step profiles some cracked structures can reach a depth of $25\,\mu$m. Although this results is not as high as initially hoped, it does look promising. With some more adjustments of the machining parameters, the depths reported in the first experiments can be reached.

3.2.2 Ruby

In contrast to quartz, no experiments were reported on ruby. Because of the similarities of sapphire and ruby, the laser parameters and etching conditions of structuring sapphire mentioned in section 2.4 will be used initially. In this section, three experiments are performed on ruby.

First experimental results: The range of pulse energies used in literature is very wide (from 90 nJ up to 1000 nJ) as well as the different writing speeds (from 100 up to 1000 μm/s). The starting pulse energy that will be used to structure ruby is around 207 nJ, which is a little higher than the pulse energy used on quartz. In the first set of experiments, three substrates of ruby are used. On one substrate (B), rectangle structures are machines and on two others substrates (C & D), square structures. These three substrates are shown in figure 3.4. The laser parameters used for substrate
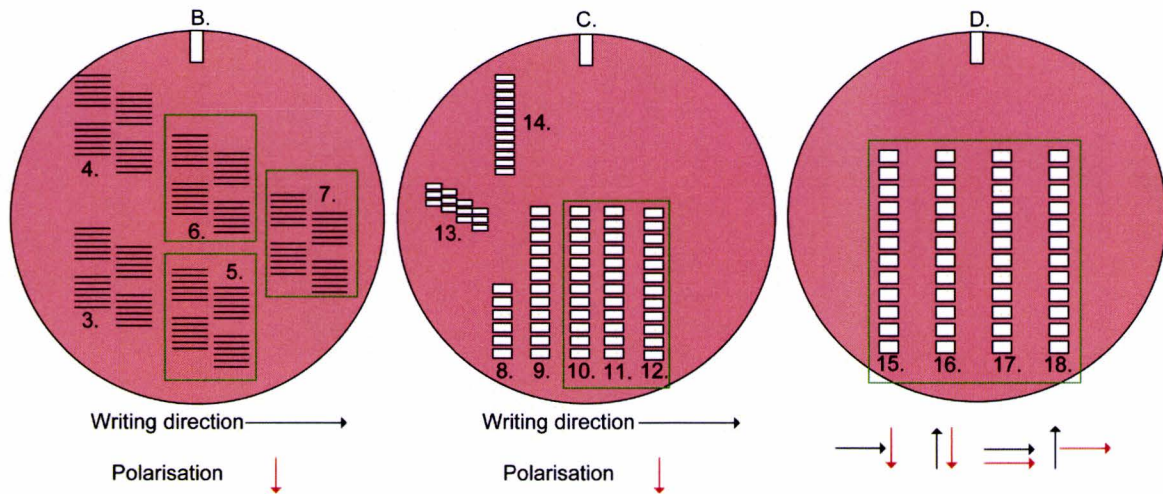

Figure 3.4: Different structures are written onto three ruby substrate. The structures within the green boxes are machined successfully and the structures are labeled with group numbers which are used throughout this chapter. The arrows below the figures are indicating the writing direction and the direction of the polarization.

B are the same as for the quartz and are mentioned in table D.1. After examining these rectangle structures (table F.1 and F.2) it was clear that parameter z should be around 6 μm and the parameter a between 10 and 30 because the structures with these parameters are not cracked while others are heavily damaged. With these parameters in mind, the more square structure are made on substrate C and D. Group 10, 11 and 12 on substrate C are irradiated with a pulse energy of 172 nJ while the other structures on that substrate where still irradiated with 207 nJ per pulse. The ones irradiated with 207 nJ per pulse are too damaged to be useful for further etching experiments. On substrate D, group 15, 16, 17 and 18 have been irradiated with the identical laser parameters as the successful structures on substrate C but, these structures are written in different directions and with different polarization directions. After irradiation the three substrates are measured and subsequently etched with different etchants. The different experiments on each substrate will be briefly described below and the results are extensively described in appendix F.

- Etching substrate B: After irradiation, this substrate tested with several etchants. First a bath in 20 % concentrated KOH during 5 minutes. During immersion, no reaction took place while KOH normally reacts heavily with Al. This was already a sign that it is not a suitable etchant and measurements did not show a difference in depth before and after this KOH bath. Secondly, the substrate is immersed in a bath of 30% NH_4OH mixed with 30% H_2O_2 and H_2O in a ratio of 1:1:3 at a temperature of 80 °C for more than 10 minutes. Still no etching of the structures was observed. The third etchant used on this substrate is 10% HF. After 24 hours, the rectangle

structures with the parameters described above (z=6 μm, a=10, 20, 30) did not become much deeper after etching. The difference was at most 0.5 μm. Nevertheless, some structures gain depth of about 5 to 7 μm but these structures were already a bit deeper and damaged. Due to a higher pulse energy, it could be that more amorphization has taken place and the etching conditions were better. Finally, HF is used one more time to etch this substrate but now with a concentration of 50% and for more than 7 hours. The results was similar to the previous tests with 10% concentrated HF. The rectangle structures without cracked did not gain depth but the damaged ones reached a depth of about 15 μm. Another final test to see if more depth will be reached with 10% HF took place for 48 hours. The depths did not change much anymore. The results of this experiment including alpha-step scans can be seen in appendix F.

- Etching substrate C: On this substrate, smaller structures are created. Because the pulse energy used was too high, only twelve squares of the 36 squares in this substrate within group 10, 11 and 12 were not cracked. On these structures the measurements are performed. After irradiation, this substrate is immersed in a bath suitable for etching aluminum. The chemical mixture consist of H_3PO_4, CH_3COOH and HNO_3. The etch temperature is about 20 °C and it is etched for more than 4 hours. The results are shown in details in appendix F and a summary is shown in figure 3.5.
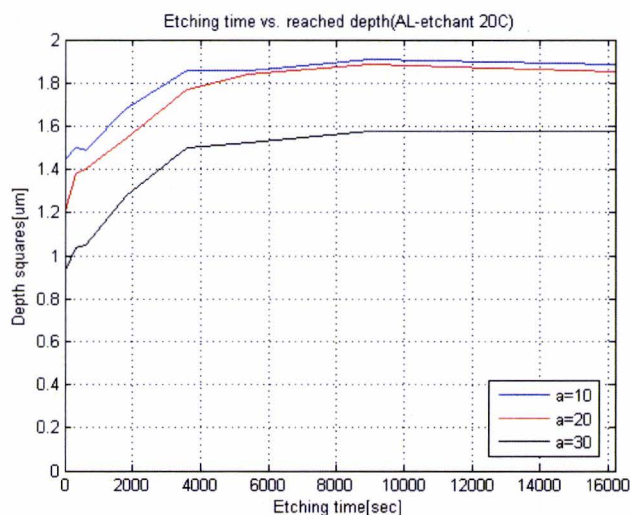

Figure 3.5: Etching depth of substrate C during 270 minutes of etching with an Al-etchant.

It can be seen that the etchant worked at the beginning of the process but after 5 minutes the depth did not further increase. After this aluminum etchant, two other etchants were tried. First the substrate is immersed in a mixture of 86% concentrated H_3PO_4 and H_2O in a ratio of 1:4 at 20 °C and secondly 95% concentrated H_2SO_4 at 40 °C was added to the existing mixture. Both mixtures had no effects on the depth.

- Etching substrate D: On this substrate, the same structures are created as the ones on substrate C, only these structures are written in different directions and with different polarization directions. After irradiation, this substrate is etched in 50% HF at a temperature of 84 °C for 150 minutes. Figure 3.6 summarizes the results from appendix F. During the the first 5 minutes etching took place but afterwards, nothing changed anymore. What can be concluded from figure 3.6 is that the structures of group 15 and 18 are deeper than structures of group 16 and 17. This indicated that writing with the polarization perpendicular to the writing direction is better. The corresponding alpha-step scans are depicted in appendix F.
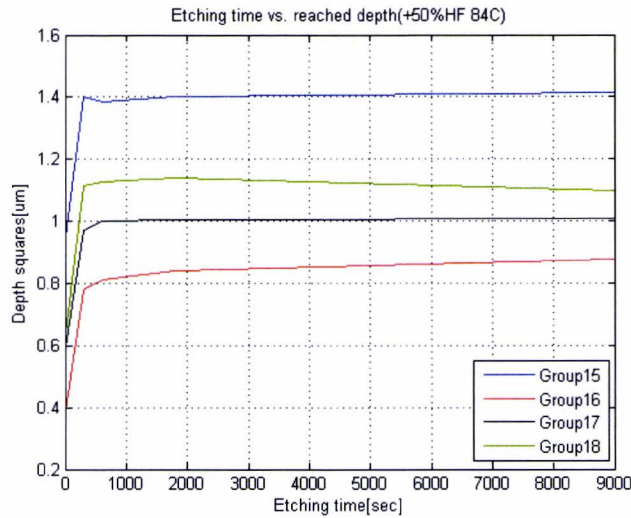
Figure 3.6: Etching depth of substrate D during 150 minutes of etching with 50% HF.

Follow-up experiment: After irradiation and etching of substrates B, C and D, it can be concluded that etching ruby is difficult. This is also caused because the laser instability mentioned earlier was not solved yet during these experiments. With this follow-up experiment, the laser parameters are exactly similar to the parameters used to machine the structures on substrate E. The experimental results are described in appendix G and because HF looked the most promising etchant during previous experiments, this was used again. At the end, the results are identical, so no real etching was achieved in ruby.

Last experiments: During these last experiments, the laser instability was totally solved and therefore if no etching is achieved, this cannot be attributed to the instability of the laser. In this experiment, the same laser pattern illustrated in figure 3.3 is used. The laser parameters used are similar except the energy per pulse is different. After earlier experiments, it turned out that ruby cracks at a lower pulse energy than quartz so the used pulse energies are 161, 172, 184 and 195 nJ. The results, obtained with an optical microscope are shown in appendix H. According to these experimental results the following parameters are advised for further machining of ruby:

- Pulse energy = 172 nJ

- X spacing = between 1.5 and 2 μm

- Z spacing = between 6 and 8 μm

- Repetition rate = 870 KHz

- Writing speed = 5000 μm/s

- Polarization perpendicular with respect to the writing direction

Etching is performed by Asulab and with 50% HF for 4 hours on 2 patterns and with 10% HF on the other two patterns. The etching depths that were achieved, are respectively 1.5 μm and 2.0 μm. Both results are disappointing. Unfortunately, during this project no real working etchant was found to etch ruby but the experiments with the etchant HF looked promising but more research in necessary to find suitable conditions.

3.3 Model to predict crack occurrence during laser machining.

Prediction of crack occurrence due to laser irradiation is complex. There are many parameters to take into account e.g. pulse energy, repetition rate, writing speed and direction but also material impurities and polarization. With Comsol simulations and some assumptions, an approximation can be made. To predict crack occurrence one must know when a material will crack. These cracks are a result of change of structure inside the material. A displacement (strain) of the material will occur and when an ultimate yield stress is reached inside the material a crack can nucleate. The strain that occurs inside the material is a result of laser treatment. Due to a certain energy deposition inside the material, some amorphisation may occur. Amorphisation leads to a change of the structure of the material and will induce some displacements i.e. strain. To simulate this behavior in a Comsol model (knowing that from the physics point of view the volume expansion is not of thermal origin), energy deposition is modeled as a heat flux. Below, the approach to predict crack occurrence is described.

First, a slit comparable in size with the cross-section of one small square-like structure showed in figure 3.2 is modeled in 2D with Comsol. This is illustrated in figure 3.7. On the edge, a heat flux
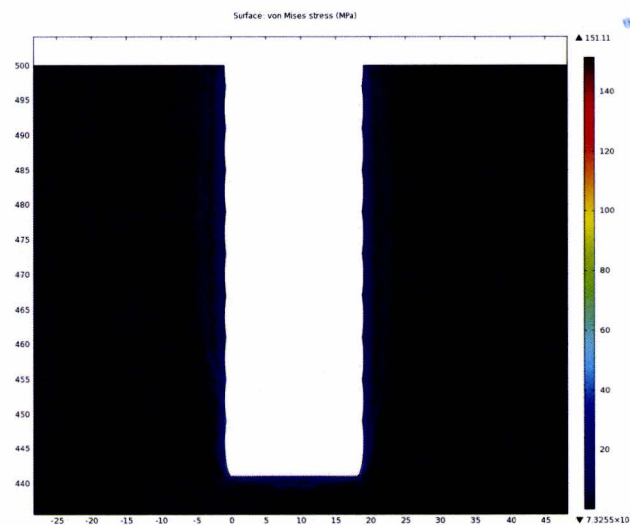

Figure 3.7: Cross-section of one small square-like structure with dimensions 20x60 μm. The thickness of this structure is modeled as 50 μm

is simulated and due to this energy deposition, strain/stress will be induced that will lead to crack occurrence. Figure 3.8 is made using Comsol and gives a clear overview of the stress and stain in anisotropic quartz when the heat flux increases from $0.5\,e^5$ MW to $5.0\,e^5$ MW. One can see that the ultimate yield stress threshold of 150 MPa has been reached at a heat flux of approximate $2.3\,e^5$ MW at an equivalent strain of 0.3 nm.

Subsequently, the equivalent heat flux has to be calculated due to the energy deposition of the laser beam. Again, this is not possible because a laser source cannot be seen as a heat source since the laser pulses are too short for the material to absorb heat. Nevertheless, this equivalent heat flux is derived with the laser parameters.

The approximation of the equivalent heat flux of the laser can be calculated as follows. First the peak pulse is calculated by dividing the pulse energy by the pulse duration of approximately 380 fs. By calculating the necessary time for machining this slit using the writing speed used, the number of laser tracks with corresponding depth, the total amount of pulses can be derived. Subsequently, the resulting heat flux, which can be derived by multiplying the number of pulses with the energy per pulse, is split up in two parts. The first part is the heat flux that is deposited directly on the edge of the slit (by the outer laser tracks). These are taken into account fully. The laser tracks inside the slit (but not on the edge) are multiplied with an overlap factor (< 1) which is dependent on the overlap
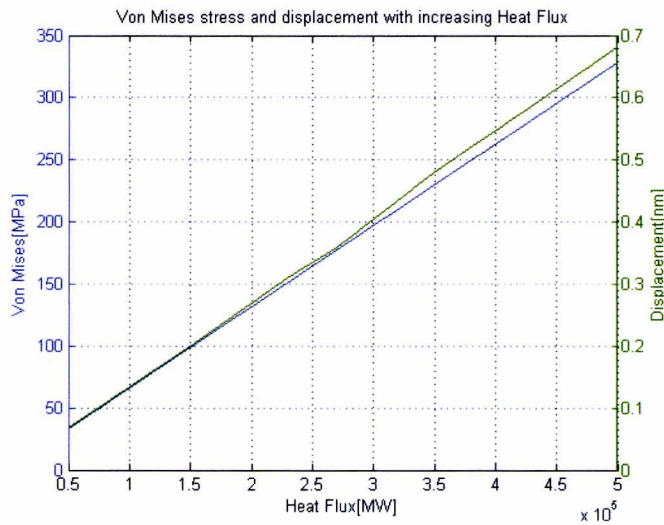
Figure 3.8: Equivalent heat flux vs. Von Mises Stress and Displacement.

distance of the adjacent laser tracks. Therefore, the energy deposition there is taken into account partly and has less influence on the total equivalent heat flux. In essence, a difference is made between these two contributions to calculate the total amount of equivalent heat flux which is deposited. With these calculations, a surface plot can be derived which gives the dependency of the number of laser tracks and the used pulse energy on the total heat flux. The surface plot is shown in figure 3.9.
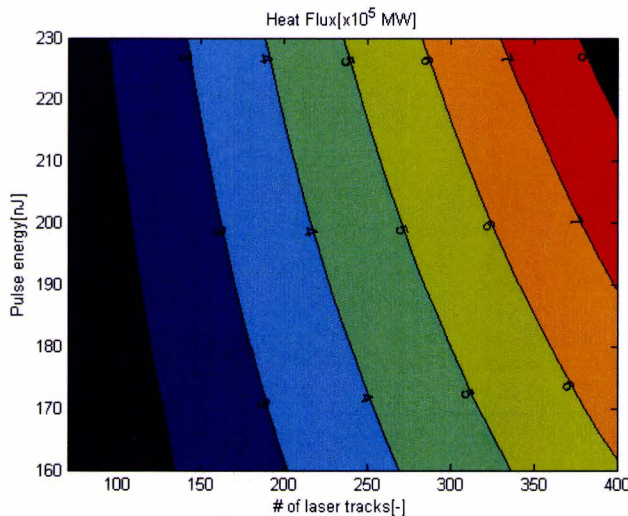
Figure 3.9: Surface plot of the derived heat flux.

With figure 3.9 a prediction can be made whether a square-like structure fabricated in quartz, described in appendix E, will crack or not due to laser irradiation. A schematic overview of the laser patterns is made and is depicted in figure 3.10(a). Each square in figure 3.10(a) represent the square-like structure at the same position in figure 3.10(b). The numbers in the squares are the number of laser track that is used the machine the specific square. A high number means that the x and/or z spacing is small and a low numbers means the opposite. If a square is green, it means that the energy deposition on the material was not too high and the machining succeeded. When a square is red, the pulse energy and/or the number of tracks is too high which will induce a high energy deposition inside the material and crack occurrence will take place. Some squares are orange which mean that
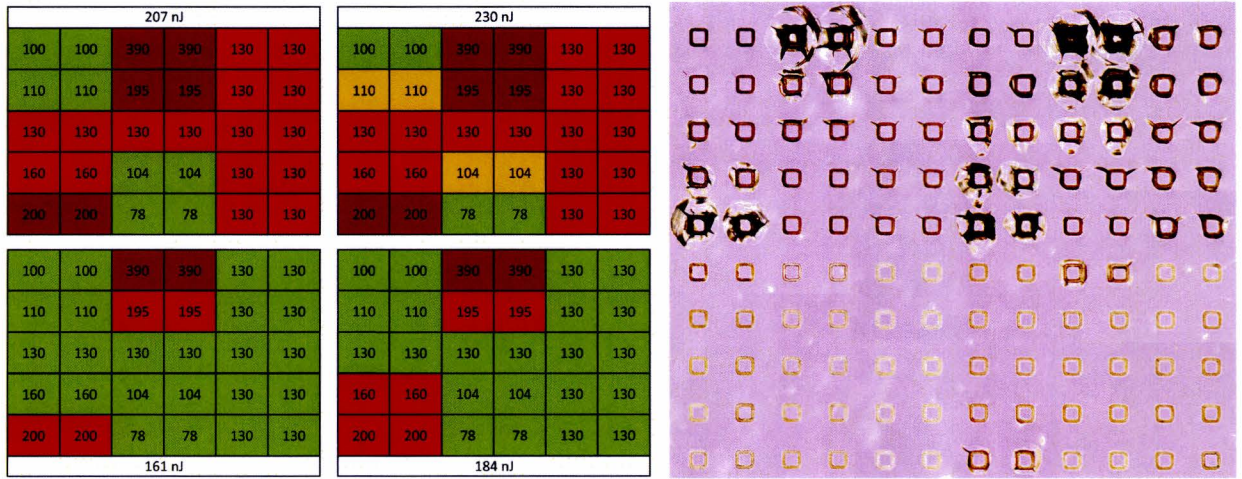
(a) Schematic overview of a laser pattern.

(b) Picture taken with an optical microscope of a laser pattern in Quartz.

Figure 3.10: Similarities between the crack prediction and experimental results.

the energy deposition is around the crack nucleation threshold which will make it impossible to predict crack occurrence. Although our modeling approach is empirical, there is a good agreement between the predicted crack cases and the observations.

Chapter 4

Shock-absorber

4.1 Introduction

Shock-absorbers are used in watches and have several functions. First, the shock-absorber holds the balance wheel in place and maintains the balance wheel rotation while the watch is hold sideways or upside down. Secondly, it protects the balance wheel against shocks during regular use of the watch. The current Ni-prototype shock-absorber has to be redesign for different materials while keeping similar mechanical specifications. The choice for the new material depends on the feasibility of fabrication of this design with femtosecond laser irradiation followed by etching techniques. The existing Ni-prototype shock-absorber is depicted in figure 4.1. Unfortunately, little information is known about
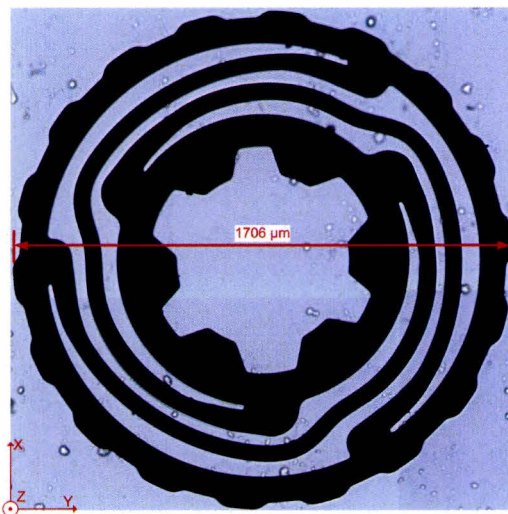
Figure 4.1: Picture with optical microscope of the Ni-prototype shock-absorber.

this element. Besides the actual parts, one measurement test is available to verify the mechanical specifications of the new prototype shock-absorber with respect to the Ni-prototype shock-absorber. This measurement illustrates the influence of an applied force. The force can be applied in vertical direction (z) or in lateral direction (xy-plane). With a force of 0.167 Newton (= 17 gram, in the watchmaking industry, they talk about grams instead of Newtons), a displacement of 26 μm and 36 μm is induced in lateral and vertical direction, respectively. The following steps (not in chronological order) have been performed until finally a new prototype shock-absorber performed in a different materials can be dimensioned.

1. Making different models: Different models are made to predict the reliability of a new prototype shock-absorber with the same characteristics as the Ni-prototype shock-absorber. Here, the

models are briefly described but more details will be provided later in this chapter.

(a) Analytical models: Analytical models are useful to test very rapidly the influence of various parameters of the model without the need for simulating it each time. Besides, multiple parameters can be varied at the same time to find optimum parameters rapidly. First a model is made by using Castigliano's theorem and secondly by using compliances and stiffness matrices.

(b) Finite element models: First a simple ANSYS model is made by copying the simple shape of the first analytical model in ANSYS for comparison. The second model is a more complex ANSYS model. This model only consists of the three arms of the Ni-prototype shock-absorber. The inner and outer ring are not generated but these parts are significantly stiffer than the arms so these could be kept out of the simulation. This simulation is used to vary the dimensions of the arms (radius, height and width) and to find optimal dimensions for the new prototype shock-absorber.

2. Comparison and optimization: The four models can be compared to the available measurement test. Error factors between the different models and the measurements are useful to determine the reliability of these models. Finally, a choice can be made and a new prototype shock-absorber can be determined in a chosen material.

4.2 Models

Two analytical and two simulation models are described below. On each model, the same measurement test is performed as on the Ni-prototype shock-absorber. The results are described in this section.

4.2.1 Analytical models

By Castigliano's theorem: The component shown in figure 4.1 has a complex shape and therefore it is difficult to compose directly an analytical model. The shock-absorber consist of three identical arms which are connected to an outer ring and an inner ring. The arms have an angular span of 195° and they are rotated with respect to the other arms with an angle of 120°. The radius of the arms with respect to the center varies over the whole angular span. Besides that, the width of the arms varies over its length. The height of the Ni-prototype shock-absorber is constant and has a value of 150 μm. To derive a suitable and reliable analytical model using Castigliano's theorem simplifications are necessary. The first step is to leave out the inner and outer ring and to rearrange the three arms. The width of each arm is derived as the average value of the varying width. The angular span of the arms will be set as 180° instead of 195° and the average radius and width that will be used are 618 and 53 μm, respectively. The simplified model is shown in figure 4.2(a).

In order to calculate the lateral displacement of this simplified model, some additional simplifications are needed. Instead of considering this model as one piece, it will be considered as three separate arms. The force applied at the center will be distributed over the three arms. The separate displacements will be averaged as the total displacement for the complete structure. This method induces a large error but is necessary when using the Castigliano's theorem. To calculate the displacement of the arm, an energy method (Castigliano's Second Theorem [12]) is used:

$$\delta_i = \frac{\partial U}{\partial Q_i} \tag{4.1}$$

where the partial derivative of the strain energy U with respect to generalized force Q_i gives the generalized displacement. The displacement in x and y direction can be calculated respectively as
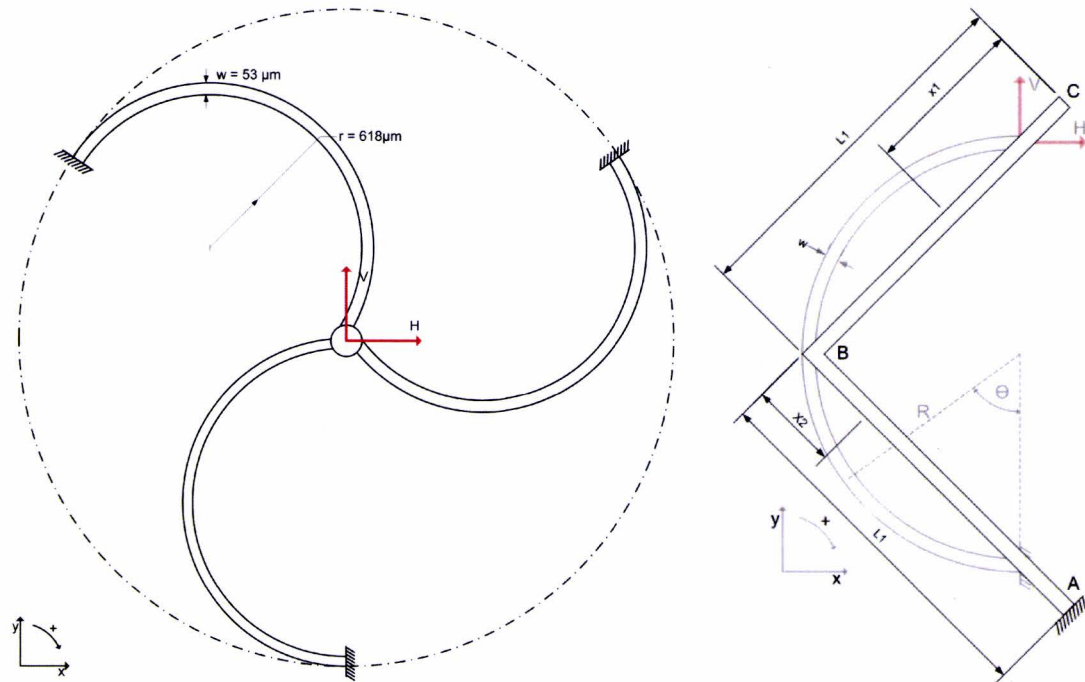
(a) Rearrangement of the 3 simplified arms for calculating the lateral displacement.

(b) Simplified arm for calculating the vertical displacement.

Figure 4.2: Simplified shock-absorber models.

$\delta_x = \partial U/\partial H$ and $\delta_y = \partial U/\partial V$, where H and V are the generalized forces in horizontal (x) and vertical (y) direction, respectively (figure 4.2(a)). The moment of one arm can be calculated with:

$$\Sigma M = VRsin\theta + HR(1 - cos\theta) = 0 \tag{4.2}$$

then δ_i can be calculated with:

$$\delta_i = \frac{1}{EI} \int_a^b M\frac{\partial M}{\partial Q_i}d\theta \tag{4.3}$$

Which will lead for the x direction to equation 4.4. The same methods can be applied for calculating the displacement along the y direction.

$$\delta_x = \frac{R^3}{EI}\left[V\left(\frac{(cos\theta - 1)^2}{2}\right) + H\left(\frac{3\theta}{2} + \frac{sin2\theta}{4} - 2sin\theta\right)\right]_0^\pi \tag{4.4}$$

This method is only valid if the radius of the curvature is large enough, i.e. the radius of curvature is greater than 10 times the width of the beam. With these dimensions the stress distribution across the width of the beam is linear in a first approximation and the complementary energy of the flexure can be calculated with sufficient accuracy. The displacements of the two other arms is then considered. The forces H and V are applied in the middle of the part i.e. on the end of every single arm. These forces need to be converted to forces H_{2x}, V_{2y}, H_{3x} and V_{3y} (see appendix I). These force are rotated

to be useful in the new orthogonal axis for respectively arm two and three. Then the formula 4.3 can also be used to calculate the displacement of those arms. Furthermore, a rotation matrix is then used to transfer these displacements in a common direction along the same orthogonal axis. The average of the three displacements can be calculated for the x and y direction and will be assumed as the total displacement of the model. To calculated the z displacement, only one arm is taken into account and therefore 1/3th of the force will be used to determine the z-displacement. The 180° ring will be substituted by two bars making a 90° angle. The total length of the two bars is equal to the length of the curvature. Figure 4.2(b) shows this simplification and formula 4.5 is used to calculate the z-displacement. Force P is the vertical force in z direction at the end of the arm.

$$\delta_z = \frac{1}{EI} \int_A^C M_f \frac{\partial M_f}{\partial P} dx + \frac{1}{GI_p} \int_B^C M_t \frac{\partial M_t}{\partial P} dx \qquad (4.5)$$

With $M_f = -x_1 P$ when $0 \leq x_1 \leq l_1$, $M_f = -x_2 P$ and $M_t = l_1 P$ when $0 \leq x_2 \leq l_2$.

With this model, the lateral displacement that occurred in response to a force of 0.167 Newton is $107\,\mu m$. The vertical displacement is $43\,\mu m$. The error (especially in lateral direction) is very large and we conclude that the approximations are too simplistic. The corresponding M-file for this first model using Castigliano's theorem can be found in appendix I. Another analytical model is derived with much less simplifications and is described in the next section.

Method using compliances/stiffness matrices: Similar to previous model, the arms have to be simplified. The width of the arms has again a constant value ($53\,\mu m$) and the distance with respect to the center (radius) is constant as well ($618\,\mu m$). But the angle between the mutual arms with respect to the center is still 120° and the angular span (195°) of the arms will not change. The height is again ($150\,\mu m$). With these simplification is not possible to get a physical possible model because the arms overlap each other. This is shown in figure 4.3.
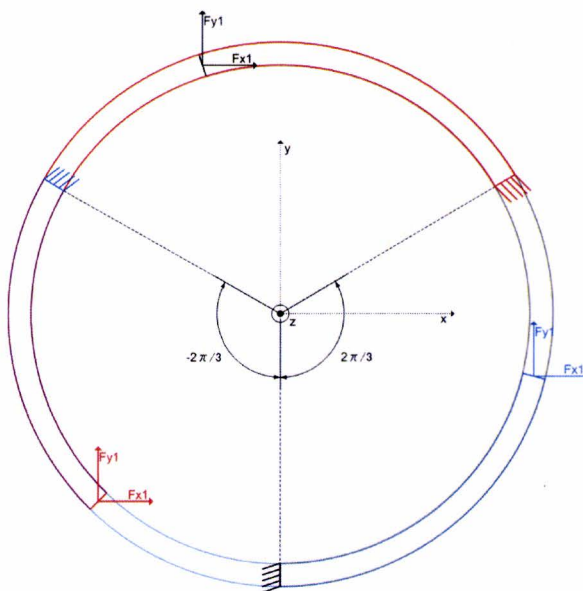
Figure 4.3: Rearrangement of the arms.

The method consists of finding the compliance matrix of infinitesimal elements along the length of one arm of the shock absorber. This method was performed earlier by X. Ding *et al.* [14]. Integration is then used for calculating the compliance of one arm. Using coordinate-frame transformation matrices, the compliance matrices for the other two arms can be calculated. The inverse of the compliance

matrix is a stiffness matrix and a summation of the three stiffness matrices produce the total stiffness matrix of the shock-absorber.

First, the compliance matrix of a straight beam of length l is given by the diagonal matrix:

$$C = \begin{bmatrix} \frac{l}{GJ} & 0 & 0 & 0 & 0 & 0 \\ 0 & \frac{l}{EI_z} & 0 & 0 & 0 & 0 \\ 0 & 0 & \frac{l}{EI_y} & 0 & 0 & 0 \\ 0 & 0 & 0 & \frac{l}{EA} & 0 & 0 \\ 0 & 0 & 0 & 0 & \frac{l^3}{12EI_z} & 0 \\ 0 & 0 & 0 & 0 & 0 & \frac{l^3}{12EI_y} \end{bmatrix} \tag{4.6}$$

Where E and G are respectively the Young's modulus and the shear modulus of the material, A the cross-sectional area of the beam and I and J the relevant second moment of inertia. Considering l infinitesimal, the matrix can be divided by l and replace by its limit when l tends to zero to find the compliance density matrix of the beam.

$$c_0 = \begin{bmatrix} \frac{1}{GJ} & 0 & 0 & 0 & 0 & 0 \\ 0 & \frac{1}{EI_z} & 0 & 0 & 0 & 0 \\ 0 & 0 & \frac{1}{EI_y} & 0 & 0 & 0 \\ 0 & 0 & 0 & \frac{1}{EA} & 0 & 0 \\ 0 & 0 & 0 & 0 & 0 & 0 \\ 0 & 0 & 0 & 0 & 0 & 0 \end{bmatrix} \tag{4.7}$$

The compliance matrix for this element is $C = c_0 \Delta \mu$.

Using this method, X. Ding *et al.* calculated the compliance matrix of a helical spring. The same approach is used to calculate the compliance matrix for one arm of the shock-absorber. However, instead of multiple rotation around the z-axis only half a round is used and a pitch of zero is used because the arm of the shock-absorber remains in the xy-plane. For a small element μ that describes the ellipse, the following geometrical relations holds:

$$\mu^2 = r^2 + \left(\frac{p}{2\pi}\right)^2 \tag{4.8}$$

Where r is the radius of the helix, that is the distance of the initial element from the origin. For convenience we pose $\gamma = \sqrt{r^2 + p^2/4\pi^2}$ and thus $d\mu = \gamma d\theta$.

We now consider the compliance matrix of the initial element. In general, the compliance matrix, or rather the compliance density, will be given by the coordinate transformation:

$$c = H^{-1} c_0 H^{-T} \tag{4.9}$$

To sum up compliance matrices, each compliance matrix has to be expressed in a common coordinate frame. The matrix H used above is a transformation matrix. Rather than finding H and inverting it, it is simpler to find H^{-1} directly. H^{-1} can be partitioned into a rotation and a transformation matrices:

$$H^{-1} = \begin{bmatrix} R & 0 \\ TR & R \end{bmatrix} \tag{4.10}$$

where the rotation matrix is about the y-axis:

$$R = \begin{bmatrix} \frac{-r}{\gamma} & 0 & \frac{-p}{2\pi\gamma} \\ 0 & 1 & 0 \\ \frac{p}{2\pi\gamma} & 0 & \frac{-r}{\gamma} \end{bmatrix} \tag{4.11}$$

where $p = 0$ and $\gamma = r$. The translation matrix is also along the y-axis:

$$T = \begin{bmatrix} 0 & 0 & r \\ 0 & 0 & 0 \\ -r & 0 & 0 \end{bmatrix} \tag{4.12}$$

Which lead to the following compliance density matrix calculated with formula 4.9:

$$c = \begin{bmatrix} \frac{1}{GJ} & 0 & 0 & 0 & 0 & \frac{-r}{GJ} \\ 0 & \frac{1}{EI_z} & 0 & 0 & 0 & 0 \\ 0 & 0 & \frac{1}{EI_y} & \frac{r}{EI_y} & 0 & 0 \\ 0 & 0 & \frac{r}{EI_y} & \frac{1}{EA} + \frac{r^2}{EI_y} & 0 & 0 \\ 0 & 0 & 0 & 0 & 0 & 0 \\ \frac{-r}{GJ} & 0 & 0 & 0 & 0 & \frac{r^2}{GJ} \end{bmatrix} \tag{4.13}$$

Subsequently this compliance density matrix has to be swept around the helix and integrated. The compliance matrix can then be found according to this formula:

$$C_1 = \int_0^{\frac{13\pi}{12}} H_1^{-1} c H_1^{-T} r d\theta \tag{4.14}$$

where $H_1^{-1}(\theta)$:

$$H_1^{-1}(\theta) = \begin{bmatrix} cos(\theta) & -sin(\theta) & 0 & 0 & 0 & 0 \\ sin(\theta) & cos(\theta) & 0 & 0 & 0 & 0 \\ 0 & 0 & 1 & 0 & 0 & 0 \\ 0 & 0 & 0 & cos(\theta) & -sin(\theta) & 0 \\ 0 & 0 & 0 & sin(\theta) & cos(\theta) & 0 \\ 0 & 0 & 0 & 0 & 0 & 1 \end{bmatrix} \tag{4.15}$$

The result of this calculation is straightforward but rather tedious and is given in appendix J. Inverting this matrix will lead to the stiffness matrix of one arm. The total stiffness of the three arms combined is simply given by calculating the compliance matrices C_2 and C_3 using formula 4.14 but with transformation matrices H_2 and H_3. Inverting the results gives K_2 and K_3. If we add the three stiffness matrices, the total stiffness matrix K is derived. This matrix is given in appendix J. Subsequently, a force of 0.167 Newton will lead to a displacement in lateral direction of 24 μm and in vertical direction of 31 μm.

4.2.2 Finite elements models

A simple model: The same structure as illustrated in figure 4.2(a) is modeled in ANSYS. In the center of the model the force is applied and at the ends of the arms a fixed displacement of zero is applied. The top view of this model is shown in figure 4.4(a) and the 3D view in figure 4.4(b).
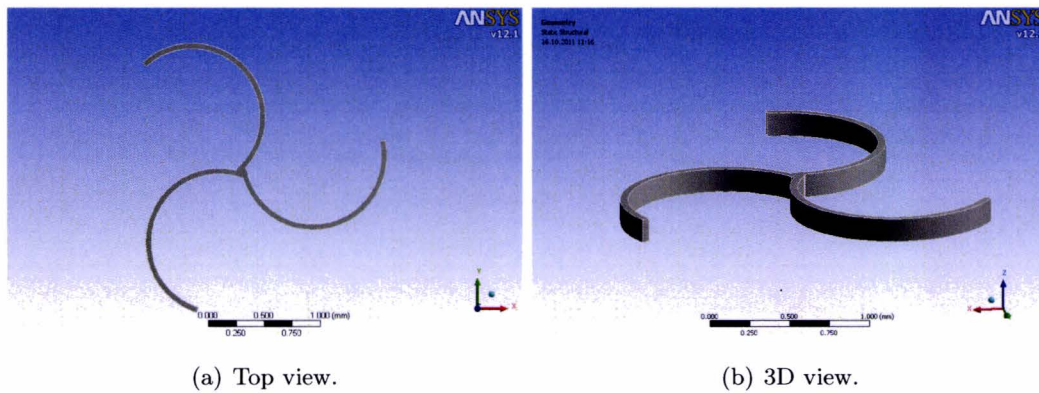
(a) Top view. (b) 3D view.

Figure 4.4: Simplified shock-absorber modeled in ANSYS.

The same force is used as before in order to compare this model with the measurements. The displacement in lateral direction is $16\,\mu$m and in vertical direction the displacement is $23\,\mu$m.

A more complex model: This model only consists of the three arms of the shock-absorber. The inner and outer ring are not generated but these parts are significantly stiffer than the arms so these could be kept out of the simulation. This simulation is used to vary the dimensions of the arms (radius, height and width) and to find optimal dimensions for the final shock-absorber. This model is shown in figure 4.5.

(a) Top view. (b) 3D view.
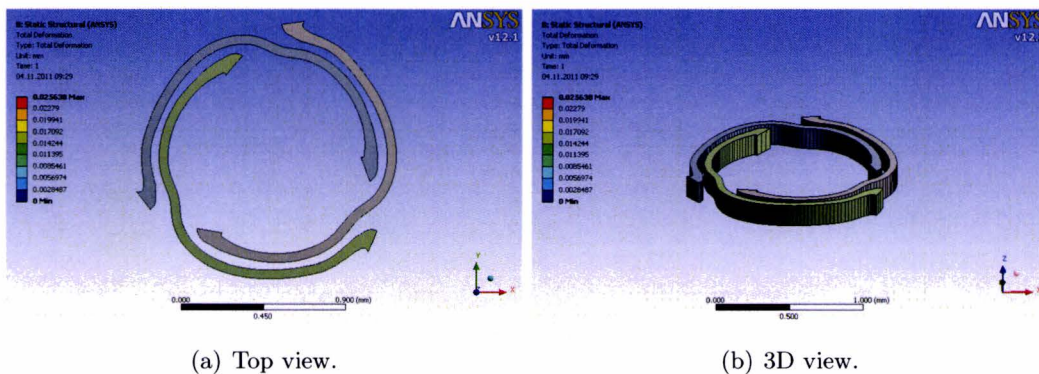
Figure 4.5: Complex shock-absorber.

When applying the force of 0.167 Newton the displacement in lateral direction is $0.23\,\mu$m and in vertical direction this is $39\,\mu$m.

4.3 Comparison and Optimization

After simulations, error factors in x, y and z are derived for all the models. A schematic overview of the models and the measurement including displacements and error factors are shown in appendix K. The error factor of the analytical model using compliances and stiffness matrices is the best approximation followed by the more complex ANSYS model. The latter one is used to run multiply simulations. The goal is to find a new prototype shock-absorber made out of one material with the same mechanical specifications as the Ni-prototype shock-absorber. The configurations will be derived for crystalline ruby and fused silica. The material parameters of these materials as well as the material parameters of Nickel are listed in table 4.1.

Material	Young's Modulus(E)[GPA]	Poisson ratio(ν)[-]	Shear Modulus(G)[GPA]
Nickel	207	0.31	79
Crystalline Ruby	320	0.34	119
Fused Silica	78	0.17	33

Table 4.1: Material Properties.

Requirements: The new prototype shock-absorber has to meet several requirements and it is limited in dimensions. The radius of the arms should be dimensioned between 500 and 700 μm. The width should be between 30 and 60 μm while the minimum height is 150 μm and the maximum height is 250 μm. With these dimensions, the new prototype shock-absorber needs to produce the displacement of 26 μm in lateral direction when applying a force of 0.167 Newton. Along the perpendicular direction, the displacement should be 36 μm. Furthermore, the gap between two arms has to be at least 25 μm when fully deformed. In addition, the maximum displacement in lateral and vertical direction due to the weight of the balance wheel, may not exceed 1/3 of the thickness of the balance wheel. The used balance wheel is 440 μm so the maximal displacement in all directions can reach a maximum of 150 μm. The weight of the balance wheel is around 100 mg.

The simulations results for crystalline ruby and fused silica are given in appendix L. When a small window of ± 1 μm variation for both directions is used, two configurations turned out suitable for ruby. These two configurations are given in table 4.2.

Dimensions[μm]			Displ.[μm]		Stress[GPA]		Gap[μm]	Defr. due to BW[μm]	
Radius	Width	Height	XY-dir.	Z-dir.	XY-dir.	Z-dir.		Lateral	Vertical
600	40	150	25.0	35.0	637	727	35	0.063	0.21
650	40	170	26.3	36.5	558	741	45	0.066	0.22

Table 4.2: Crystalline Ruby shock-absorber configurations.

The same is done for the shock-absorber performed in fused silica. The results are given in appendix L as well. The design space is a little bit larger to find suitable configurations. The tolerances considered are ± 3 μm. Two configurations turned out suitable and are given in table 4.3.

Dimensions[μm]			Displ.[μm]		Stress[GPA]		Gap[μm]	Defr. due to BW[μm]	
Radius	Width	Height	XY-dir.	Z-dir.	XY-dir.	Z-dir.		Lateral	Vertical
600	50	250	28.6	33.3	274	310	28	0.072	0.20
650	60	230	29.0	33.1	253	312	25	0.074	0.20

Table 4.3: Fused Silica shock-absorber configurations.

For these four configurations, some additional simulations are performed. The width and height are varied with 10% of its length. This is interesting because manufacturing such small model brings relatively large tolerances. These results are also given in appendix L. With all these simulations, the most suitable dimensions can be chosen for ruby and for fused silica. These configurations are colored gray in table 4.2 and 4.3.

4.4   Final design

The initial goal was the fabricate the shock absorber in ruby. Due to the late and disappointing etching results of ruby, the new shock-absorber will be made out of fused silica (from now called fs-prototype). Figure 4.6 shows the fs-prototype realized in fused silica. In this drawing a taped hole is present in the center of the design. The axis of the balance wheel will go into that hole.
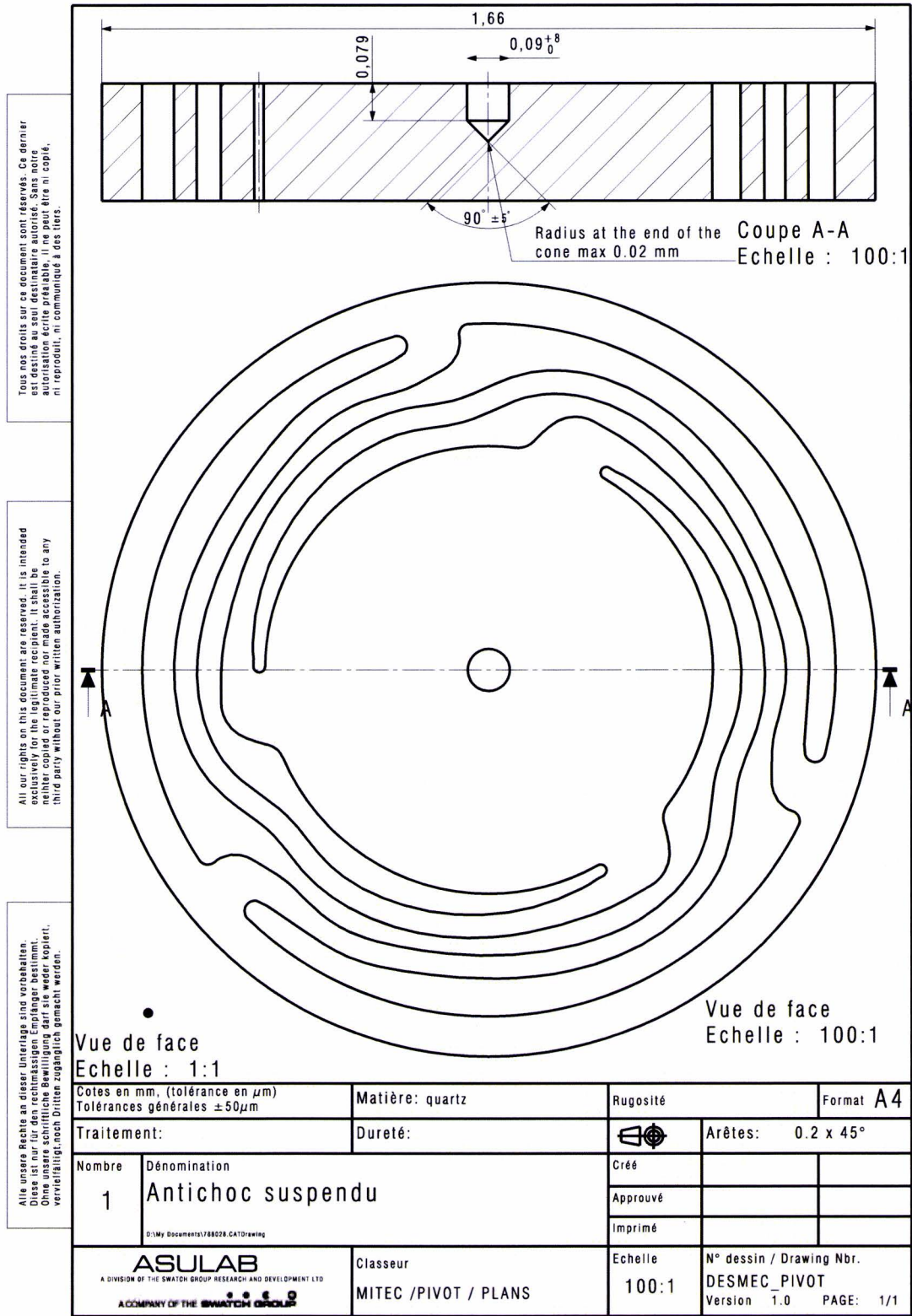
Figure 4.6: Fs-prototype realized in fused silica.

Chapter 5

Fabrication

This chapter describes the machining strategy, expectations and the achieved results. The fs-prototype has to be made out of a $250\,\mu$m thick fused silica substrate. The fs-prototype sketch is shown in figure 5.1. The taped hole in the center (not shown in figure 5.1) has to be machined using the same process.
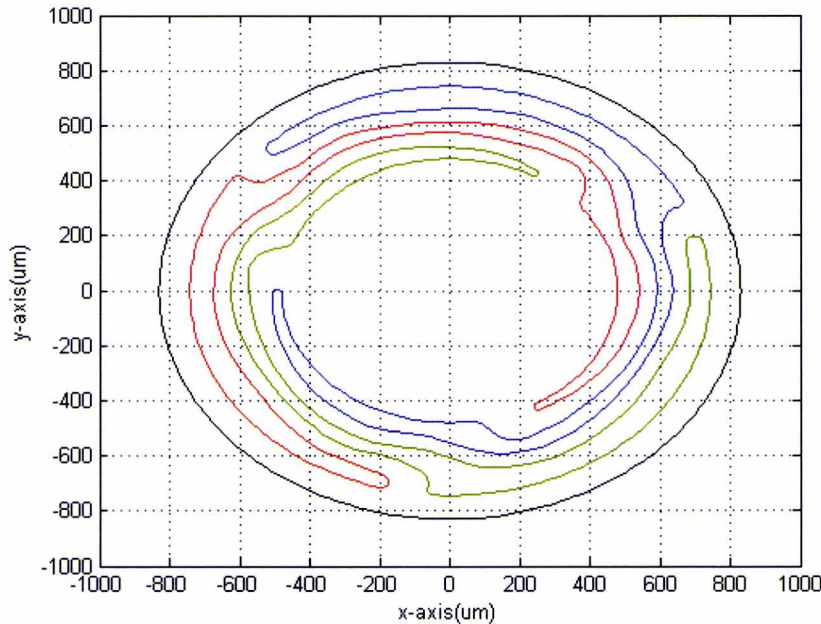
Figure 5.1: The curvatures of the fs-prototype. It consists of four curves. The taped hole in the middle is not illustrated here.

5.1 Machining strategy

The focus of the machining strategy is on the moving part of the setup i.e. the PI-stages and the flexure. This moving part in shown in figure 5.2. The moving part of the setup consists of two large PI-stages which enable to move the substrate in x and y direction over a large domain. However, the accuracy of these stages is in microns. On top of these stages, high-accuracy piezo-driven flexure stages are mounted. These stages are much more accurate (nano-scale) but have a much shorter range motion ($100 \times 100\,\mu$m). The third moving part is the z-stage. This stage has similar specifications as the PI-stages used for the x and y directions. Ideally, the whole fs-prototype should be made with

Figure 5.2: PI-stages and flexure stages

the flexure stages in order to obtain a high accuracy. However, the dimensions of the fs-prototype are too large to be made using only the high-accuracy stages. The CNC commanding the PI-stages is not sufficiently accurate to synchronize the stages so that complex curves can be made. Here, we explore an approach where we combined both stages: the PI-stages for the coarse motion a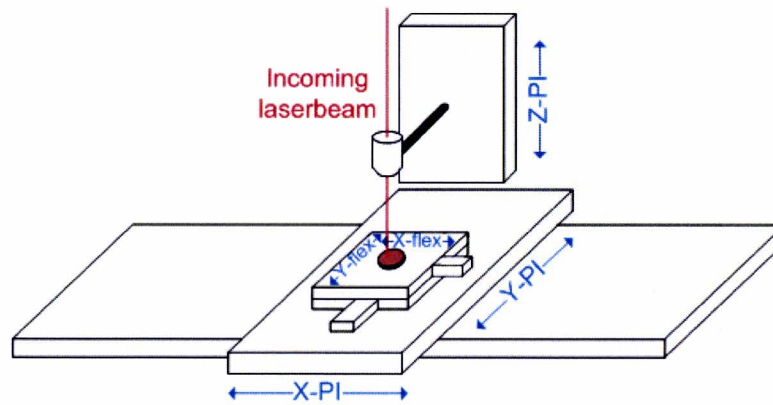nd the flexures for the fine motion. The flexure stages will move during machining and the PI-stages will move between machining. With this machining strategy a large domain can be reached with a high accuracy. This strategy leads to the following curve trajectory depicted in figure 5.3. In this figure only one loop is
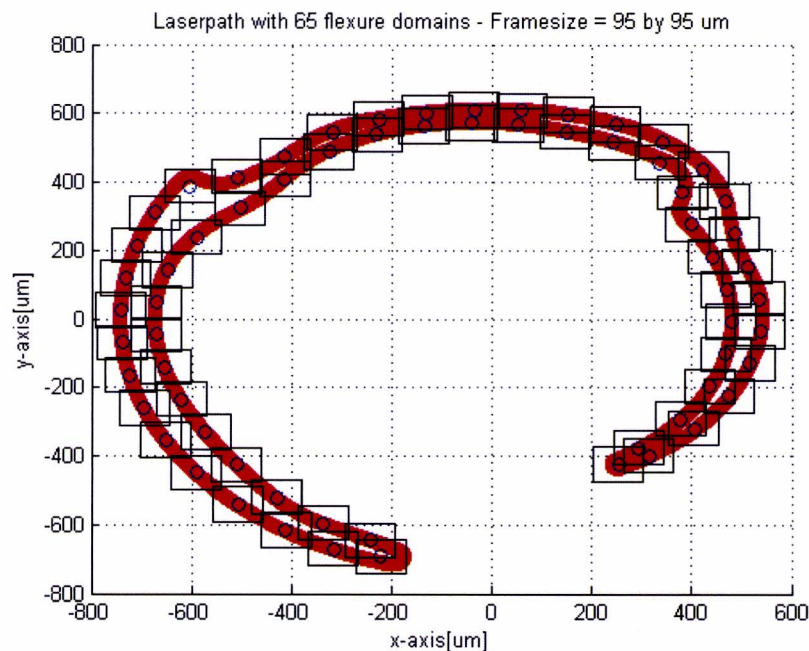
Figure 5.3: Curvature of one of the arms with flexure stages domain.

shown but the rest of the design will be executed in the exact same way. The PI-stages move from blue dot to blue dot: point-to-point motion. When a blue dot is reached, the middle of the flexure stages is positioned at the coordinates of the blue dots. The PI-stage will pause and the flexure stages will start moving so that the laser spot will follow the curvature within the corresponding black square around that blue dot. The black square represent the $100 \times 100\,\mu$m working domain of the flexure stages. This strategy will ensure that the curvatures of the component will be followed with high accuracy. The M-file of this algorithm is shown in appendix M. Executing this process with all the curves leads to a

complete trajectory of the design. This machining strategy have to be executed from the bottom to the top surface of the substrate. A fixed z-step is used to ensure a homogeneous irradiation of the curves from bottom surface up to the top surface. The last part of machining is the taped hole in the center of the design which is shown in figure 5.4(a). The machining strategy shown in figure 5.4(b). As one

(a) Draft of the taped hole

(b) Machining strategy: the ellipses represent the cross-section of the laser tracks at one side, the symmetric axis is at $x = 0$

Figure 5.4: Taped hole.

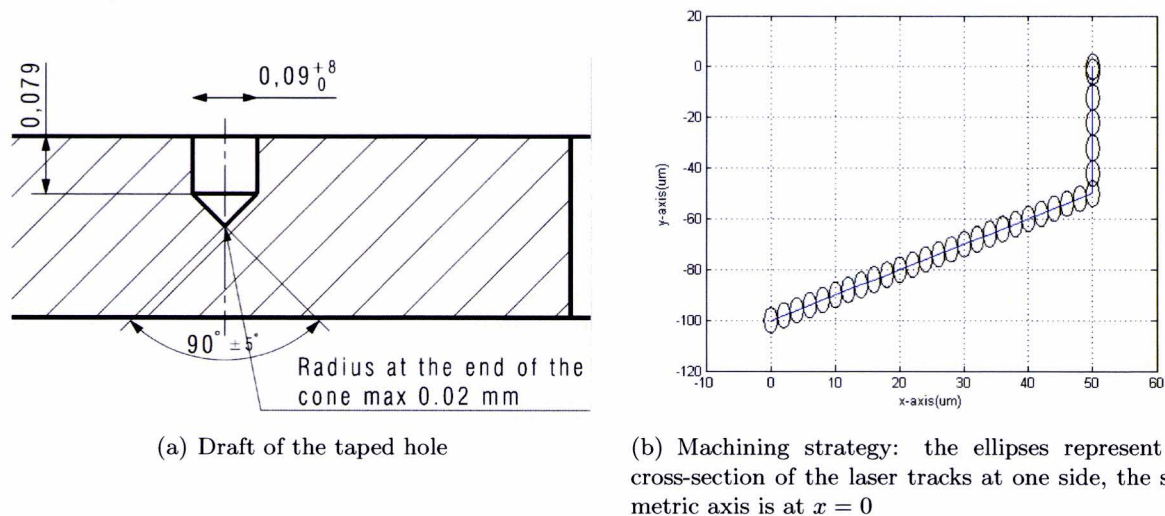can see, instead of irradiating the whole volume inside the taped hole, only the sides are irradiated. The volume inside the taped hole will be cut out during the etching process. The same strategy is applied in section 2.3.2. After laser irradiation of the fs-prototype it is immersed in a 2.5% HF wet chemical etching bath.

5.2 Machining input

From the design of the fs-prototype until the machining strategy, some steps have to be taken in between. First the design is converted to a .svg document file which stand for Scalable Vector Graphics. Such a file consists different codes for predefined shape elements e.g. rectangles, circle and ellipses. Simple or compound shape outlines can be drawn with curved or straight lines that can be filled in, outlined or used as a clipping path. Paths have a compact coding. An example is shown in figure 5.5. These codes have to be converted to x-y coordinates which represent the points of the curved shape of

```
<path style="stroke-width:0.0283;stroke-linecap:butt;stroke-linejoin:miter;" d="M46.616,2.365c0-
1.299-1.053-2.353-2.353-2.353s-2.353,1.054-2.353,2.353c0,1.3,1.054,2.354,2.353,2.354s2.353-
1.054,2.353-2.354z"/>
<path style="stroke-width:0.0283;stroke-linecap:butt;stroke-linejoin:miter;" d="M46.066,3.2051-0.045-
0.0421-0.03-0.0551-0.009-0.0411-0.002-0.02810-0.05710.003-0.12510.007-0.0710.015-0.06810.02-
0.06710.031-0.13910.009-0.06910.003-0.0711-0.003-0.07L46.051,2.21-0.016-0.0661-0.04-0.1311-0.053-
0.1441-0.06-0.14 1-0.089-0.1781-0.103-0.171-0.117-0.1611-0.133-0.148L45.364,0.991-0.08-0.0671-0.079-
0.0591-0.083-0.051L45,0.7551-0.13-0.0411-0.072-0.016L44.724,0.691-0.066-0.0031-
0.065,0.004L44.492,0.71L44.427,0.731-0.126,0.0551-0.125,0.0531-0.066,0.021L44.01,0.882 1-0.1,0.0141-
0.1,0.0171-0.098,0.0241-0.094,0.0361-0.12,0.0631-0.111,0.0781-0.103,0.0881-0.109,0.1171-0.097,0.1271-
0.082,0.1371-0.067,0.1451-0.05,0.1511-0.033,0.1561-0.016,0.159v0.05110.004,0.0511-
0.001,0.055c0.003,0.019,0.019,0.031,0.038,0.03 c0.019-0.002,0.033-0.017,0.034-0.035c0.005-
0.387,0.175-0.752,0.466-1.006s0.676-0.372,1.06-0.325c0.042,0.006,0.085-0.01,0.114-0.041c0.031-
0.032,0.064-0.063,0.1-0.09110.044-0.0310.051-0.01910.053-
```

Figure 5.5: Example of a .svg code.

the fs-prototype. These coordinates are shown in figure 5.6. The four loops of the fs-prototype consists

1104 coordinates. These coordinates cannot be implemented into the machining strategy program
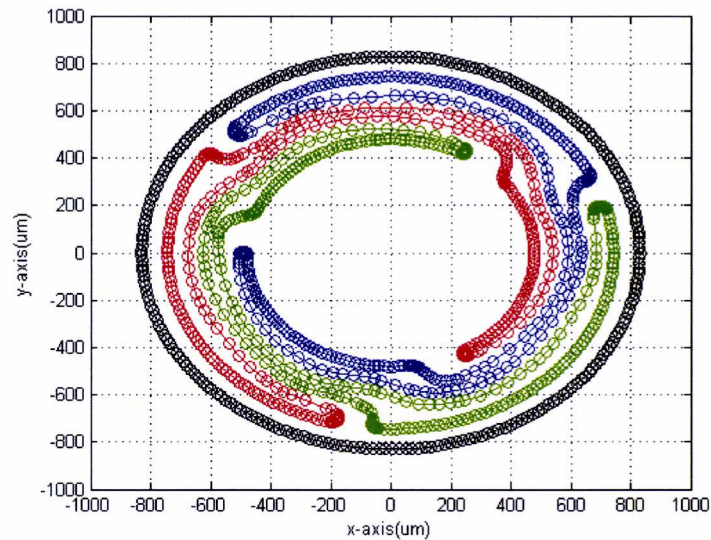
Figure 5.6: x-y coordinates of the fs-prototype.

directly. First new x-y coordinates between the original points have to be generated. This is necessary because of the configuration of the flexure stages that is used to move the substrate. The configuration of the flexure stages needs to have, in order to move at a constant speed, an equal distance between every mutual points on the curvature. This step changes figure 5.6, consisting 1104 coordinates into figure 5.7, consisting 23250 coordinates. The output of previous calculations can be written in text
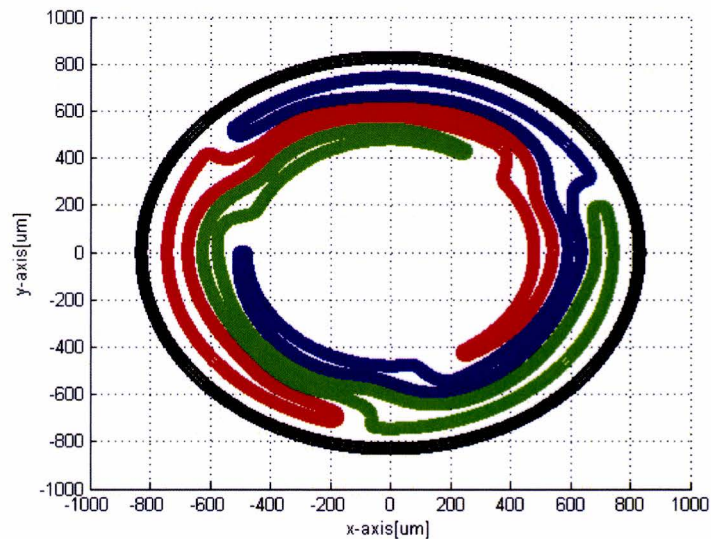
Figure 5.7: x-y coordinates after inserting intermediate points of the fs-prototype.

files. Two arrays of x-y coordinates are sufficient to be readable by the machining strategy program. Since, the input file is generated and the strategy is known, the fs-prototype can be fabricated.

5.3 Improvements

After testing the whole machining strategy, some errors in the results occur. The main errors are summarized below and a solution for these errors is given.

- No continuous line: Due to bad system control and a low accuracy of the PI-stages, sometimes the written track are not continuous (but they are still in line with each other). After implementing an overlap factor in the algorithm of the machining strategy this error was solved. The difference is shown in figure 5.8.

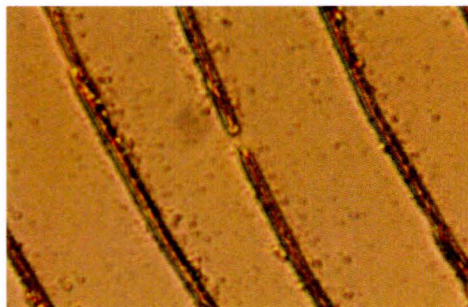(a) No continuous laser track   (b) After implementing an overlap factor, the line is continuous.
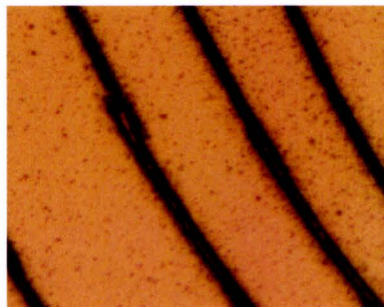
Figure 5.8: Pictures taken with an optical microscope. The difference between before and after implementing an overlap factor.

- Mismatching lines: Again, due to the same causes, another problem occurred. Adjacent lines are not connected to one another (and are not written in line with each other) because the PI-stages are not accurate enough to position the substrate. This can be seen clearly in figure 5.9. The solution to this problem is to write three lines next to each other with a mutual distance of $1\,\mu$m.
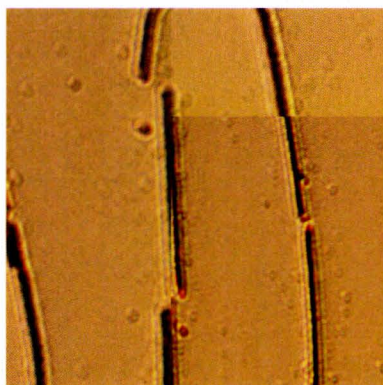
(a) One single line is written. The middle line is not in line with the adjacent lines.   (b) Three lines are written next to one another to ensure that adjacent lines are connected.
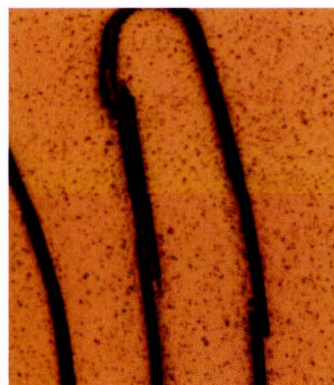
Figure 5.9: Pictures taken with an optical microscope.

- Difference in etching depth: After the first etching tests, difference in etching speed on the same sample occurred. Because these parts were written with a polarization in one direction, the angle

between the writing direction and the polarization was changing constantly. In figure 5.10, the red line represents the polarization direction. When the writing direction is perpendicular to the polarization, the etching speed is higher (more etched). The curves which are written parallel with respect to the polarization are etched less. The solution is to use a circular polarization. The etching speed is then decreased (with respect to the etching speed when the writing direction is perpendicular w.r.t. the polarization) but it will be homogeneous over the irradiated areas.
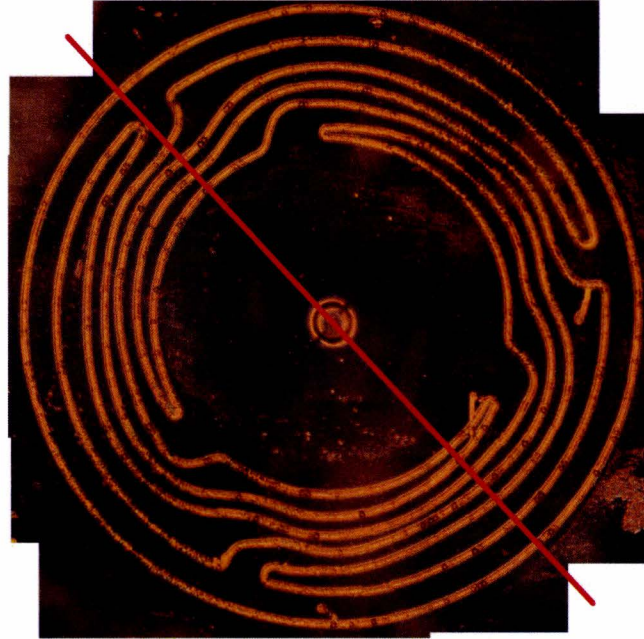
Figure 5.10: The curves are not etched homogeneous, the red line indicates the polarization direction. When the curves are written parallel to this red line, the etching speed is low.

5.4 Expectations

With this machining strategy including the applied improvements the curvatures should be irradiated completely (from bottom surface up to the top surface) and the taped hole should be irradiated, starting at the bottom and moving up to the top surface. The laser parameters and etching conditions are described in section 2.4 for fused silica. Unfortunately, during experiments we discovered that a maximum writing speed of $300\,\mu$m/s can be used for the taped hole and a maximum speed of $500\,\mu$m/s for the curvatures. According to figure 2.3, the repetition rate has to be around $100\,$kHz (with these writing speeds) to achieve an energy deposition between 10 and 20 J/mm^2. With these laser parameters and a circular polarization, the expected etching speed of the irradiated area will be between 0.5 and $1\,\mu$m/min with using 2.5% HF which is slower than the values described in literature. The etching speed of the non-irradiated area will be the same as the literature values, which are around $1\,\mu$m/hour with 2.5% HF. If, with these etching speeds, the substrate with the irradiated areas is immersed for five hours, it will be sufficient to get released from the substrate. The irradiated areas will gain between 300 and $600\,\mu$m in depth. The thickness of the substrate will be reduced with about $10\,\mu$m. Therefore, the component should be released from the substrate without losing much height.

5.5 Results

This section describes the achieved results of machining strategy and the femtosecond laser technique followed by etching. A difference is made in this section between machining the curvatures and ma-

chining the taped hole.

In total the fs-prototype is written seven times on different substrates but finally none of these fs-prototype did go out of the substrate after etching (even after etching for 24 hours). Table 5.1 indicates if a picture is taken with the optical microscope after irradiation or etching. These pictures are shown in appendix N.

Fs-protype	Irradiation	2 hours	6 hours	20 hours	24 hours
1	X				X
2	X				
3	X	X	X		
4	X		X	X	
5	X		X	X	
6	X(back & front)				
7					X

Table 5.1: Behind the number of the prototype, the cross indicates if a picture is taken of the component after irradiation and/or after etching for 2, 6, 20 and/or 24 hours, respectively.

5.5.1   Curvatures

Looking at the pictures, differences between the various fs-prototypes are visible. The first two fs-prototype are written before the improvements were applied on the machining strategy and for this reason interruptions occur during machining. By slowing down the speed of the PI-stages (they move between machining), the errors which are visible on the first three components are solved on the next fs-prototype. The drawback of slowing down the speed of these stages is that the production time of one fs-prototype became 20 hours.

Fs-prototype 6 and 7 are written with a different laser. The energy deposition during these processes was too high (minimum frequency of the laser is 400 kHz) and as a results etching speeds are slower.

Etching for 6 hours produced a smooth line of the separate adjacent laser tracks. Because the components did not fall out of the substrate, etching is proceeded in some cases for 24 hours. Since wet etching is an isotropic process, the laser tracks are getting wider as well until they merge.

While trying to get fs-prototype 4 out of the substrate it broke. This gave the opportunity to look at the surface and edge of an etched curve with the SEM. Figure 5.11(a) illustrates this substrate with the fs-prototype in the center. The dashed gray line indicates the entire substrate before it broke and the dashed black line indicates where it broke. The crack propagated from the edges toward the outer curve of the fs-prototype and continued along this curve. Figure 5.11(b) shows the SEM image. The red arrows of both figures correspond to one another. What can be seen is that it was almost etched through the substrate. Around $8\,\mu$m thick material is present at the bottom of the substrate (which mean that the bottom of this fs-prototype was never irradiated by the laser beam). Although, etching was not successful, we can conclude that the edge of the curve is sharp and the etched surface is smooth as well.

5.5.2   Taped hole

The figures in appendix N show that the results for the taped hole varies as well. With fs-prototype 3, 6 and 7 the volume inside the whole was etched out of the substrate completely. With the optical microscope, pictures are made of the taped hole in different depths of fs-prototype 3. Figure 5.12 shows these pictures and indicates at what approximated depth they were made. We can concludes that the edge is sharp and that the walls are smooth. In addition, the taped hole has its desired shape.
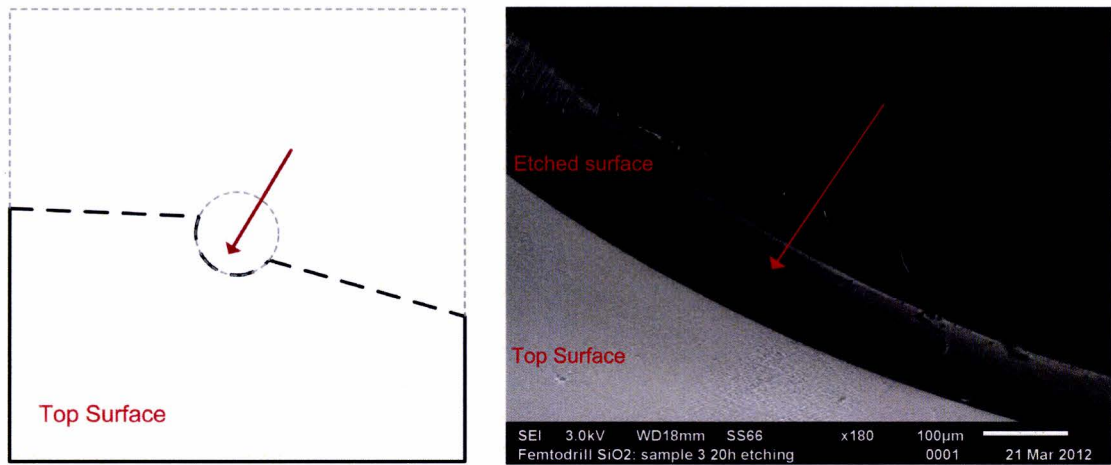
(a) Substrate with the fs-prototype curvature in the middle. The black dashed line indicates where it broke.

(b) SEM image: the surface and edge of the etched curve. Around $8\,\mu$m thick material is present at the bottom of the substrate.

Figure 5.11: Fs-prototype 4 broke on along the outer curve which gave the opportunity to study the etched surface: the red arrows correspond to one another.

Due to the fact that non of the irradiated and etched fs-prototypes is fallen out of the substrate, mechanical testing is not possible. Consequently, the comparison with the analytical and simulation model can not be made.
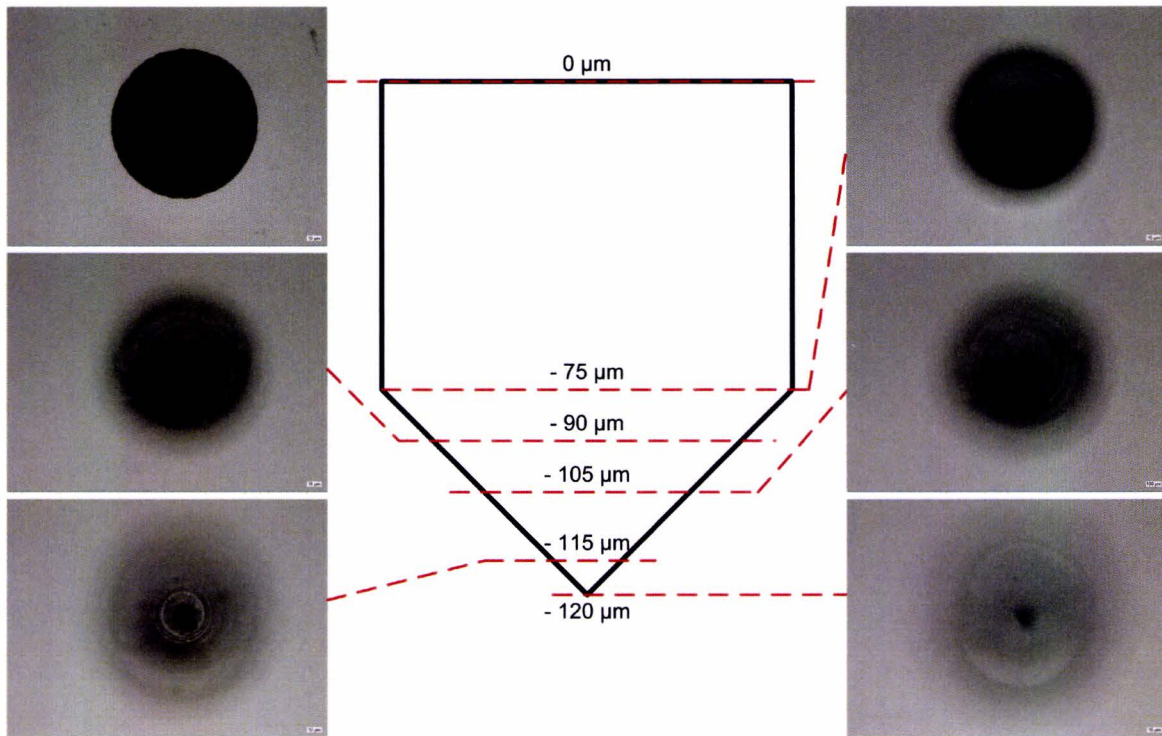
Figure 5.12: Pictures are taken with an optical microscope. The picture are made of the taped hole in different depths. The depths are approximated with the microscope.

5.6 Recommendations

Although, mechanical testing can not be performed, there is still hope for fabricating a fs-prototype shock-absorber. Some recommendations are given below:

- Perform the same experiment but with improved stages or new stages. The stages that are used right now are a limited factor. Because of these stages, the used machining strategy had to be implemented and this strategy combined with the stages limits the writing speed at $500\,\mu m/s$. These stages also bring errors which are described in section 5.3. When new stages are used, this strategy is not necessary anymore and the speed can be increased. The new stages need to have a writing domain of 10x10 cm and have to be very accurate (nanoscale).

- Etching can be performed in KOH. Recently, it was shown by Kiyama *et al.* [15] that heated-KOH might offer significantly better aspect ratio than HF.

- In literature, etching with HF is also performed with higher temperatures under pressure. This might be an option to see if better results can be achieved.

With these recommendations taken into account, the fs-prototype shock-absorber can be fabricated with femtosecond laser irradiation followed by wet chemical etching in such way that the component can be etched out of the substrate.

Chapter 6

Conclusion

The goals of this project is to redesign and manufacture the existing Ni-prototype shock-absorber for different materials while keeping similar mechanical specifications. The techniques femtosecond laser irradiation was used to structure quartz and ruby. For both materials suitable laser parameters are found. The difference in laser parameters between the two materials is the pulse energy used. For quartz a pulse energy of 184 nJ turned out suitable while for ruby a lower energy pulse (173 nJ) is needed to avoid crack occurrence. For both materials a repetition rate of 870 kHz with a writing speed of 5000 μm will lead to successful structures if the mutual distance in x and z direction between the laser tracks is around 1.5 and 7 μm, respectively. After irradiation the substrate are immersed in 2.5% HF. Quartz and especially ruby turned out difficult to etch with the available etching setup. During the experiments with quartz some structures reached a sufficient depth, although it took more time that it should have according to literature. Etching ruby was very difficult. Practically no structures reached the desired depth, especially when a structure was machined without cracks.

Because structuring quartz and ruby was not successful, we decided to manufacture the shock-absorber out of fused silica. For this material the shock-absorber was redesigned in order to meet the mechanical specifications, the requirements and pass the qualifying shock tests. This component is structured several times on a 250 μm thick fused silica substrate and is immersed in 2.5% HF. Unfortunately, the shock-absorber did not come out of the substrate. Mechanical testing was therefore not possible during the time of this diploma project but the substrate showed that the edges of the etched curves were sharp and the etched surface was smooth. The taped hole in the center of the substrate was successfully irradiated and etched out. These results are hopeful for further investigation. Replacing the current manufacturing setup will improve the results. New stages should replace the current two stages. These new stages need to have a writing domain of 10x10 cm and have to be very accurate (nanoscale). Irradiation will be more homogeneous over the curvatures of the shock-absorber and this improves a constant etching speed which may finally lead to a successful manufacturing approach and a working shock-absorber.

Bibliography

[1] http://en.wikipedia.org/wiki/Watch

[2] Sheeba Rajesh, Yves Bellouard, "Towards fast femtosecond laser micromachining of fused silica: The effect of deposited energy", Optics Express 21490, Vol. 18, No. 20, 2010

[3] Chiwon Moon, Shingo Kanehira, Masayuki Nishi, Kiyotaka Miura, Takayuki Nakaya, Eita Tochigi, Noaya Shibata, Yuichi Ikuhara, Kazuyuki Hirao, "Crack Propagation in a Ruby Single Crystal by Femtosecond Laser Irradiation", J. Am. Ceram. Soc 92 [12] 3118-3121 (2009)

[4] Litao Qi, Kazuhiro Nishii, Motohiro Yasui, Hikoharu Aoki, Yoshiharu Namba, "Femtosecond laser ablation of sapphire on different crystallographic facet planes by single and multi laser pulses irradiation", Optics and Lasers in Engineering 48(2010) 1000-1007

[5] Y. Kondo, J. Qiu, T. Mitsuyu, K. Hirao, T. Yoko, "Three-dimensional microdrilling of glass by multiphoton process and chemical etching", Japanese Journal of Applied Physics, vol. 38, no 10A, (1999)

[6] Dirk Wortmann, Jens Gottmann, Nelli Brandt, Herbert Horn-Solle, "Micro- and nanostructures inside sapphire by fs-laser irradiation and selective etching", Optics Express 1517 Vol. 16, No 3, (2008)

[7] Y. Bellouard, A. Said, M. Dugan, P. Bado, "Fabrication of high-aspect ratio, micro-fluidic channels and tunnels using femtosecond laser pulses and chemical etching", Optics Express Vol. 12, No. 12, 2004

[8] Maren Hörstmann-Jungemann, Jens Gottmann, Martin Keggenhoff, "3D-Microstructuring of sapphire using fs-laser irradiation and selective etching", JLMN-Journal of Laser Micro/Nanoengineering Vol 5. No.2 (2010)

[9] Shigeki Matsuo, Kensuke Tokumi, Takuro Tomita, Shuichi Hashimoto, "Three-Dimensional Residue-Free Removal inside sapphire by high-temperature etching after irradiation of femtosecond laser pulses", Hindawi Publishing Corporation, (2008)

[10] Shigeki Matsuo, Yoshinori Shichijo, Takuro Tomita and Shuichi Hashimoto, "Laser fabrication of ship-in-a-bottle microstructures in sapphire", JLMN-Journal of Laser Micro/Nanoengineering Vol. 2, No. 2, 2007

[11] Saulius Juodkazis, Yasufumi Nishi and Hiroaki Misawa, "Femtosecond laser-assisted formation of channels using KOH solution", Phys. stat. sol. (RRL) 2, No. 6, 275-277 (2008)

[12] Warren C. Young, Richard G. Budynas, "Roark's Formulas for Stress and Strain", McGraw-Hill, ISBN 0-07-072542-X, 2002

[13] Michel del Pedro, Thomas Gmür, John Botsis, "Introduction à la mécanique des solides et des structures", Presses polytechniques et universitaires romandes, 2001

[14] X. Ding, J.M. Selig, "On the compliance of coiled springs", International Journal of Mechanical Sciences 46 (2004) 703-727

[15] S. Kiyama, S. Matsuo, S. Hashimoto and Y. Morihira, "Examination of Etching Agent and Etching Mechanism on Femotosecond Laser Microfabrication of Channels Inside Vitreous Silica Substrates", J. Phys. Chem. C 113(27), 11560-11566(2009)

Appendix A

Laser parameters

Material	Laser number	Etchant	Time [hour]	Depth [μm]	Etching Speed	Tempe-rature	Micro-structure	Ratio	Remarks
Fused Silica	A	5% HF	3	1200	$6.6\,\mu m/min$	-	Channel	130	-
Fused Silica	B	2.5% HF	4	275	$1.15\,\mu m/min$	20	Channel	-	-
Fused Silica	C	2.5% HF	2	675	$1.2\,\mu m/min$	-	Channel	-	-
Sapphire	D	40% HF	24	680	$28\,\mu m/u$	-	Channel	-	-
Sapphire	E	40% HF	24	920	$38\,\mu m/u$	-	Channel	-	-
Sapphire	F	48% HF	49	560	$10\,\mu m/u$	-	Cutting	-	-
Sapphire	G	48% HF	49	1732	$35\,\mu m/u$	-	Channels	-	-
Sapphire	H	-	-	-	-	-	Hollow vol.	-	-
Sapphire	I	10% HF	24	-	-	120	Hollow vol.	-	Pits appear
Sapphire	J	10% HF	20	-	-	100	Hollow vol.	-	Cracks appear
Sapphire	K	10% HF	Sev. days	-	-	-	Hollow vol.	-	-
Sapphire	L	1 M KOH	1	-	-	-	Void struct.	-	-
Sapphire	M	1 M KOH	12	65	$5.4\,\mu m/u$	-	Channels	-	-
Sapphire	N	2 M KOH + 0.1 M HF	-	-	Around $20\,\mu m/u$	-	Channels	-	Tapering occurred

Table A.1: Parameters used with femtosecond laser irradiation technique including results.

Letter	Laser type	Wave-length [nm]	Pulse duration [fs]	Repetition rate [kHz]	Pulse energy [nJ]	Numerical aperture	Polari-zation	Mutual Distance[μm] XY	Z	Writing Speed [$\mu m/s$]
A	Ti:sapphire	800	100	250	135	0.6	-	4	-	100
B	Ytterbium-KGW	1024	500	100-860	215	0.45	Perp.	-	-	10 - 35000
C	Ti:sapphire	800	100	250	135-270	0.6	-	2	-	100
D	Fiber chirped amplifier	1045	400	500	300-1000	0.55 / 0.7	Perp.	4	-	100-1000
E	Fiber chirped amplifier	1045	400	1000	300-1000	0.55 / 0.7	Perp.	4	-	100-1000
F	Yb-glass fiber chirped pulse amplifier	1045	450	500	232	0.6	-	-	-	1000
G	Yb-glass fiber chirped pulse amplifier	1045	450	500	185	0.6	-	0.55	-	
H	Yb-glass fiber chirped pulse amplifier	1045	450	500	240	0.6	-	0.55	3.5	100
I	Unknown	800	130		40		-	0.2	1	
J	Unknown	800	130		40		-	0.2	2	
K	Unknown	-	-	-	-		-	0.25	1	-
L	Unknown	800	150	0.02	90 to 150		-	0.7	-	
M	Unknown	800	150	0.02	140		-	0.7	-	
N	Unknown	800	150	0.02	100 to 200		-	0.05-1.9	-	

Table A.2: Femtosecond laser parameters from table A.1.

Appendix B

Material properties

	Quartz	Fused Silica	Sapphire	Ruby
Chemical formula	SiO_2	SiO_2	Al_2O_3	$Al_2O_3+Cr_2O_3$
Crystal System	Trigonal	Amorphous	Hexagonal	Hexagonal
Density[kg/m^3]	2650	2203	3980	3990
Youngs Modulus[GPa]	perp. 76.5 / par 97.2	78	350	320
Poission ratio	0.17	0.17	0.31	0.34
Shear modulus[GPA]	31.14	33	150	119
Ultimate Yield strength[MPa]	150	50	400	300
Hardness[Mohs scale]	7	5.3-6.5	9	9
Melting point[°C]	1670	1723	2040	2044
Coef. of thermal expansion K^{-1}	perp 7.14e4 / par 1.30e5	1.8e6	6e6	5.8e6
Thermal conductivity[W/mK]	perp 6.2 / par 10.7	1.3	40	46.02
Refractive index	1.53	1.45	1.74	1.76

Table B.1: Material properties(values vary due to different varieties, impurities et cetera).

Appendix C

Quartz: results follow-up experiments 1

The results of this experiment were not similar to the results of the research performed earlier. Where in earlier research depths of 15 to 20 μm were reached within 4 minutes, the etching depths of these experiments were extremely low. Only one structures reached a depth of 12 μm within 4 minutes. Depths of 45 to 60 μm are reached after 20 minutes of etching, the results were disappointing. The used laser parameters, machined structures, experimental etching depths, alpha-steps scans and pictures taken with a optic microscope are shown in the rest of this appendix.

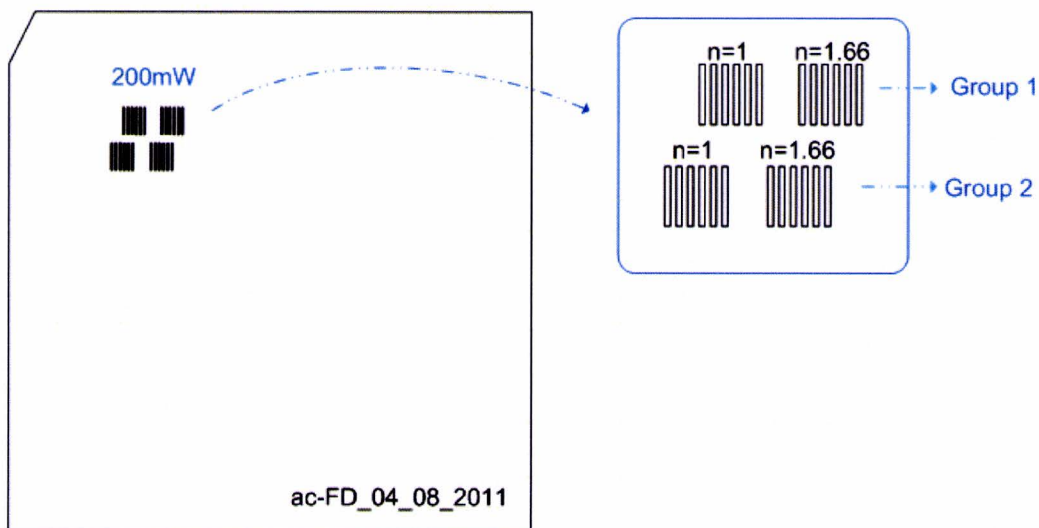| n=1.0(z=10)				n=1.66(z=6)			
a	n	f(KHz)	v(mm/s)	a	n	f(KHz)	v(mm/s)
10	1	300	30	10	1.66	100	16.6
20	1	600	30	20	1.66	200	16.6
30	1	800	26.7	30	1.66	400	22.1
40	1	800	20	40	1.66	400	16.6
50	1	800	16	50	1.66	800	16.6

Table C.1: Used laser parameters.

Figure C.1: Structures machined on Quartz substrate.

| After irradiation | After 2 min etching | After 4 min etching | After 20 min etching |

Group 1(n=1)

a	Depth(µm)
10	1.3
20	1.8
30	1.5
40	-
50	-

Group 1(n=1)

a	Depth(µm)
10	1.4
20	1.8
30	1.5
40	-
50	-

Group 1(n=1)

a	Depth(µm)
10	-
20	-
30	3.5
40	-
50	-

Group 1(n=1)

a	Depth(µm)
10	10.0
20	30.0
30	35.0
40	35.0
50	45.0

Group 1(n=1.66)

a	Depth(µm)
10	1.8
20	1.6
30	-
40	-
50	1.2

Group 1(n=1.66)

a	Depth(µm)
10	1.8
20	1.6
30	1.6
40	-
50	1.2

Group 1(n=1.66)

a	Depth(µm)
10	1.0
20	-
30	12.0
40	-
50	4.24

Group 1(n=1.66)

a	Depth(µm)
10	30.0
20	25.0
30	40.0
40	30.0
50	30.0

Group 2(n=1)

a	Depth(µm)
10	0
20	0
30	0
40	0
50	2.6 Picture(1)

Group 2(n=1)

a	Depth(µm)
10	0
20	0
30	0
40	0
50	2.6 Picture(2,3)

Group 2(n=1)

a	Depth(µm)
10	0
20	0
30	0
40	0
50	-

Group 2(n=1)

a	Depth(µm)
10	0
20	0
30	0
40	60.0
50	55.0

Group 2(n=1.66)

a	Depth(µm)
10	1.7
20	1.7
30	1.9
40	2.2
50	1.0

Group 2(n=1.66)

a	Depth(µm)
10	1.7
20	1.8
30	1.9
40	2.2
50	1.0

Group 2(n=1.66)

a	Depth(µm)
10	2.0
20	2.2
30	2.0
40	2.2
50	1.2

Group 2(n=1.66)

a	Depth(µm)
10	40.0 Picture(4,5)
20	3.0
30	17.0
40	2.3
50	1.2

Figure C.2: Results etching depths.
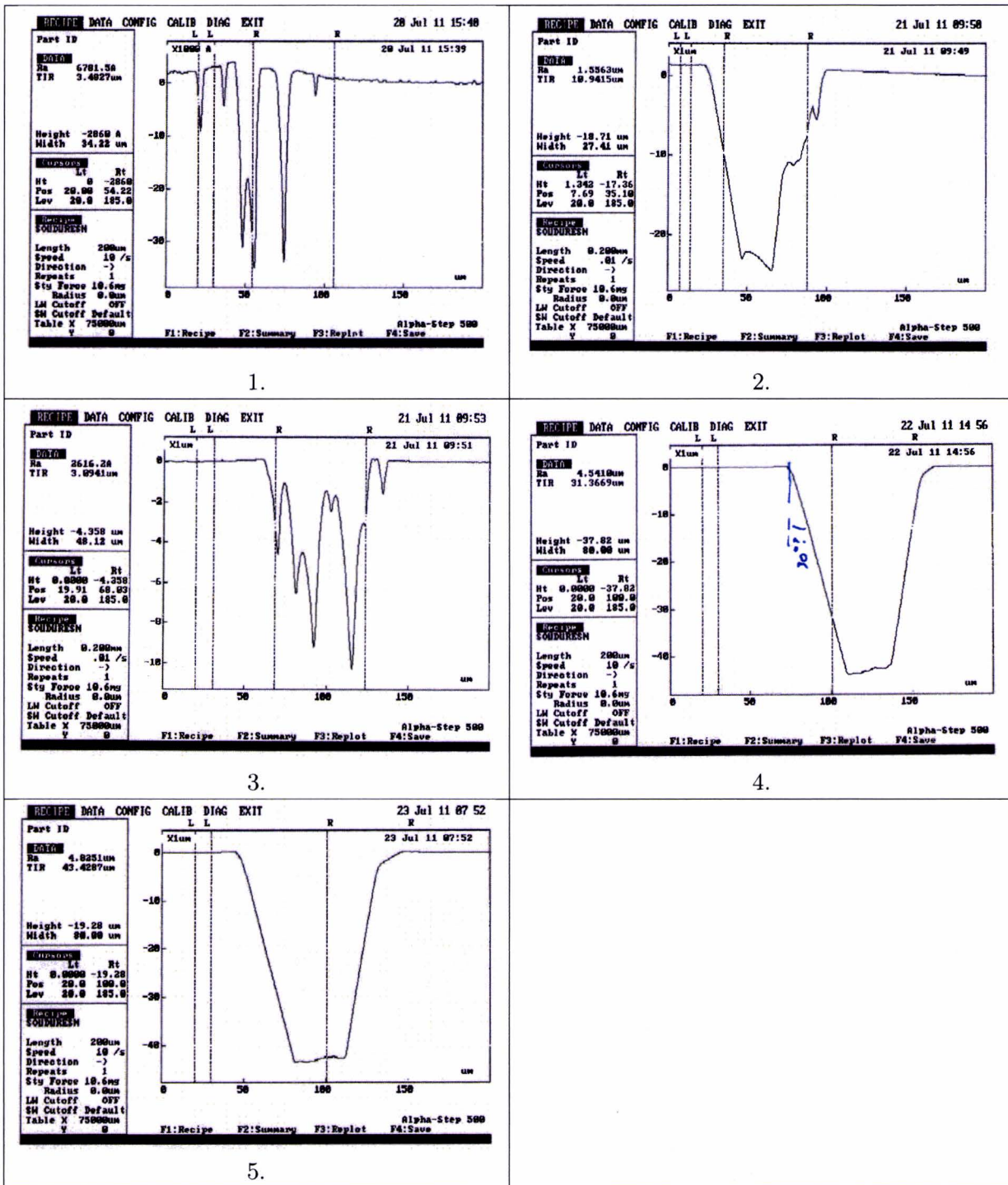
Table C.2: Alpha-step scans: the numbers correspond with the numbers in table C.2.

After 2 min etching	After 4 min etching	After 20 min etching
Group 1(n=1)		
Group 1(n=1.66)		
Group 2(n=1)		
Group 2(n=1.66)		

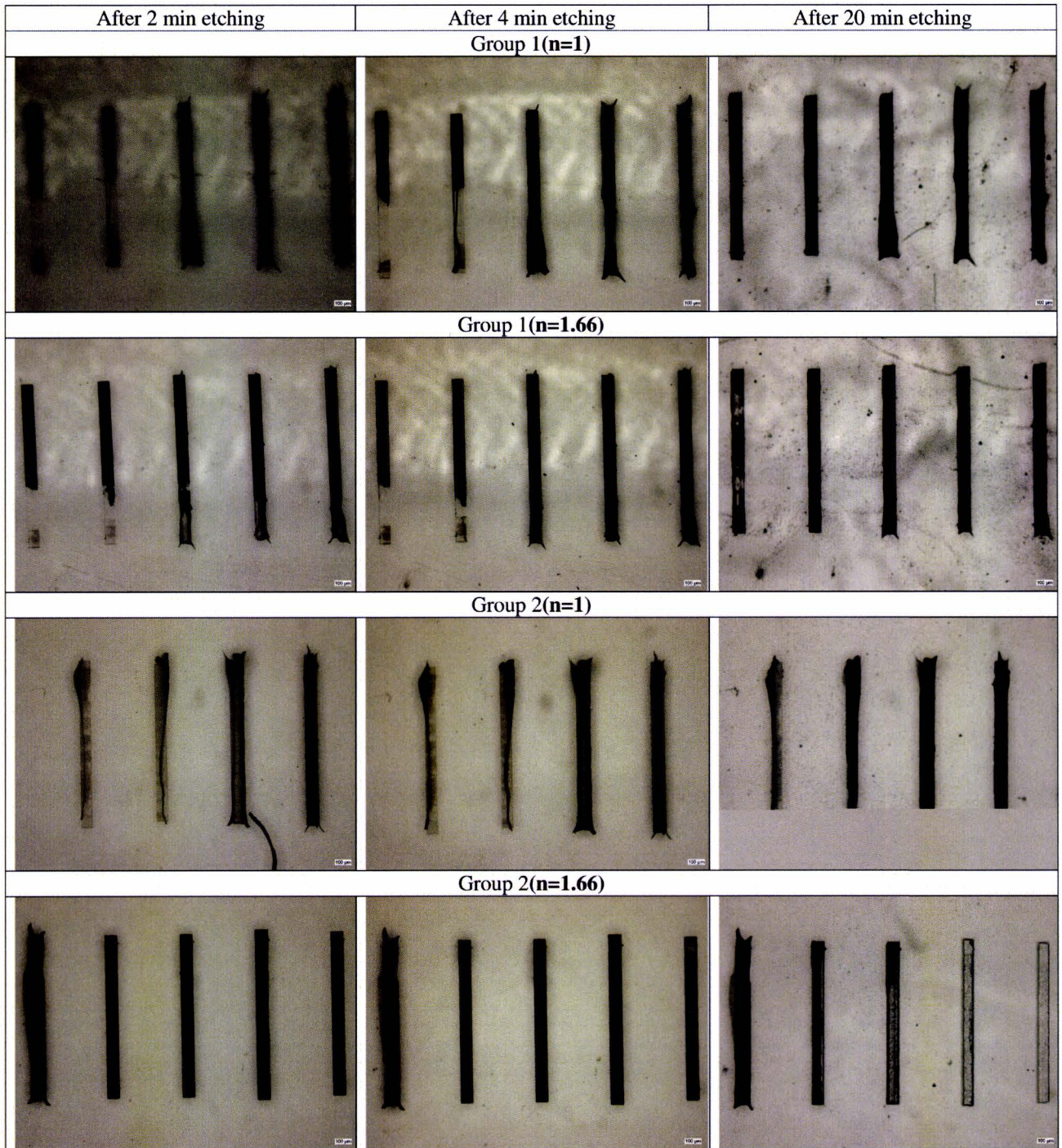Figure C.3: Pictures optic microscope.

Appendix D

Quartz: results follow-up experiments 2

In these experiments, the range of pulse energy is increased as well as the a and n parameters mentioned in equation 3.1 and 3.2. These laser parameters and machined structures are described below. After laser irradiation and etching of the substrates the etched patterns did not reach the desired depths. The structures which reached the depths of about 15 to 20 μm within 4 minutes were heavily damaged. Material was ablated and cracks were introduced. The ones without cracks were shallow and reached a depth of about 5 to 10 μm. The etching depths, pictures and alpha-step scans are shown in the rest of this appendix.

n=1.0(z=10)				n=1.66(z=6)			
a	n	f(KHz)	v(mm/s)	a	n	f(KHz)	v(mm/s)
10	1	300	30	10	1.66	100	16.6
20	1	600	30	20	1.66	200	16.6
30	1	800	26.7	30	1.66	400	22.1
40	1	800	20	40	1.66	400	16.6
50	1	800	16	50	1.66	800	16.6
60	1	800	13.3	60	1.66	800	22.1
n=1.25(z=8)				n=2.5(z=4)			
a	n	f(KHz)	v(mm/s)	a	n	f(KHz)	v(mm/s)
10	1.25	200	25	10	2.5	100	25
20	1.25	400	25	20	2.5	200	25
30	1.25	700	29.2	30	2.5	300	25
40	1.25	800	25	40	2.5	400	25
50	1.25	800	20	50	2.5	600	30
60	1.25	800	16.7	60	2.5	700	29.2

Table D.1: Used laser parameters.
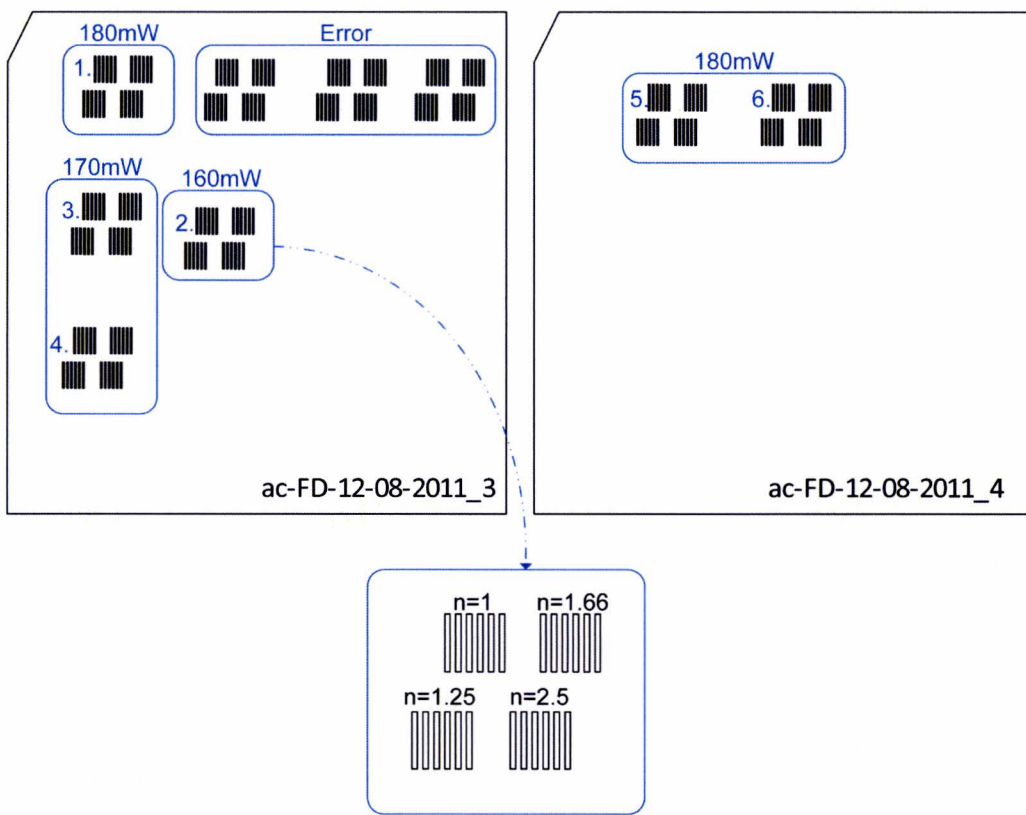
Figure D.1: Structures machined on Quartz substrate.

After laser machining, without any etching(497um)

Group 2 (160mW)

Group 2.1 (z=10)

a	n	f (KHz)	v (mm/s)	d(um)	Remarks	Picture
10	1	300	30			
20	1	600	30			
30	1	800	26,7		Under the surface/ not measurable	
40	1	800	20			
50	1	800	16			
60	1	800	13,3			

Group 2.2 (z=6)

a	n	f (KHz)	v (mm/s)	d(um)	Remarks	Picture
10	1,66	100	16,6			
20	1,66	200	16,6			
30	1,66	400	22,1		Under the surface/ not measurable	
40	1,66	400	16,6			
50	1,66	800	26,6			
60	1,66	800	22,1			

Group 2.3 (z=8)

a	n	f (KHz)	v (mm/s)	d(um)	Remarks	Picture
10	1,25	200	25			
20	1,25	400	25			
30	1,25	700	29,2		Under the surface/ not measurable	
40	1,25	800	25			
50	1,25	800	20,0			
60	1,25	800	16,7			

Group 2.4 (z=4)

a	n	f (KHz)	v (mm/s)	d(um)	Remarks	Picture
10	2,5	100	25			
20	2,5	200	25			
30	2,5	300	25,0		Under the surface/ not measurable	
40	2,5	400	25			
50	2,5	600	30,0			
60	2,5	700	29,2			

After laser machining, without any etching(497um)

Group 3 (170mW)

Group 3.1 (z=10)

a	n	f (KHz)	v (mm/s)	d(um)	Remarks	Picture
10	1	300	30	0,4	Hole of 2 um, bad	
20	1	600	30			
30	1	800	26,7	1,3	Not uniform	4
40	1	800	20			
50	1	800	16			
60	1	800	13,3	1,0	Not uniform with upright edge of 0,5 um	

Group 3.2 (z=6)

a	n	f (KHz)	v (mm/s)	d(um)	Remarks	Picture
10	1,66	100	16,6	1,5	Not uniform	
20	1,66	200	16,6			
30	1,66	400	22,1	1,7	Not uniform	
40	1,66	400	16,6			
50	1,66	800	26,6			
60	1,66	800	22,1	1,8	Not uniform	

Group 3.3 (z=8)

a	n	f (KHz)	v (mm/s)	d(um)	Remarks	Picture
10	1,25	200	25	1,4	Not uniform, variate ± 0,5 um	
20	1,25	400	25	1,5	Tolerable uniform with upright edges	
30	1,25	700	29,2	2,0	Tolerable uniform	5
40	1,25	800	25	1,9	Tolerable uniform	
50	1,25	800	20,0	1,5	Tolerable uniform with upright edges	
60	1,25	800	16,7	1,5	Bad	

Group 3.4 (z=4)

a	n	f (KHz)	v (mm/s)	d(um)	Remarks	Picture
10	2,5	100	25	3,0	Not uniform, variate ± 1,0 um	6
20	2,5	200	25	3,0	Not uniform, variate ± 1,0 um	
40	2,5	400	25	4,9	Bottom uniform but with slopes and high edges	
50	2,5	600	30,0	4,5	Hole up to 6um, rest around 4um	

Figure D.2: Depths after irradiation.

After laser machining, without any etching(497um)

Group 4 (170mW)

Group 4.1 (z=10)

a	n	f (KHz)	v (mm/s)	d(um)	Remarks	Picture
10	1	300	30	1,3	Measured at dark part, not uniform	
20	1	600	30			
30	1	800	26,7	1,0	Measured at dark part, rest under surface	
40	1	800	20			
50	1	800	16			
60	1	800	13,3		Under the surface/ not measurable	

Group 4.2 (z=6)

a	n	f (KHz)	v (mm/s)	d(um)	Remarks	Picture
10	1,66	100	16,6			
20	1,66	200	16,6	1,0	Bad with high peaks	
30	1,66	400	22,1			
40	1,66	400	16,6	1,0	Very rough	
50	1,66	800	26,6			
60	1,66	800	22,1	1,0	Bad with high peaks	

Group 4.3 (z=8)

a	n	f (KHz)	v (mm/s)	d(um)	Remarks	Picture
10	1,25	200	25	1,0	Very rough	
20	1,25	400	25			
30	1,25	700	29,2	1,2	Rough with variation ± 1,0 um	
40	1,25	800	25			
50	1,25	800	20,0			
60	1,25	800	16,7	0,7	Rough	

Group 4.4 (z=4)

a	n	f (KHz)	v (mm/s)	d(um)	Remarks	Picture
10	2,5	100	25	2,0	Two depths, 2,5um and 2,0um. In between high	
20	2,5	200	25	2,5	Big broad peak up to 1um under surface	
50	2,5	600	30,0	3,0	High left edge 3um above surface, not uniform	

After laser machining, without any etching(497um)

Group 1 (180mW)

Group 1.1 (z=10)

a	n	f (KHz)	v (mm/s)	d(um)	Remarks	Picture
10	1	300	30	1,0	Tolerable uniform, ± 0,4 um	
20	1	600	30			
30	1	800	26,7	1,3	Tolerable uniform, ± 0,5 um	
40	1	800	20			
50	1	800	16			
60	1	800	13,3	1,0	Not uniform	

Group 1.2 (z=6)

a	n	f (KHz)	v (mm/s)	d(um)	Remarks	Picture
10	1,66	100	16,6	1,5	Variate ± 0,5 um	
20	1,66	200	16,6			
30	1,66	400	22,1	1,9	Variate ± 0,5 um	
40	1,66	400	16,6			
50	1,66	800	26,6			
60	1,66	800	22,1	1,8	Variate ± 0,5 um	

Group 1.3 (z=8)

a	n	f (KHz)	v (mm/s)	d(um)	Remarks	Picture
10	1,25	200	25		Max depth=2 um but very bad	1
20	1,25	400	25	1,5	Uniform(1 small hole(2,5 um)	2
30	1,25	700	29,2			
40	1,25	800	25			
50	1,25	800	20,0			
60	1,25	800	16,7	1,7	Uniform except for 1 hole and peak	

Group 1.4 (z=4)

a	n	f (KHz)	v (mm/s)	d(um)	Remarks	Picture
10	2,5	100	25	2,0	2 platforms, depths are 1,5 and 2.5 um	
20	2,5	200	25	3,2	Variate ± 1,0 um	

After laser machining, without any etching(497um)
Group 5 (180mW)

Group 5.1 (z=10)

a	n	f (KHz)	v (mm/s)	d(um)	Remarks	Picture
10	1	300	30	1,7	Tolerable uniform	
20	1	600	30			
30	1	800	26,7	1,7	Two depths of 1,7, in between high	
40	1	800	20			
50	1	800	16			
60	1	800	13,3	1,5	1 peak of 0,5um but reasenable	

Group 5.2 (z=6)

a	n	f (KHz)	v (mm/s)	d(um)	Remarks	Picture
10	1,66	100	16,6	1,5	Bad, high peak up to surface	
20	1,66	200	16,6			
30	1,66	400	22,1	2,0	Hole up to 4um	
40	1,66	400	16,6			
50	1,66	800	26,6			
60	1,66	800	22,1	3,0	Tolerable uniform	

Group 5.3 (z=8)

a	n	f (KHz)	v (mm/s)	d(um)	Remarks	Picture
10	1,25	200	25		Very bad	8
20	1,25	400	25			
30	1,25	700	29,2	2,0	Good, very uniform	
40	1,25	800	25	2,0	Reasonable uniform with upright edges	
50	1,25	800	20,0	1,8	Reasonable uniform with upright edges	
60	1,25	800	16,7	2,0	Good, very uniform	

Group 5.4 (z=4)

a	n	f (KHz)	v (mm/s)	d(um)	Remarks	Picture
10	2,5	100	25	3,0	Big peak up to 1,5um	
20	2,5	200	25	3,0	Not really uniform but nog big peaks/holes	

After laser machining, without any etching(497um)
Group 6 (180mW)

Group 6.1 (z=10)

a	n	f (KHz)	v (mm/s)	d(um)	Remarks	Picture
10	1	300	30			
20	1	600	30			
30	1	800	26,7		Under the surface/ not measurable	
40	1	800	20			
50	1	800	16			
60	1	800	13,3			

Group 6.2 (z=6)

a	n	f (KHz)	v (mm/s)	d(um)	Remarks	Picture
10	1,66	100	16,6	1,0	Bad, lot of peaks and holes	
20	1,66	200	16,6			
30	1,66	400	22,1	1,0	Bad, lot of peaks and holes	
40	1,66	400	16,6	1,0	Bad, lot of peaks and holes	
50	1,66	800	26,6	2,5	Variate ± 1,0 um	
60	1,66	800	22,1	2,0	Tolerable uniform	

Group 6.3 (z=8)

a	n	f (KHz)	v (mm/s)	d(um)	Remarks	Picture
10	1,25	200	25	1,0	Bad, lot of peaks and holes	
20	1,25	400	25			
30	1,25	700	29,2	1,2	Big peak of 1um	
40	1,25	800	25			
50	1,25	800	20,0			
60	1,25	800	16,7	0,7	Peaks up to surface	

Group 6.4 (z=4)

a	n	f (KHz)	v (mm/s)	d(um)	Remarks	Picture
10	2,5	100	25	3,0	Reasonable with upright edge	
20	2,5	200	25	3,9	Reasonable with upright edge, variate ± 0,5 um	

Figure D.4: Depths after irradiation.

After laser machining, with 2 minutes etching(490um)

Group 2 (160mW)

Group 2.1 (z=10)

a	n	f (KHz)	v (mm/s)	d(um)	Remarks	Picture
10	1	300	30			
20	1	600	30			
30	1	800	26,7		Under the surface/ not measurable	
40	1	800	20			
50	1	800	16			
60	1	800	13,3			

Group 2.2 (z=6)

a	n	f (KHz)	v (mm/s)	d(um)	Remarks	Picture
10	1,66	100	16,6			
20	1,66	200	16,6			
30	1,66	400	22,1		Under the surface/ not measurable	
40	1,66	400	16,6			
50	1,66	800	26,6			
60	1,66	800	22,1			

Group 2.3 (z=8)

a	n	f (KHz)	v (mm/s)	d(um)	Remarks	Picture
10	1,25	200	25			
20	1,25	400	25			
30	1,25	700	29,2		Under the surface/ not measurable	
40	1,25	800	25			
50	1,25	800	20,0			
60	1,25	800	16,7			

Group 2.4 (z=4)

a	n	f (KHz)	v (mm/s)	d(um)	Remarks	Picture
10	2,5	100	25			
20	2,5	200	25			
30	2,5	300	25,0	2,0	deep hole up to 11 um	
40	2,5	400	25			
50	2,5	600	30,0			
60	2,5	700	29,2	15,0	Slope edges, not uniform	

After laser machining, with 2 minutes etching(490um)

Group 3 (170mW)

Group 3.1 (z=10)

a	n	f (KHz)	v (mm/s)	d(um)	Remarks	Picture
10	1	300	30	1,5	Bad, 4 deep holes à 2,5 um	
20	1	600	30			
30	1	800	26,7	2,0	Not uniform with 4 deep holes à 3,5 um	
40	1	800	20			
50	1	800	16			
60	1	800	13,3	1,5	Uniform, only 1 hole to 4um	

Group 3.2 (z=6)

a	n	f (KHz)	v (mm/s)	d(um)	Remarks	Picture
10	1,66	100	16,6	1,5	Hole to 4,1um, variate ± 1,0 um	
20	1,66	200	16,6			
30	1,66	400	22,1	7,5	Bad, lot of depth differences	
40	1,66	400	16,6			
50	1,66	800	26,6			
60	1,66	800	22,1	7,0	Bad, Plateau of 4um, depth 25 and 11 um around it	

Group 3.3 (z=8)

a	n	f (KHz)	v (mm/s)	d(um)	Remarks	Picture
10	1,25	200	25	1,5	Not uniform, variate ± 0,5 um	
20	1,25	400	25	2,1	Tolerable uniform, , variate ± 0,4 um	
30	1,25	700	29,2	2,5	Tolerable uniform but with hole to 4,5 um	
40	1,25	800	25	2,0	Tolerable uniform but with hole to 4,0 um	
50	1,25	800	20,0	2,0	Variate ± 0,6 um, upright edges, not uniform	
60	1,25	800	16,7	1,5	Bad	

Group 3.4 (z=4)

a	n	f (KHz)	v (mm/s)	d(um)	Remarks	Picture
10	2,5	100	25	6,0	Bad, big plateau 5um, depth 11 and 13 around it	
20	2,5	200	25	5,0	Bad, big plateau 5um, depth 15 and 10 around it	
30	2,5	300	25,0	20,0	Bad	13&
40	2,5	400	25	15,0	Big peak up to 7um under surfacae, holes of 25um	
50	2,5	600	30,0	15,0	Big peak up to 5um under surfacae, holes 20 and 11	
60	2,5	700	29,2	17,0	Plateau of 7um, depths of 23 and 15 around it	

Figure D.5: Depths after 2 minutes etching with 50% concentrated HF.

After laser machining, with 2 minutes etching(490um)

Group 4 (170mW)

Group 4.1 (z=10)

a	n	f (KHz)	v (mm/s)	d(um)	Remarks	Picture
10	1	300	30	2,0	Measured at dark part, not uniform	
20	1	600	30			
30	1	800	26,7	1,0	Bad	
40	1	800	20			
50	1	800	16			
60	1	800	13,3		Under the surface/ not measurable	

Group 4.2 (z=6)

a	n	f (KHz)	v (mm/s)	d(um)	Remarks	Picture
10	1,66	100	16,6			
20	1,66	200	16,6	1,0	Bad with high peaks	
30	1,66	400	22,1			
40	1,66	400	16,6	2,0	Rough, holes to 8um	
50	1,66	800	26,6			
60	1,66	800	22,1	1,0	2 holes, 17 and 10 um	

Group 4.3 (z=8)

a	n	f (KHz)	v (mm/s)	d(um)	Remarks	Picture
10	1,25	200	25	1,1	Very rough	
20	1,25	400	25			
30	1,25	700	29,2	1,5	Rough with variation ± 0,5 um	
40	1,25	800	25			
50	1,25	800	20,0			
60	1,25	800	16,7	1,5	Rough with variation ± 0,5 um	

Group 4.4 (z=4)

a	n	f (KHz)	v (mm/s)	d(um)	Remarks	Picture
10	2,5	100	25	4,4	Picture	14
20	2,5	200	25	4,0	One big hole to 13 um, bad	
30	2,5	300	25,0	15,0	Not uniform, lowest point 28 um, bad	
40	2,5	400	25	12,0	Not uniform, lowest point 24 um, bad	
50	2,5	600	30,0	17,0	Not good, peak up to 11 um under surface	
60	2,5	700	29,2	20,0	Picture	15

After laser machining, with 2 minutes etching(490um)

Group 1 (180mW)

Group 1.1 (z=10)

a	n	f (KHz)	v (mm/s)	d(um)	Remarks	Picture
10	1	300	30	1,5	Not uniform, variate ± 0,7 um	
20	1	600	30			
30	1	800	26,7	1,7	Not uniform, variate ± 0,7 um	
40	1	800	20			
50	1	800	16			
60	1	800	13,3	1,5	Not uniform, big hole 3,5um	

Group 1.2 (z=6)

a	n	f (KHz)	v (mm/s)	d(um)	Remarks	Picture
10	1,66	100	16,6	1,8	Not uniform, hole 3,0um	
20	1,66	200	16,6			
30	1,66	400	22,1	6,0	Picture	11
40	1,66	400	16,6			
50	1,66	800	26,6			
60	1,66	800	22,1	3,0	Big holes to 9 um	

Group 1.3 (z=8)

a	n	f (KHz)	v (mm/s)	d(um)	Remarks	Picture
10	1,25	200	25	1,5	More uniform but still bad	
20	1,25	400	25	2,0	Tolerabel uniform	
30	1,25	700	29,2			
40	1,25	800	25			
50	1,25	800	20,0			
60	1,25	800	16,7	2,2	Rough, variate ± 0,7 um	

Group 1.4 (z=4)

a	n	f (KHz)	v (mm/s)	d(um)	Remarks	Picture
10	2,5	100	25	3,0	Not uniform	
20	2,5	200	25	5,0	Big holes to 14 um	
30	2,5	300	25,0	17,4	Picture	12
40	2,5	400	25	22,7	2 big holes to 17 and 24um	
50	2,5	600	30,0	17,0	Slopes edges en small plateau	
60	2,5	700	29,2	23,0	Picture	13

Figure D.6: Depths after 2 minutes etching with 50% concentrated HF.

After laser machining, with 2 minutes etching(490um)
Group 5 (180mW)

Group 5.1 (z=10)

a	n	f (KHz)	v (mm/s)	d(um)	Remarks	Picture
10	1	300	30	2,1	Tolerable uniform	
20	1	600	30			
30	1	800	26,7	2,0	Bad, high peak up to surface	
40	1	800	20			
50	1	800	16			
60	1	800	13,3	2,0	Not uniform	

Group 5.2 (z=6)

a	n	f (KHz)	v (mm/s)	d(um)	Remarks	Picture
10	1,66	100	16,6	2,0	Peak is gone, variate ± 1,0 um	
20	1,66	200	16,6			
30	1,66	400	22,1	2,5	Hole up to 4,5um	
40	1,66	400	16,6			
50	1,66	800	26,6			
60	1,66	800	22,1	3,5	Tolerable uniform	

Group 5.3 (z=8)

a	n	f (KHz)	v (mm/s)	d(um)	Remarks	Picture
10	1,25	200	25		Very bad	
20	1,25	400	25			
30	1,25	700	29,2	3,0	Not uniform, rough	
40	1,25	800	25	3,0	Uniform except hole to 8um	
50	1,25	800	20,0	5,0	Bad, 3 plateau's with holes, 7, 7 and 13 um	
60	1,25	800	16,7	3,0	Bad, 2 holes 15 and 12 um	

Group 5.4 (z=4)

a	n	f (KHz)	v (mm/s)	d(um)	Remarks	Picture
10	2,5	100	25	3,0	Big peak up to 2,0um	
30	2,5	300	25,0	5,0	big holes 10 um, pretty uniform except hole	
40	2,5	400	25	6,0	uniform around 6um, 2 holes 8 um	
50	2,5	600	30,0	9,0	Picture	16
60	2,5	700	29,2	8,5	Plateau 6 um, bottom 10 um, not uniform	

Group 6 (180mW)

Group 6.1 (z=10)

a	n	f (KHz)	v (mm/s)	d(um)	Remarks	Picture
10	1	300	30		Still under the surface	
20	1	600	30			
30	1	800	26,7		Measure crack 3,0 um(under surface)	
40	1	800	20			
50	1	800	16			
60	1	800	13,3		Measure crack 6,0 um(under surface)	

Group 6.2 (z=6)

a	n	f (KHz)	v (mm/s)	d(um)	Remarks	Picture
10	1,66	100	16,6	1,5	Bad, lot of peaks and holes, depth max 3,5 um	
20	1,66	200	16,6			
30	1,66	400	22,1	1,5	Bad, lot of peaks and holes, depth max 8um	
40	1,66	400	16,6			
50	1,66	800	26,6			
60	1,66	800	22,1	2,5	Tolerable uniform but holes up to 7um	

Group 6.3 (z=8)

a	n	f (KHz)	v (mm/s)	d(um)	Remarks	Picture
10	1,25	200	25	1,5	Bad, lot of peaks and holes, rough	
20	1,25	400	25			
30	1,25	700	29,2	2,0	Big holes up to 6um, not uniform	
40	1,25	800	25			
50	1,25	800	20,0			
60	1,25	800	16,7	2,0	Rough, holes up to 6,5 , 5 and 4 um	

Group 6.4 (z=4)

a	n	f (KHz)	v (mm/s)	d(um)	Remarks	Picture
10	2,5	100	25	7,0	Bad, holes up to 17 um, not uniform	
20	2,5	200	25	10,0	Bad, picture	17
30	2,5	300	25,0	15,0	Comparable to picture 17	
50	2,5	600	30,0	20,0	Comparable to picture 17	
60	2,5	700	29,2	15,0	Deep but shape like a traingle, not uniform	

Figure D.7: Depths after 2 minutes etching with 50% concentrated HF.

After laser machining, with 4 minutes etching(482um)
Group 2 (160mW)

Group 2.1 (z=10)						
a	n	f (KHz)	v (mm/s)	d(um)	Remarks	Picture
10	1	300	30			
20	1	600	30			
30	1	800	26,7		STOPPED MEASURING	
40	1	800	20			
50	1	800	16			
60	1	800	13,3			

Group 2.2 (z=6)						
a	n	f (KHz)	v (mm/s)	d(um)	Remarks	Picture
10	1,66	100	16,6			
20	1,66	200	16,6			
30	1,66	400	22,1		STOPPED MEASURING	
40	1,66	400	16,6			
50	1,66	800	26,6			
60	1,66	800	22,1			

Group 2.3 (z=8)						
a	n	f (KHz)	v (mm/s)	d(um)	Remarks	Picture
10	1,25	200	25			
20	1,25	400	25			
30	1,25	700	29,2		STOPPED MEASURING	
40	1,25	800	25			
50	1,25	800	20,0			
60	1,25	800	16,7			

Group 2.4 (z=4)						
a	n	f (KHz)	v (mm/s)	d(um)	Remarks	Picture
10	2,5	100	25			
20	2,5	200	25			
30	2,5	300	25,0		STOPPED MEASURING	
40	2,5	400	25			
50	2,5	600	30,0			
60	2,5	700	29,2			

After laser machining, with 4 minutes etching(482um)
Group 3 (170mW)

Group 3.1 (z=10)						
a	n	f (KHz)	v (mm/s)	d(um)	Remarks	Picture
10	1	300	30	2,0	Bad, 1 deep hole of 16, rest around 1um deep	
20	1	600	30			
30	1	800	26,7	10,0	2 holes of 18 and 15 um with a peak of 6 under surface in betweer	
40	1	800	20			
50	1	800	16			
60	1	800	13,3	18,0	V'shape, max depth 30 um	

Group 3.2 (z=6)						
a	n	f (KHz)	v (mm/s)	d(um)	Remarks	Picture
10	1,66	100	16,6	1,6	Bad, 3um max depth	
20	1,66	200	16,6			
30	1,66	400	22,1	15,0	V-shape, 26 um is max depth	
40	1,66	400	16,6			
50	1,66	800	26,6			

Group 3.3 (z=8)						
a	n	f (KHz)	v (mm/s)	d(um)	Remarks	Picture
10	1,25	200	25	1,5	Not uniform, variate ± 0,5 um	
20	1,25	400	25			
30	1,25	700	29,2	20,0	2 holes of 20 and 15 um with a peak of 3 under surface in betweer	
40	1,25	800	25			
50	1,25	800	20,0			
60	1,25	800	16,7	15,0	Picture	20

Group 3.4 (z=4)						
a	n	f (KHz)	v (mm/s)	d(um)	Remarks	Picture
10	2,5	100	25	8,0	3 depths of 20, 25 en 1C	
20	2,5	200	25			
40	2,5	400	25			
50	2,5	600	30,0			
60	2,5	700	29,2	50,0	V-shape with depth 65 um	

Figure D.8: Depths after 4 minutes etching with 50% concentrated HF.

After laser machining, with 4 minutes etching(482um)

Group 4 (170mW)

Group 4.1 (z=10)

a	n	f (KHz)	v (mm/s)	d(um)	Remarks	Picture
10	1	300	30	2,0	Hole to 5,5 um	
20	1	600	30			
30	1	800	26,7	1,0	Still bad	
40	1	800	20			
50	1	800	16			
60	1	800	13,3		Under the surface/ not measurable	

Group 4.2 (z=6)

a	n	f (KHz)	v (mm/s)	d(um)	Remarks	Picture
10	1,66	100	16,6			
20	1,66	200	16,6	1,0	Bit uniform	
30	1,66	400	22,1			
40	1,66	400	16,6	2,0	2 holes, 20 en 18 with a peak of 10 in between	
50	1,66	800	26,6			
60	1,66	800	22,1	1,0	Bad, 2 holes of 20 en 30 um	

Group 4.3 (z=8)

a	n	f (KHz)	v (mm/s)	d(um)	Remarks	Picture
10	1,25	200	25	1,1	Very rough	
20	1,25	400	25			
30	1,25	700	29,2	2,0	1 hole of 16 um, rest is around 2 um	
40	1,25	800	25			
50	1,25	800	20,0			
60	1,25	800	16,7	1,5	big hole of 20 um	

Group 4.4 (z=4)

a	n	f (KHz)	v (mm/s)	d(um)	Remarks	Picture
10	2,5	100	25	4,4	Picture	21
20	2,5	200	25			
30	2,5	300	25,0	20,0	V-shape of 40	
40	2,5	400	25			
50	2,5	600	30,0			
60	2,5	700	29,2	20,0	V-shape of 42	

After laser machining, with 4 minutes etching(482um)

Group 1 (180mW)

Group 1.1 (z=10)

a	n	f (KHz)	v (mm/s)	d(um)	Remarks	Picture
10	1	300	30	1,6	1 hole to 9 um	
20	1	600	30			
30	1	800	26,7	13,0	Picture	18
40	1	800	20			
50	1	800	16	15,0	2 holes with dept 22	
60	1	800	13,3	15,0	V-shape, 28 um deep	

Group 1.2 (z=6)

a	n	f (KHz)	v (mm/s)	d(um)	Remarks	Picture
10	1,66	100	16,6	1,6	Tolerable uniform	
20	1,66	200	16,6			
40	1,66	400	16,6			
50	1,66	800	26,6			

Group 1.3 (z=8)

a	n	f (KHz)	v (mm/s)	d(um)	Remarks	Picture
20	1,25	400	25	2,0	Really bad	
30	1,25	700	29,2			
40	1,25	800	25			
50	1,25	800	20,0			
60	1,25	800	16,7	2,2	Rough, 3 deep holes of 5, 18 en 8 um	

Group 1.4 (z=4)

a	n	f (KHz)	v (mm/s)	d(um)	Remarks	Picture
10	2,5	100	25	3,0	Bad, hole to 10um	
20	2,5	200	25			
40	2,5	400	25			
50	2,5	600	30,0			
60	2,5	700	29,2	23,0	V-shaped with 2 bottoms, 30 en 48 um	

Figure D.9: Depths after 4 minutes etching with 50% concentrated HF.

After laser machining, with 4 minutes etching(482um)

Group 5 (180mW)

Group 5.1 (z=10)

a	n	f (KHz)	v (mm/s)	d(um)	Remarks	Picture
10	1	300	30	2,0	1 hole of 7 um	
20	1	600	30			
30	1	800	26,7	5,0	hole of 18 um	
40	1	800	20			
50	1	800	16			

Group 5.2 (z=6)

a	n	f (KHz)	v (mm/s)	d(um)	Remarks	Picture
10	1,66	100	16,6	2,0	Uniform bottom	
20	1,66	200	16,6			
30	1,66	400	22,1	2,0	2 depths(plateaus(of 4 en 2 um	
40	1,66	400	16,6			
50	1,66	800	26,6			
60	1,66	800	22,1	3,5	Tolerable uniform	

Group 5.3 (z=8)

a	n	f (KHz)	v (mm/s)	d(um)	Remarks	Picture
10	1,25	200	25		Still very bad	
20	1,25	400	25	2,2	Hole up to 6.1 um	
30	1,25	700	29,2	7,0	Lot of big peaks and holes	
40	1,25	800	25	10,0	Rough slopes and depth of 15um, not good	

Group 5.4 (z=4)

a	n	f (KHz)	v (mm/s)	d(um)	Remarks	Picture
10	2,5	100	25	3,0	Not uniform, rough bottom	
20	2,5	200	25	4,0	Reasonable uniform	
30	2,5	300	25,0	5,0	big holes 11 and 8 um, not uniform	
40	2,5	400	25	6,0	uniform around 6um, 2 holes 8 um	
50	2,5	600	30,0	9,0	Very rough bottom	
60	2,5	700	29,2	6,0	Plateau 4um, 2 holes of 10 um with peak of 5 between, bac	

Group 6 (180mW)

Group 6.1 (z=10)

a	n	f (KHz)	v (mm/s)	d(um)	Remarks	Picture
10	1	300	30	15	3 depths 17, 24 en 10 um	
20	1	600	30			
30	1	800	26,7	13	2 holes of 25 and 21, peak of 3 um between	
40	1	800	20			
50	1	800	16			
60	1	800	13,3	3	Bad, lot of peaks and holes, max depth is 13	

Group 6.2 (z=6)

a	n	f (KHz)	v (mm/s)	d(um)	Remarks	Picture
10	1,66	100	16,6	1,5	Bad, lot of peaks and holes, depth max 4 um	
20	1,66	200	16,6			
30	1,66	400	22,1	15,0	2 depths 28 and 25 um with peak between	
40	1,66	400	16,6			
50	1,66	800	26,6	4,0	2 big holes of 30 and 35 with peak of 5 um between	
60	1,66	800	22,1	15,0	Picture	22

Group 6.3 (z=8)

a	n	f (KHz)	v (mm/s)	d(um)	Remarks	Picture
10	1,25	200	25	1,0	Bad, lot of peaks and holes, rough	
20	1,25	400	25			
30	1,25	700	29,2	12,0	Big holes up to 30 um	
40	1,25	800	25			
50	1,25	800	20,0			
60	1,25	800	16,7	10,0	V-shaped with big hole of 28 um	

Group 6.4 (z=4)

a	n	f (KHz)	v (mm/s)	d(um)	Remarks	Picture
10	2,5	100	25	17,0	Holes with depth 22 and 30 um, peak of 18 under surf	
20	2,5	200	25	10,0	Bad, V-shaped 25 um hole	

Figure D.10: Depths after 4 minutes etching with 50% concentrated HF.

After laser machining, with 20 minutes etching

Group 2 (160mW)

Group 2.1 (z=10)

a	n	f (KHz)	v (mm/s)	d(um)	Remarks	Picture
10	1	300	30			
20	1	600	30			
30	1	800	26,7			
40	1	800	20		STOPPED MEASURING	
50	1	800	16			
60	1	800	13,3			

Group 2.2 (z=6)

a	n	f (KHz)	v (mm/s)	d(um)	Remarks	Picture
10	1,66	100	16,6			
20	1,66	200	16,6			
30	1,66	400	22,1			
40	1,66	400	16,6		STOPPED MEASURING	
50	1,66	800	26,6			
60	1,66	800	22,1			

Group 2.3 (z=8)

a	n	f (KHz)	v (mm/s)	d(um)	Remarks	Picture
10	1,25	200	25			
20	1,25	400	25			
30	1,25	700	29,2			
40	1,25	800	25		STOPPED MEASURING	
50	1,25	800	20,0			
60	1,25	800	16,7			

Group 2.4 (z=4)

a	n	f (KHz)	v (mm/s)	d(um)	Remarks	Picture
10	2,5	100	25			
20	2,5	200	25			
30	2,5	300	25,0			
40	2,5	400	25		STOPPED MEASURING	
50	2,5	600	30,0			
60	2,5	700	29,2			

After laser machining, with 20 minutes etching

Group 3 (170mW)

Group 3.1 (z=10)

a	n	f (KHz)	v (mm/s)	d(um)	Remarks	Picture
10	1	300	30			
20	1	600	30			
40	1	800	20	20,0	2 holes, V-shape with depth 31, peak 15 depth 25	
50	1	800	16			
60	1	800	13,3	30,0	Broad B-shape with depth 30 and hole of 40	

Group 3.2 (z=6)

a	n	f (KHz)	v (mm/s)	d(um)	Remarks	Picture
10	1,66	100	16,6	2,0	Bad, hole of 10um, rest 2,0 um	
20	1,66	200	16,6			
30	1,66	400	22,1	30,0	V-shape, 45 um is max depth	
40	1,66	400	16,6			
50	1,66	800	26,6			
60	1,66	800	22,1	30,0	V-shape of 46 um depth	

Group 3.3 (z=8)

a	n	f (KHz)	v (mm/s)	d(um)	Remarks	Picture
10	1,25	200	25			
20	1,25	400	25	15,0	Broad V-shape with peak of 10 um, rest is uniform at 20 um	
30	1,25	700	29,2			
40	1,25	800	25	28,0	Broad V-shape with depth of 35 um	
50	1,25	800	20,0			
60	1,25	800	16,7	30,0	V-shape with depth of 58 um	20

Group 3.4 (z=4)

a	n	f (KHz)	v (mm/s)	d(um)	Remarks	Picture
10	2,5	100	25	20,0	broad V-shape with 2 peaks with heigth 7 and 3 um	
20	2,5	200	25			
30	2,5	300	25,0	33,0	Plateau at 30 um, hole to 45 um	
40	2,5	400	25			
50	2,5	600	30,0			
60	2,5	700	29,2	50,0	V-shape with depth 65 um	

Figure D.11: Depths after 20 minutes etching with 50% concentrated HF.

After laser machining, with 20 minutes etching

Group 4 (170mW)

Group 4.1 (z=10)

a	n	f (KHz)	v (mm/s)	d(um)	Remarks	Picture
10	1	300	30			
20	1	600	30			
30	1	800	26,7			
40	1	800	20		STOPPED MEASURING	
50	1	800	16			
60	1	800	13,3			

Group 4.2 (z=6)

a	n	f (KHz)	v (mm/s)	d(um)	Remarks	Picture
10	1,66	100	16,6			
20	1,66	200	16,6			
30	1,66	400	22,1			
40	1,66	400	16,6			
50	1,66	800	26,6			
60	1,66	800	22,1	1,0	Broad V-shape with depth 55 um, plateau at 35 um	

Group 4.3 (z=8)

a	n	f (KHz)	v (mm/s)	d(um)	Remarks	Picture
10	1,25	200	25			
20	1,25	400	25			
30	1,25	700	29,2	2,0	Bad, 2 holes to 22 and 25 um with peak of 10um betweer	
40	1,25	800	25			
50	1,25	800	20,0	20,0	V-shaped with depth of 28 and 35 um	
60	1,25	800	16,7			

Group 4.4 (z=4)

a	n	f (KHz)	v (mm/s)	d(um)	Remarks	Picture
10	2,5	100	25			
20	2,5	200	25			
30	2,5	300	25,0	20,0	plateau of 40 and V-shape of 35	
40	2,5	400	25			
50	2,5	600	30,0			
60	2,5	700	29,2	20,0	V-shape of 65	

After laser machining, with 20 minutes etching

Group 1 (180mW)

Group 1.1 (z=10)

a	n	f (KHz)	v (mm/s)	d(um)	Remarks	Picture
10	1	300	30	4,0	3 holes of 10, 20 and 10 um	
20	1	600	30	20,0	V-shape with peak at the bottom of 4 um	
30	1	800	26,7	20,0	holes of 31 um, peak to 15 and hole to 24	
40	1	800	20			
50	1	800	16	25,0	Broad V-shape, bottom is slope, max depth is 35 um	
60	1	800	13,3	25,0	Broad V-shape, bottom is slope, max depth is 35 um	

Group 1.2 (z=6)

a	n	f (KHz)	v (mm/s)	d(um)	Remarks	Picture
10	1,66	100	16,6		BAD	
20	1,66	200	16,6			
30	1,66	400	22,1	22,0	Broad V-shape with peaks at bottom of 10, max depth 38um	
40	1,66	400	16,6			
50	1,66	800	26,6			
60	1,66	800	22,1	28,0	V-shape with peaks of 18 um, max dept 42 um	

Group 1.3 (z=8)

a	n	f (KHz)	v (mm/s)	d(um)	Remarks	Picture
10	1,25	200	25		Bad	
20	1,25	400	25			
40	1,25	800	25			
50	1,25	800	20,0	24,0		

Group 1.4 (z=4)

a	n	f (KHz)	v (mm/s)	d(um)	Remarks	Picture
10	2,5	100	25	4,0	3 holes with depth 10, 14 and 10 um	
20	2,5	200	25			
30	2,5	300	25,0	30,0	Bad, plateau at 25, hole to 45 um	
40	2,5	400	25			
50	2,5	600	30,0			
60	2,5	700	29,2	25,0	Plateau at 30 um, V-shape with depth of 48 um	

Figure D.12: Depths after 20 minutes etching with 50% concentrated HF.

After laser machining, with 20 minutes etching
Group 5 (180mW)

Group 5.1 (z=10)

a	n	f (KHz)	v (mm/s)	d(um)	Remarks	Picture
10	1	300	30	2,0	1 hole of 4 um	
20	1	600	30			
30	1	800	26,7	12,0	Broad V-shape with depth 17 um	
40	1	800	20			
50	1	800	16			
60	1	800	13,3	14,0	Not bad, V-shaped with unifrom bottom at 15 um	

Group 5.2 (z=6)

a	n	f (KHz)	v (mm/s)	d(um)	Remarks	Picture
10	1,66	100	16,6			
20	1,66	200	16,6			
30	1,66	400	22,1			
40	1,66	400	16,6			
50	1,66	800	26,6			
60	1,66	800	22,1		BAD, very rough	

Group 5.3 (z=8)

a	n	f (KHz)	v (mm/s)	d(um)	Remarks	Picture
10	1,25	200	25		Still very bad	
20	1,25	400	25	5,0	3 holes with depth 8, 8 and 7um...rough	
30	1,25	700	29,2	8,0	V-shaped with depth 15 um and hole 10 um	
40	1,25	800	25	10,0	V-shape with depth 14 um	
50	1,25	800	20,0	14,0	Tolerable uniform, OK, edged could be steeper	
60	1,25	800	16,7	13,0	V-shape with depth 15 um	

Group 5.4 (z=4)

a	n	f (KHz)	v (mm/s)	d(um)	Remarks	Picture
10	2,5	100	25	3,0	Not uniform, rough bottom	
20	2,5	200	25	4,0	Reasonable uniform	
30	2,5	300	25,0	5,0	Big hole of 8 um, not uniform	
40	2,5	400	25	6,0	Around 6 um, peak of 1 um	
50	2,5	600	30,0	9,0	v-shape with depth 10 um	
60	2,5	700	29,2	7,0	plateau of 6 um, V-shape of 10 um depth	

After laser machining, with 20 minutes etching
Group 6 (180mW)

Group 6.1 (z=10)

a	n	f (KHz)	v (mm/s)	d(um)	Remarks	Picture
10	1	300	30	25	V-shape with max depth of 40 um	
20	1	600	30			
60	1	800	13,3	40	V-shape with max depth of 60 um	

Group 6.2 (z=6)

a	n	f (KHz)	v (mm/s)	d(um)	Remarks	Picture
10	1,66	100	16,6	4,0	Bad, lot of peaks and holes, depth max 11 um	
20	1,66	200	16,6	10,0	3 holes with depth 12, 25 and 40 um	
30	1,66	400	22,1	25,0	V-shape with depth 40 um	
40	1,66	400	16,6			
50	1,66	800	26,6			
60	1,66	800	22,1	30,0	V-shape with flat bottom 35 um, with hole of 45 um	

Group 6.3 (z=8)

a	n	f (KHz)	v (mm/s)	d(um)	Remarks	Picture
10	1,25	200	25	1,0	Bad, lot of peaks and holes, rough	
20	1,25	400	25			
30	1,25	700	29,2	35,0	V-shape with depth 52	
40	1,25	800	25			
50	1,25	800	20,0			
60	1,25	800	16,7	30,0	V-shaped with peak of 5 um in flat bottom	

Group 6.4 (z=4)

a	n	f (KHz)	v (mm/s)	d(um)	Remarks	Picture
10	2,5	100	25	30,0	Broad V-shape with hole of 10 um	
20	2,5	200	25	25,0	plateau 25, hole of 42 um	
30	2,5	300	25,0	35,0	V-shape with depth 55	
40	2,5	400	25	50,0	V-shape with depth 65	
50	2,5	600	30,0	50,0	V-shape with depth 65	
60	2,5	700	29,2	40,0	V-shape with depth 60	

Figure D.13: Depths after 20 minutes etching with 50% concentrated HF.

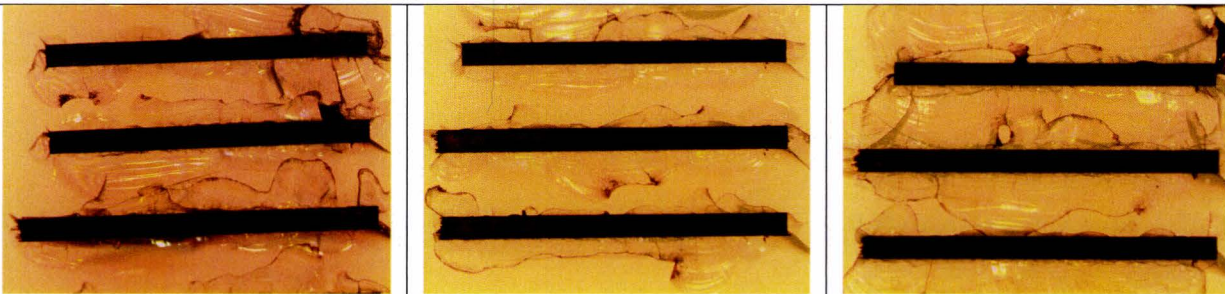| Group1-1 | Group1-2 | Group1-3 | Group1-4 |
Group2-1	Group2-2	Group2-3	Group2-4
Group3-1	Group3-2	Group3-3	Group3-4
Group4-1	Group4-2	Group4-3	Group4-4
Group5-1	Group5-2	Group5-3	Group5-4
Group6-1	Group6-2	Group6-3	Group6-4
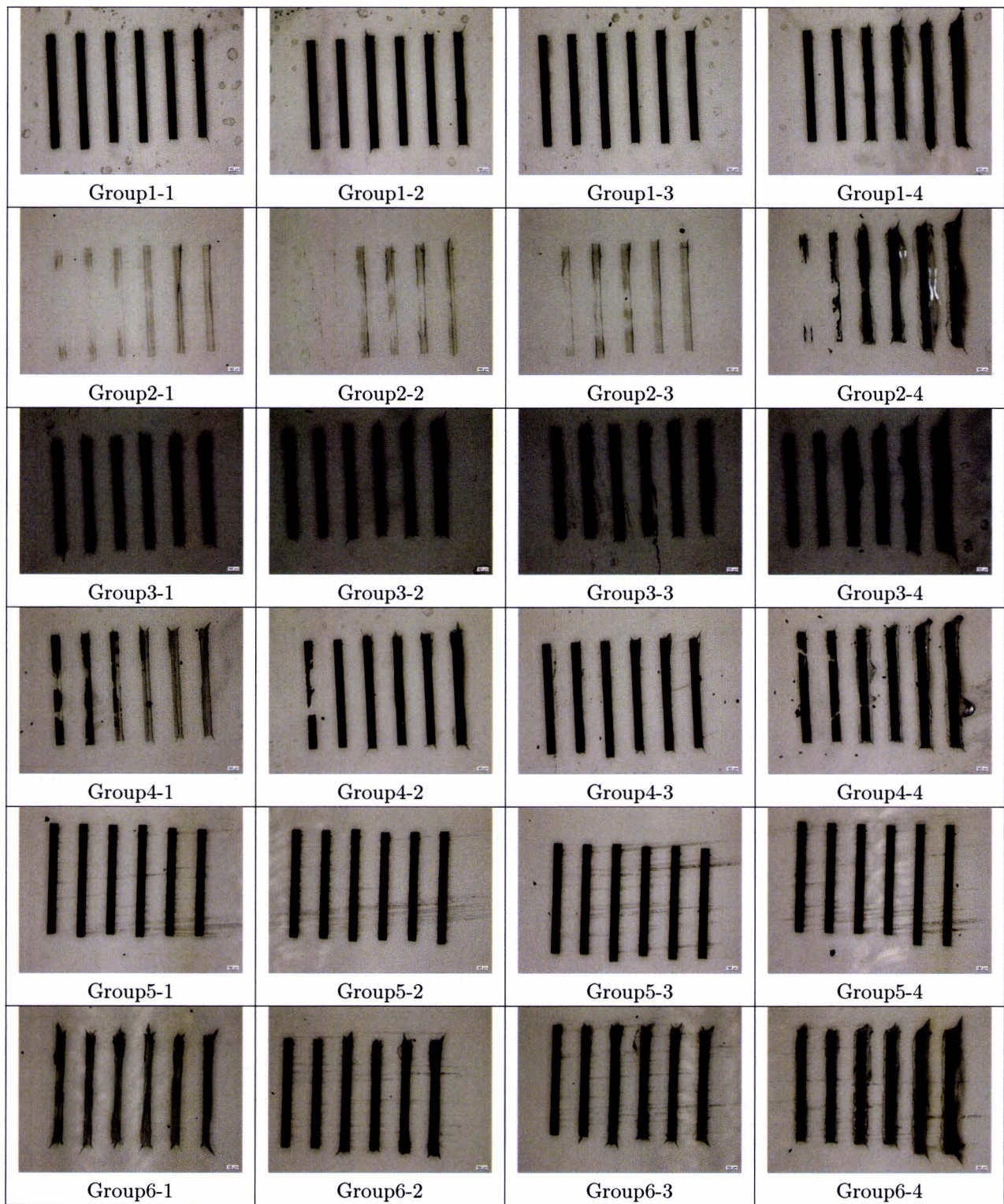
Table D.2: Pictures optic microscope after irradiation.

Group1-1	Group1-2	Group1-3	Group1-4
Group2-1	Group2-2	Group2-3	Group2-4
Group3-1	Group3-2	Group3-3	Group3-4
Group4-1	Group4-2	Group4-3	Group4-4
Group5-1	Group5-2	Group5-3	Group5-4
Group6-1	Group6-2	Group6-3	Group6-4
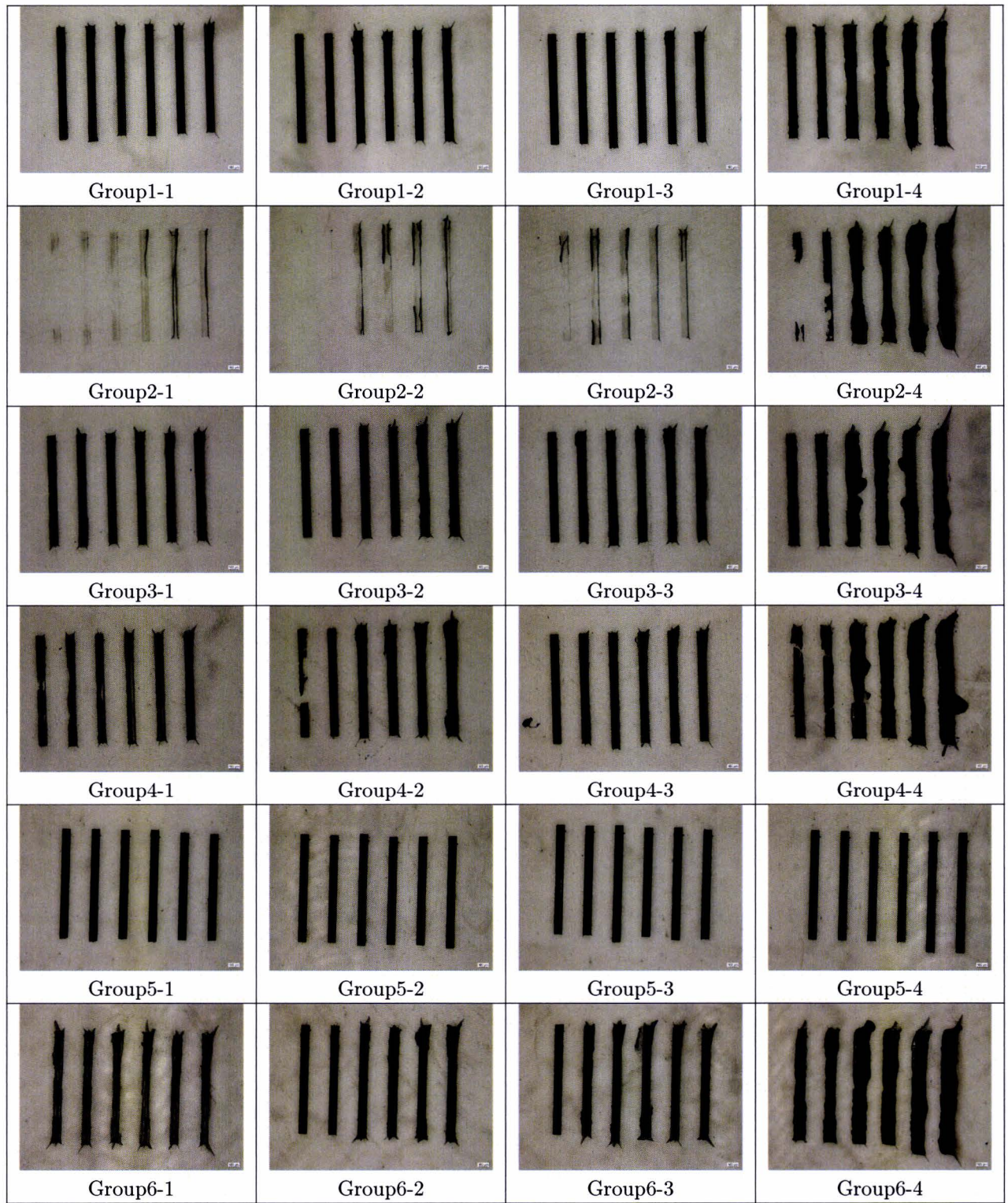
Table D.3: Pictures optic microscope after 2 minutes etching in 50 % concentrated HF.

Group1-1	Group1-2	Group1-3	Group1-4
Group2-1	Group2-2	Group2-3	Group2-4
Group3-1	Group3-2	Group3-3	Group3-4
Group4-1	Group4-2	Group4-3	Group4-4
Group5-1	Group5-2	Group5-3	Group5-4
Group6-1	Group6-2	Group6-3	Group6-4
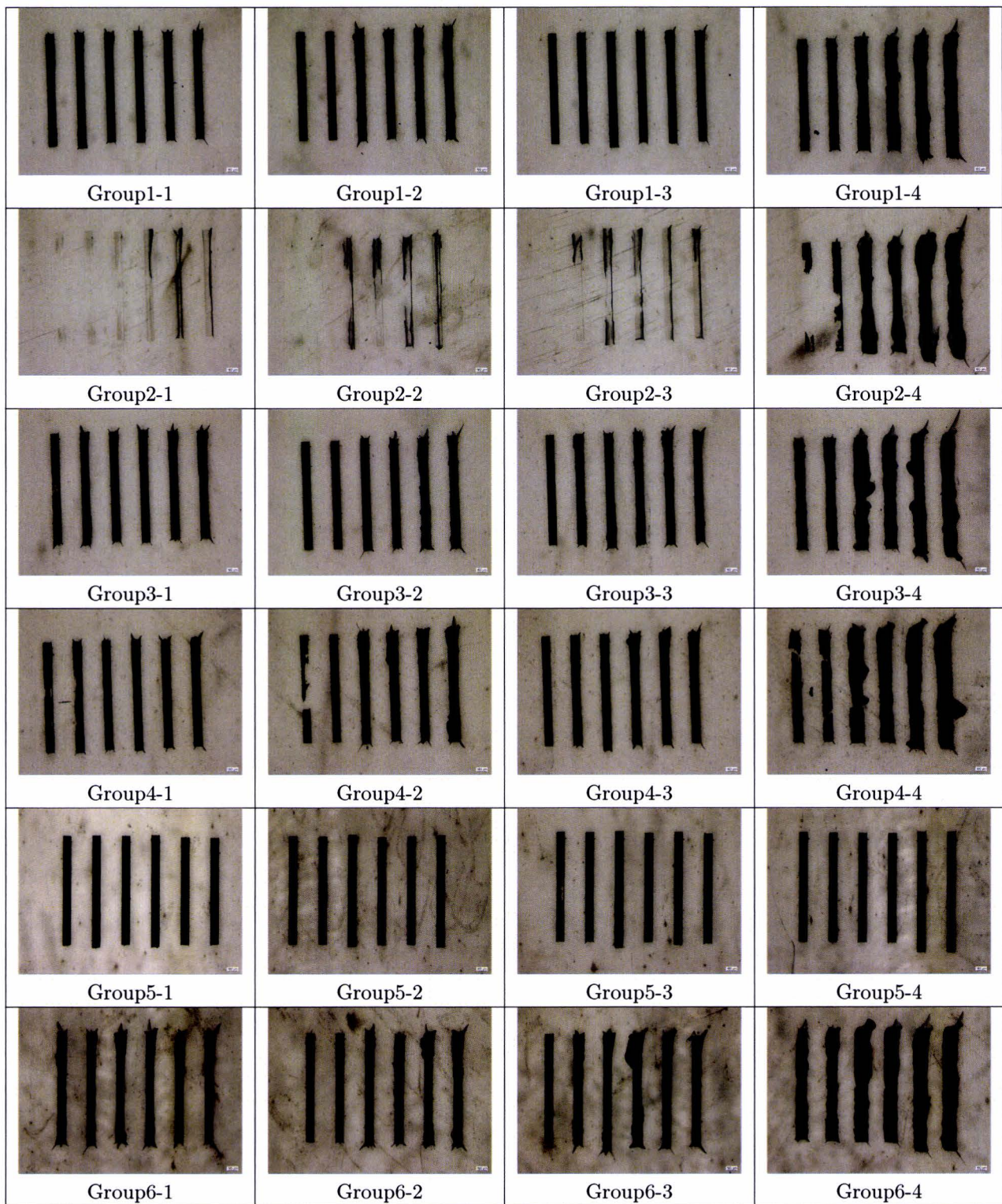
Table D.4: Pictures optic microscope after 4 minutes etching in 50 % concentrated HF.
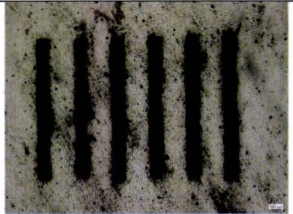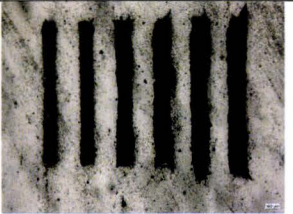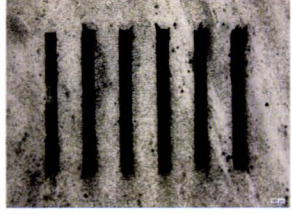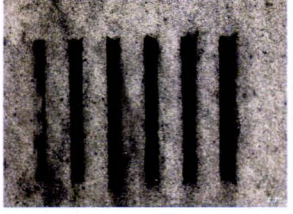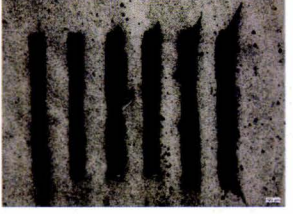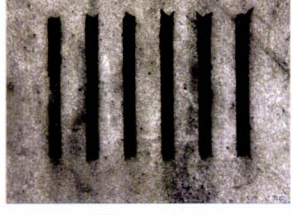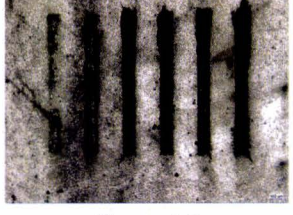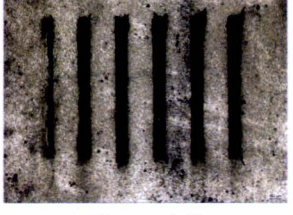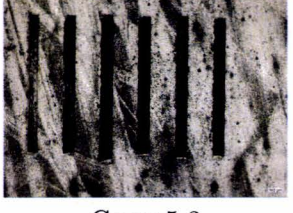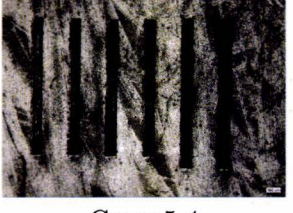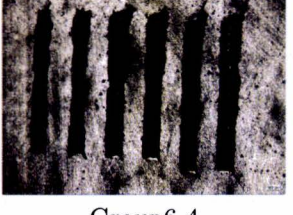
Table D.5: Pictures optic microscope after 20 minutes etching in 50 % concentrated HF.
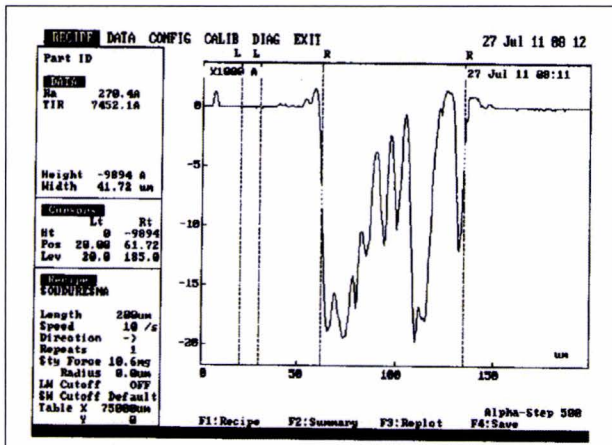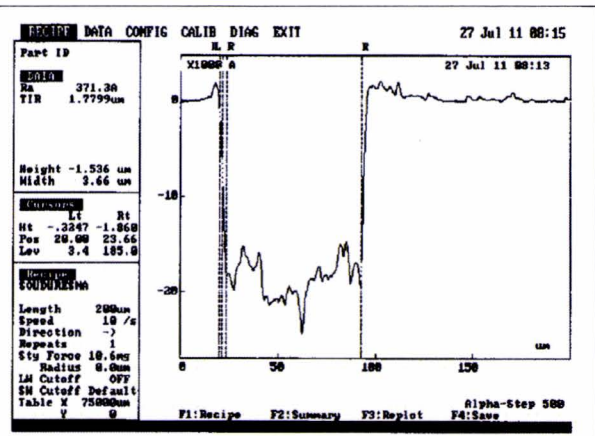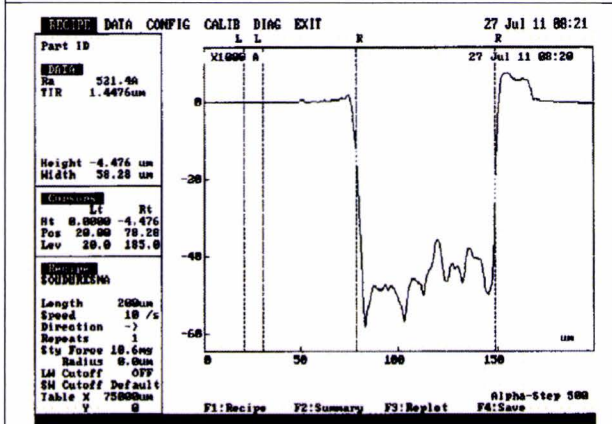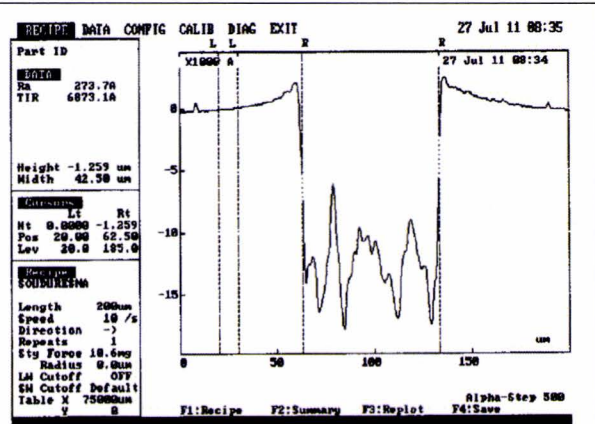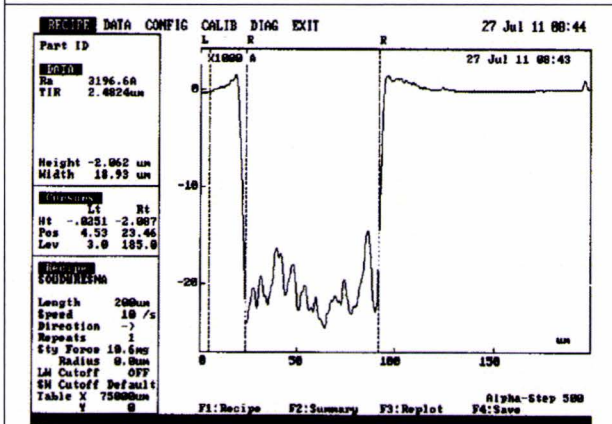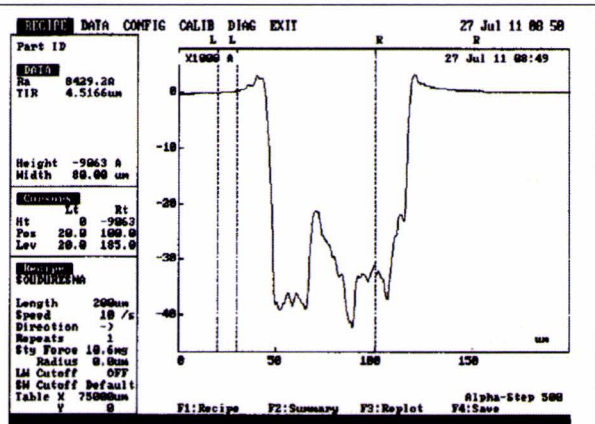
Table D.6: Alpha-step scans: the numbers correspond with the numbers in previous tables.
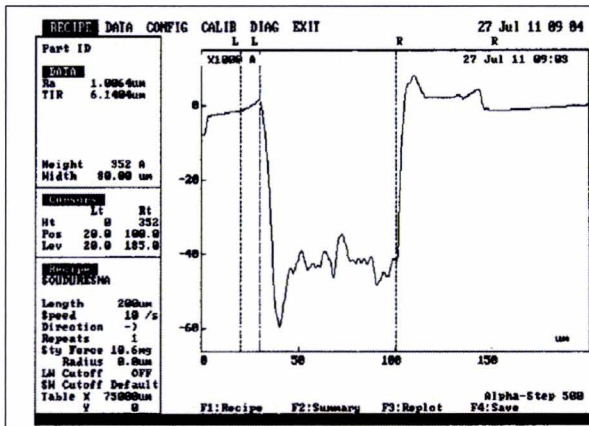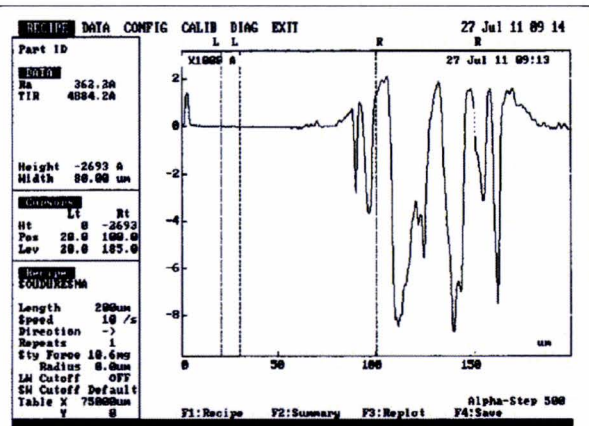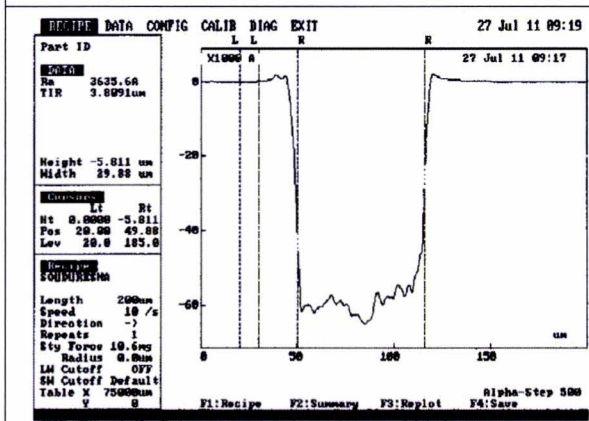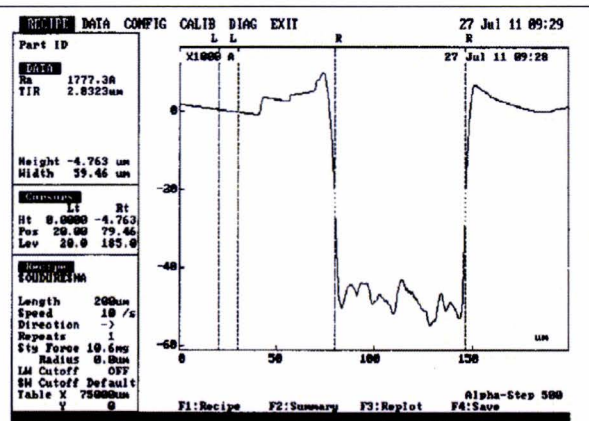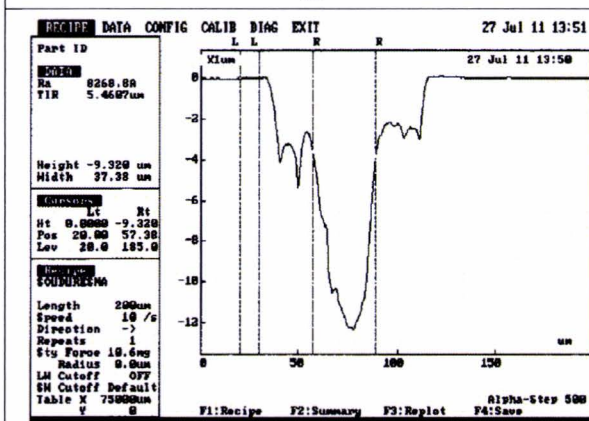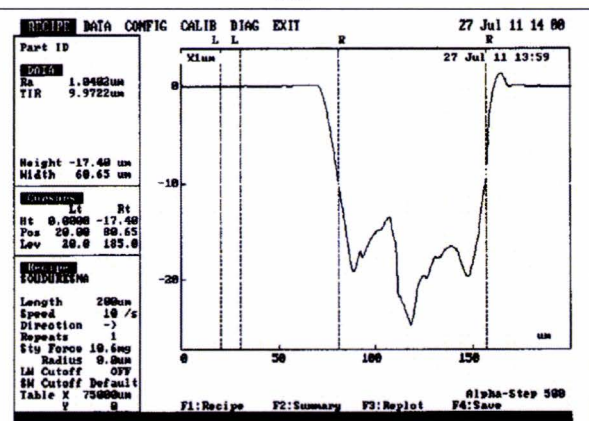
Table D.7: Alpha-step scans: the numbers correspond with the numbers in tables.
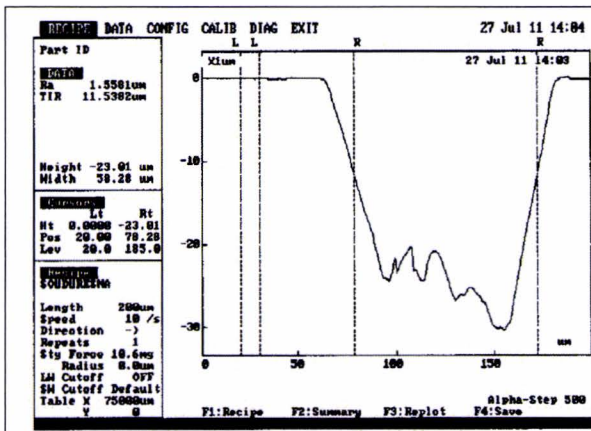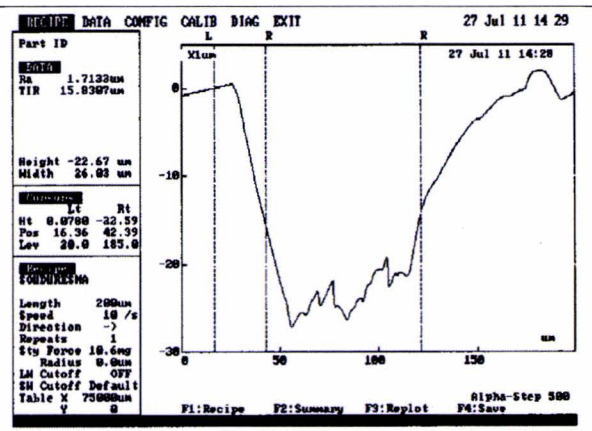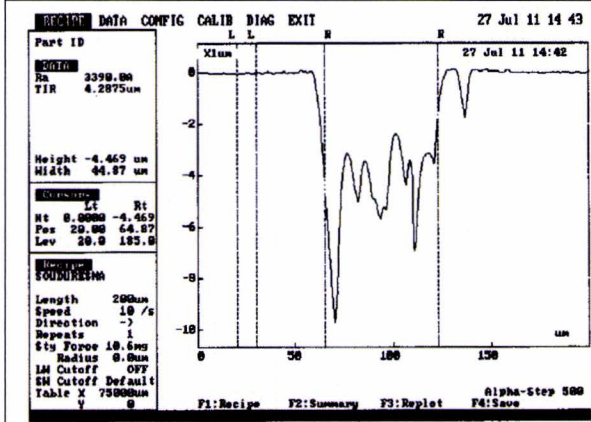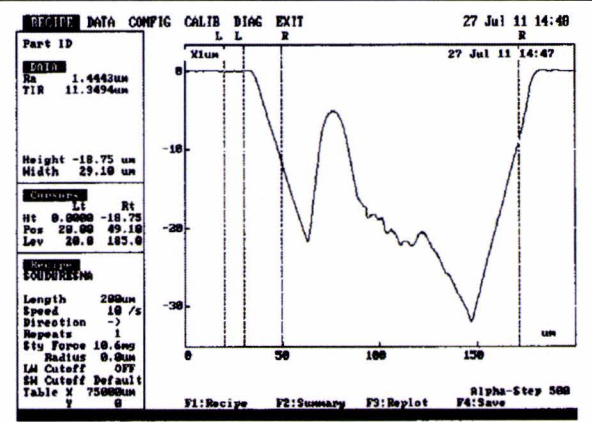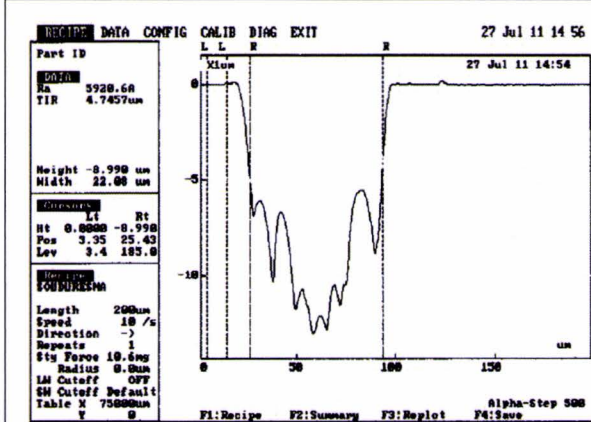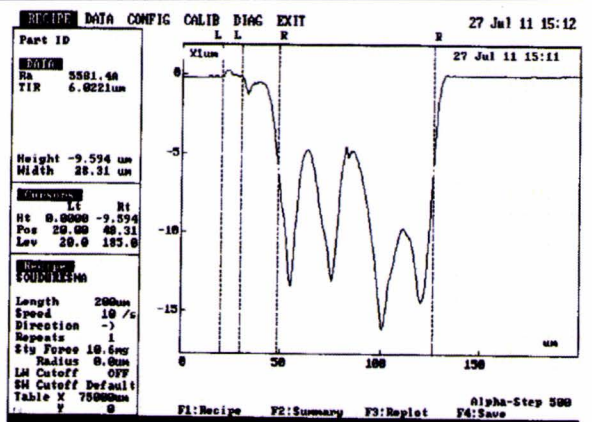
Table D.8: Alpha-step scans: the numbers correspond with the numbers in tables.
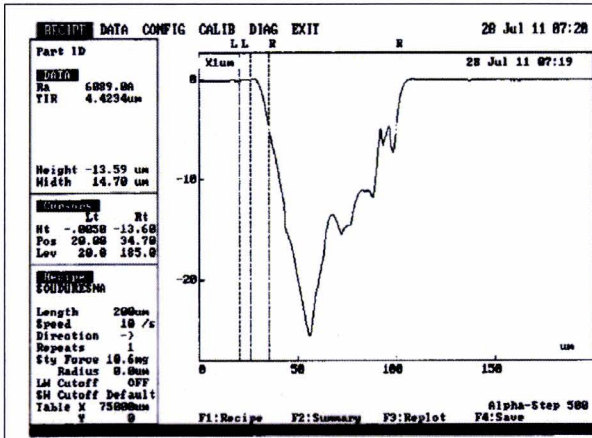
18.
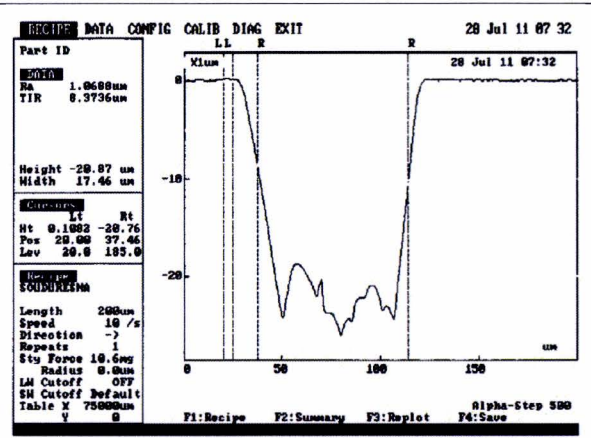
19.
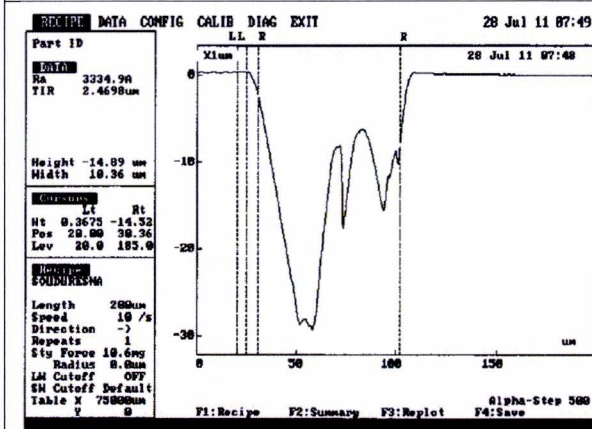
20.
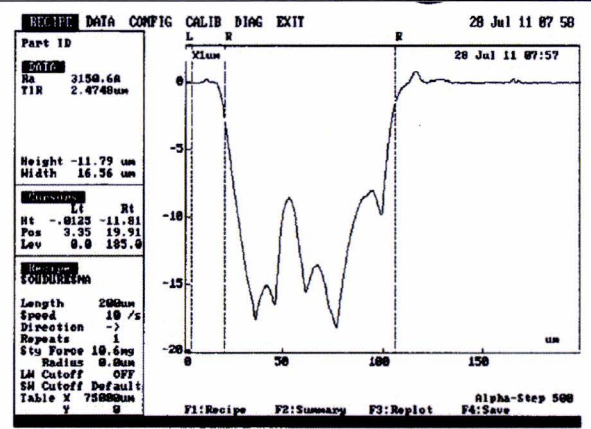
21.
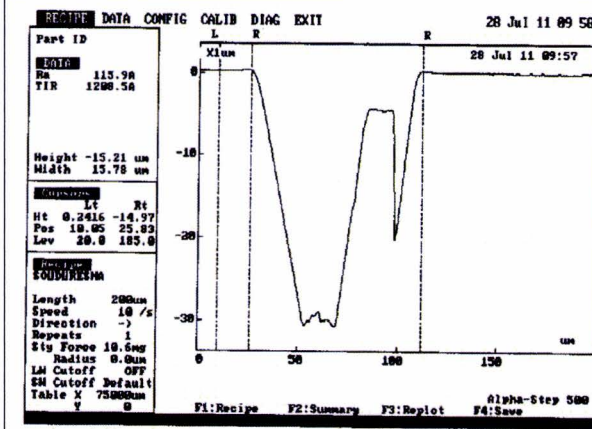
22.
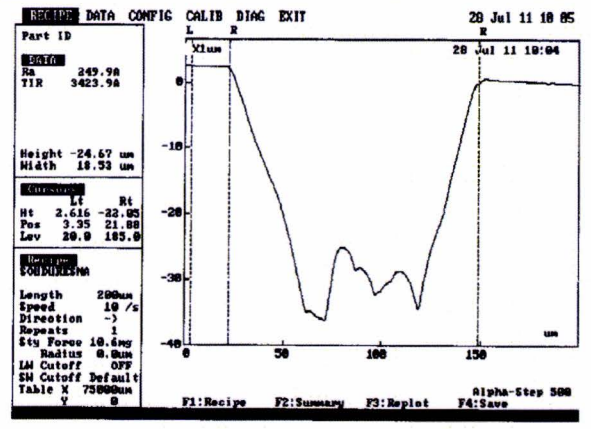
23.

Table D.9: Alpha-step scans: the numbers correspond with the numbers in tables.
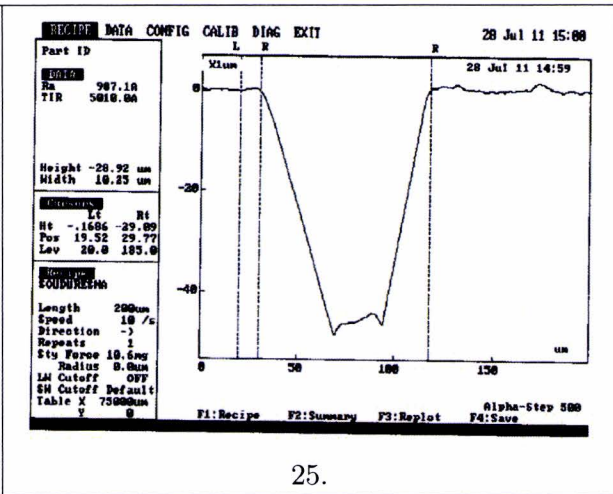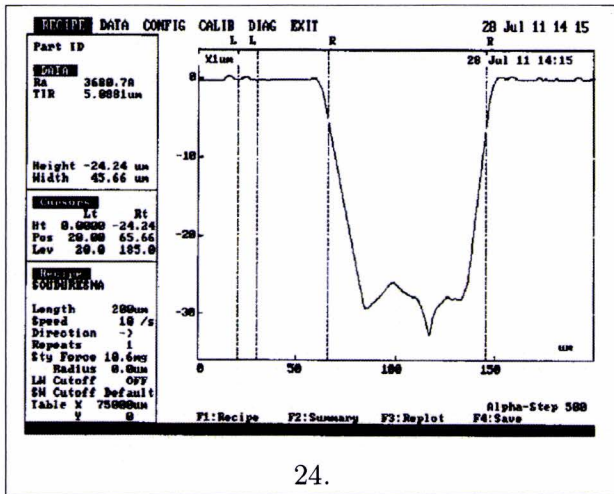
Table D.10: Alpha-step scans: the numbers correspond with the numbers in tables.

Appendix E

Quartz: results last experiments
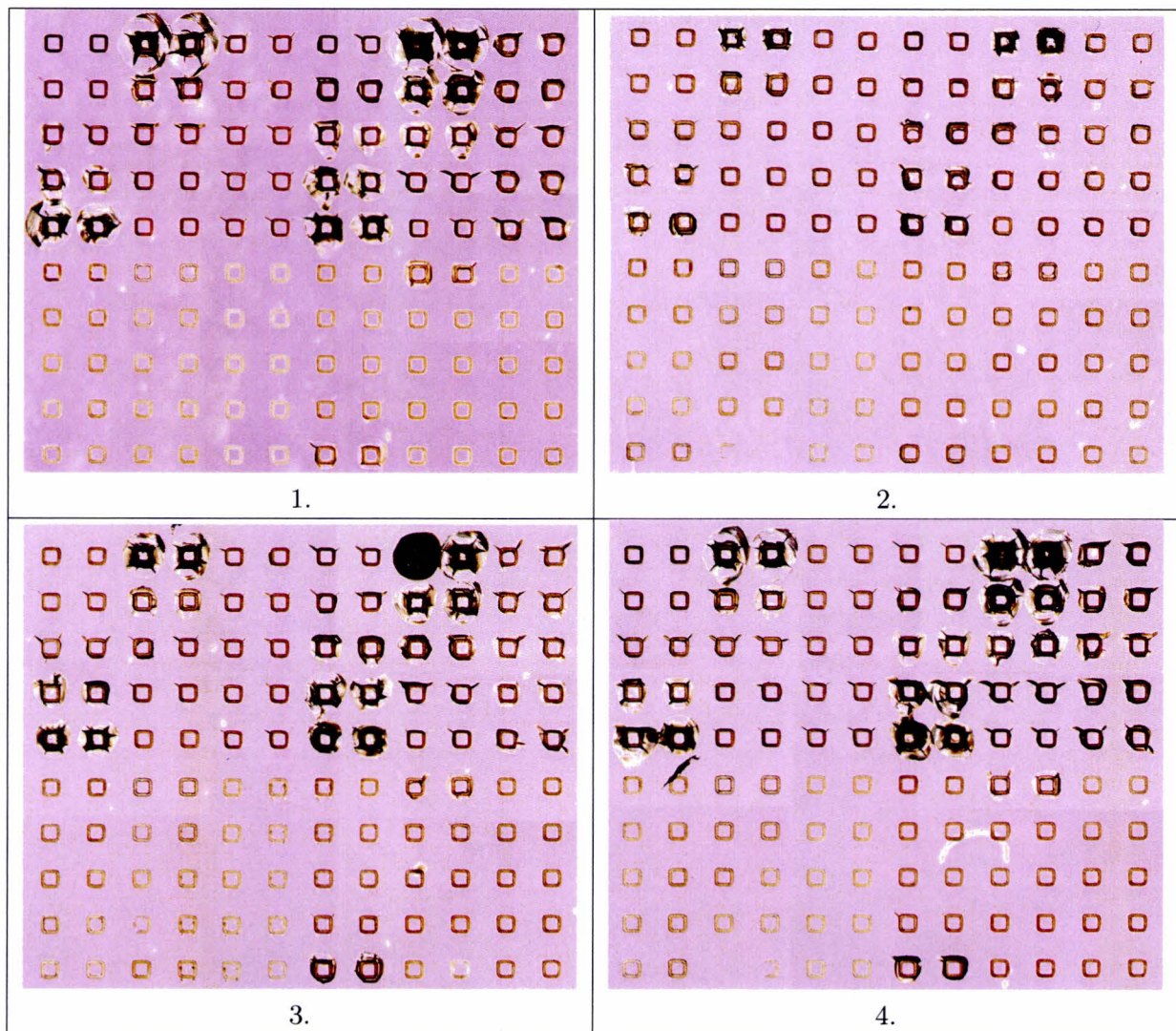
Table E.1: Pictures optic microscope after irradiation.

CONFIDENTIEL   Essais gravure laser fs (TU Eindhoven)   16/02/2012

Pictures done at Asulab and etching

The following pictures are taken with the orientation shown on the right and structures are on the visible surface. It is a mirror image (central symmetry) compared to the pictures done at Eindhoven and the plan in Figure 1, but it corresponds to the wafers descriptions.

1e (before etching)	1e (after 2 min etching)
1e_01_01 : 2 min : 3.8 um ; 4 min : 3.5 um	1e_03_02r : : 2 min : 2.2um ; 4 min : 2.1 um
2min_03_03 : 2 min : 1.6 um ; 4 min : 2.5 um	2min_05_10 : 2 min : 3 um ; 4 min : 3 um
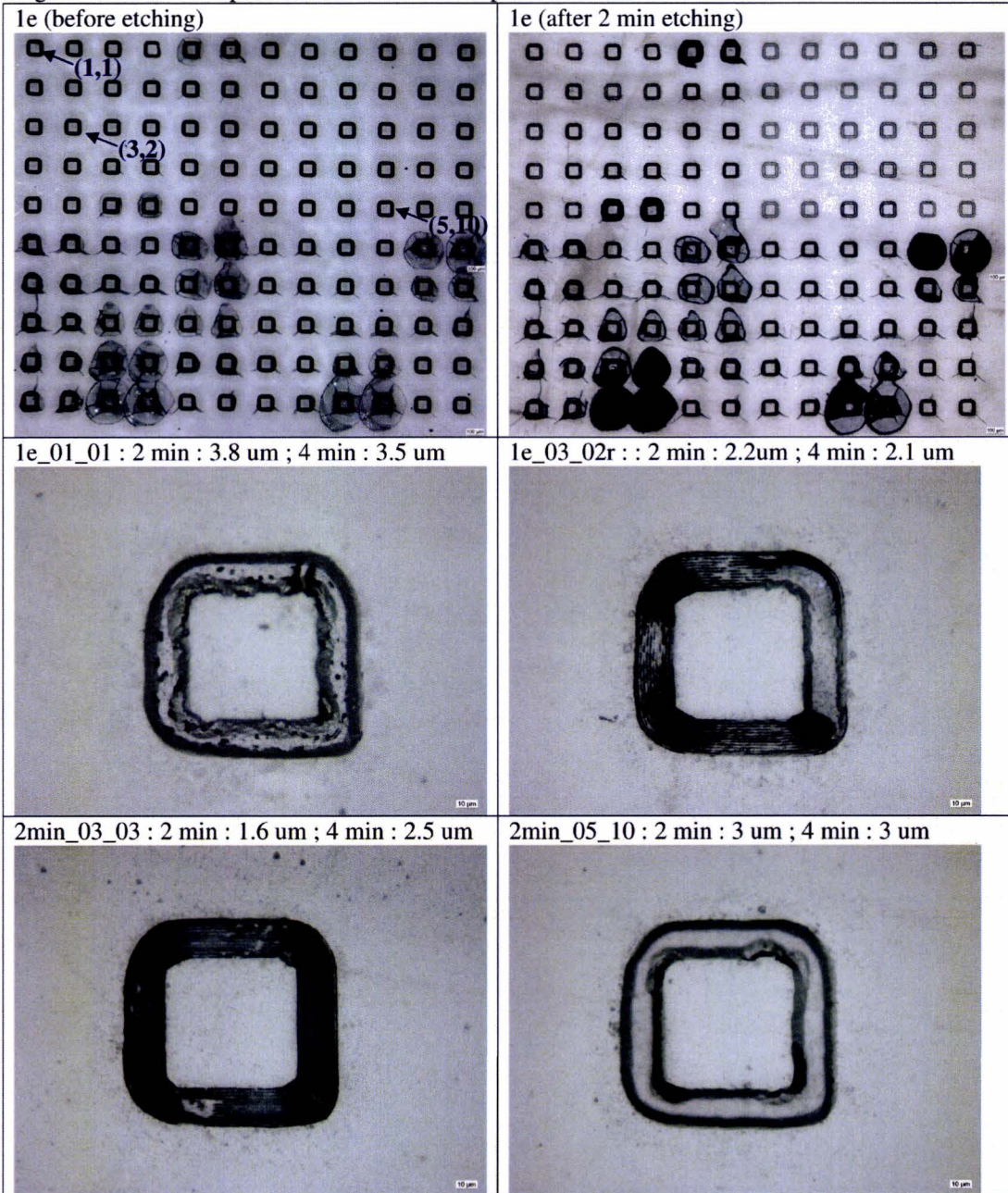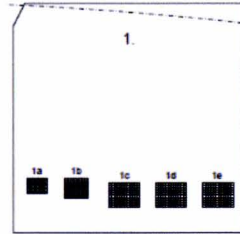
Figure 3: Pictures done at Asulab with depth measurements (picture after 2 min).

Figure E.1: Etching results by Asulab(1of2).

The structures are numbered from the upper left corner as shown on Figure 3. First some of the "nice looking" (without craks) structures have been measured by alpha-step. Etching 2 min more does not change much the depth of these structures.

Sample 2 has been sent to Micro Crystal to perform a 4 min etch in their bath to compare with our bath. The substrate thickness after etching is 481 um. The depth of the measured "nice looking structures" is similar to the one shown above. Both baths give similar results.

Some of the "cracked" structures have been measured as well and some can be deep! The final depth is often difficult to be measured by alpha-step because the width of the structures is too small (we have a 60° tip). For instance the (6;9) looks promising. (alpha step profiles are attached).

C:\DATA\EMIT\
FemtoDrill\quartz_20:

2a after 4 min etch at Micro Crystal

2a_06_09 : 4 min : 10 um

2a_09_10 : 4 min : 24 um
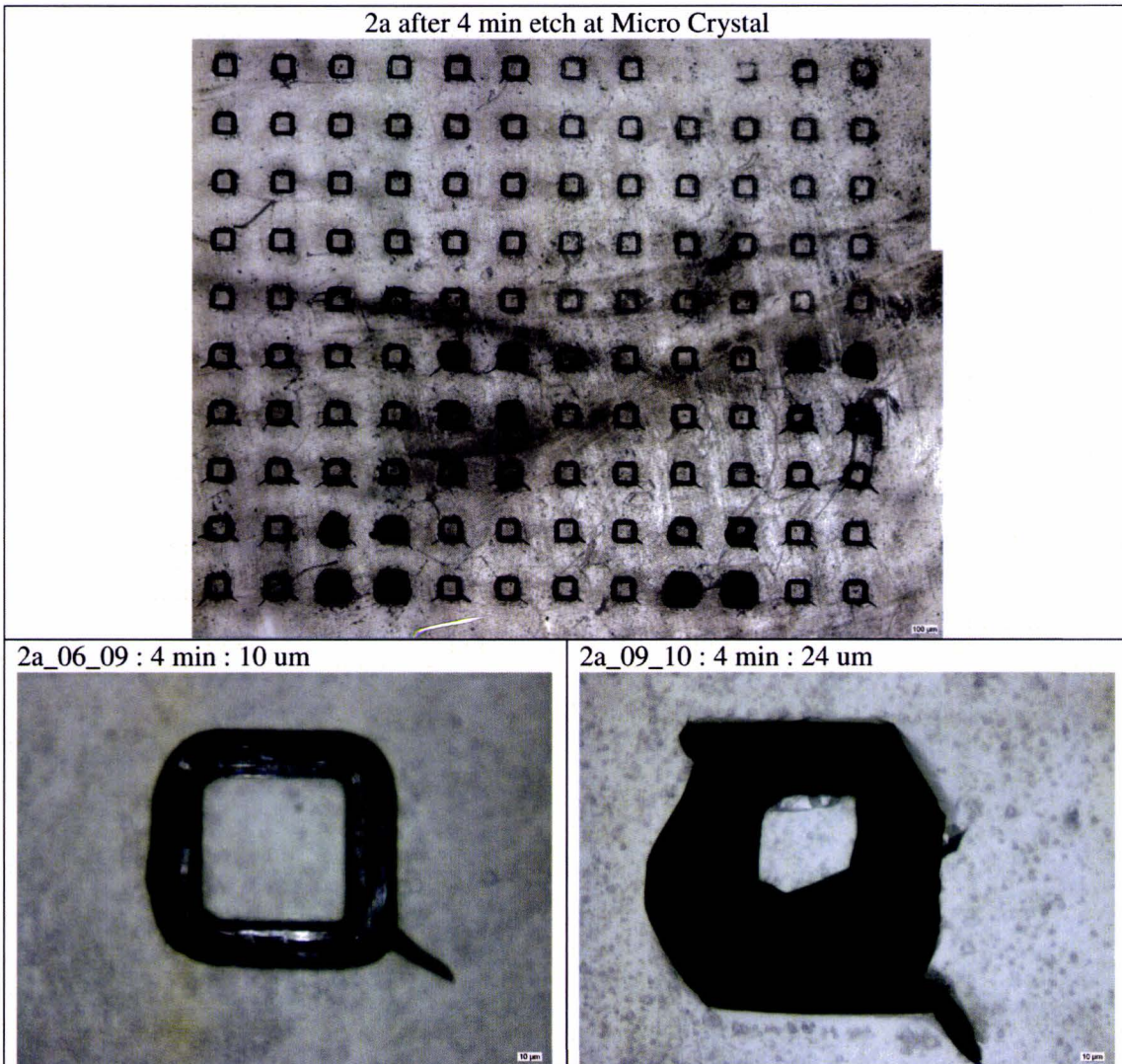
Figure 4: Pictures done at TU Eindhoven (before etching)
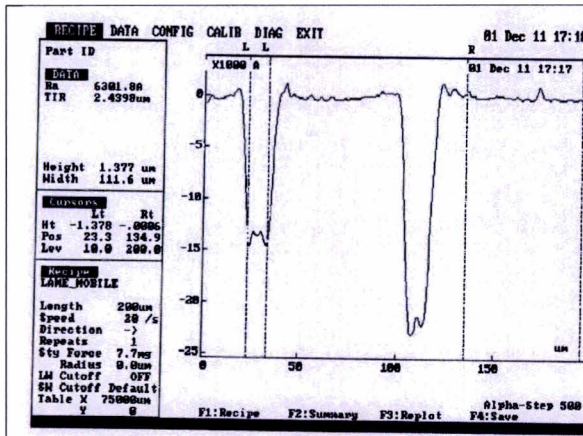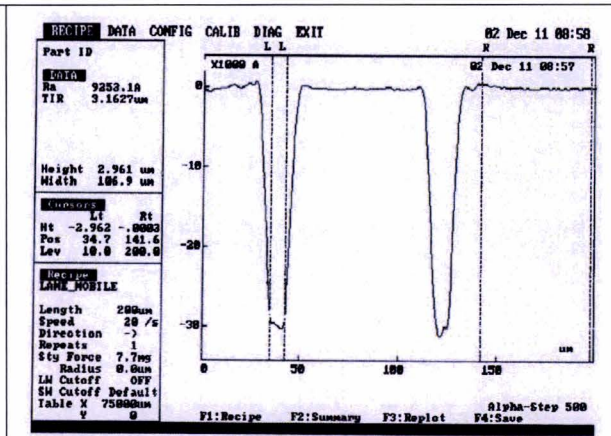
1e (3,2) for 2 min.	1e (5,11) for 2min.
2a (3,3) for ? min.	2a (6,9) for ? min.
2a (9,10) for ? min.	2a (10,12) for ? min.
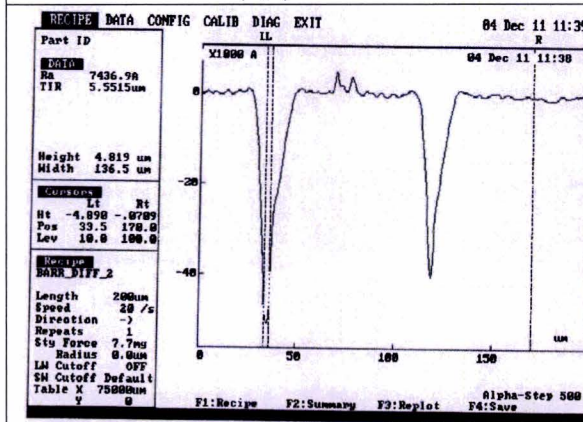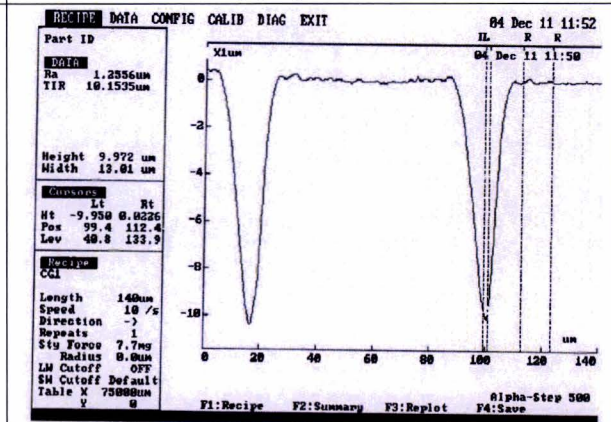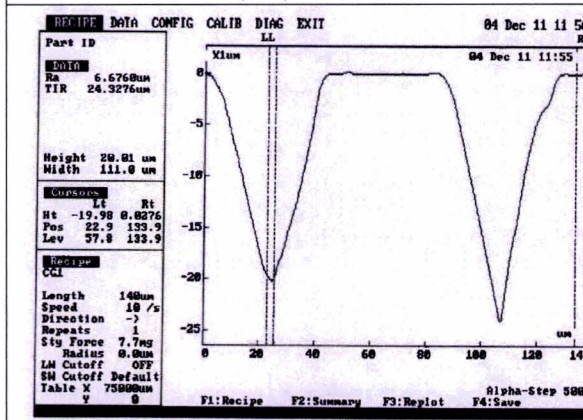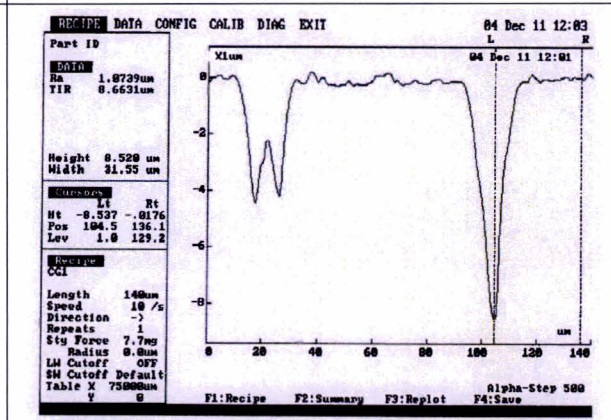
Table E.2: Alpha-step scans of the different structures.

Appendix F

Ruby: results first experiments

Group 5	Group 6	Group 7
n=1, from top to bottom a=10, a=20, a=30		
n=1, from top to bottom a=40, a=50, a=60		
n=1.66, from top to bottom a=10, a=20, a=30		
n=1.66, from top to bottom a=40, a=50, a=60		

Table F.1: Pictures optic microscope after irradiation.
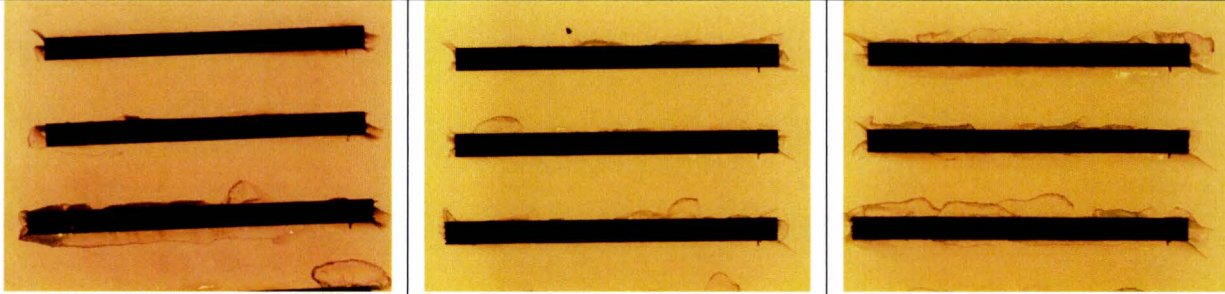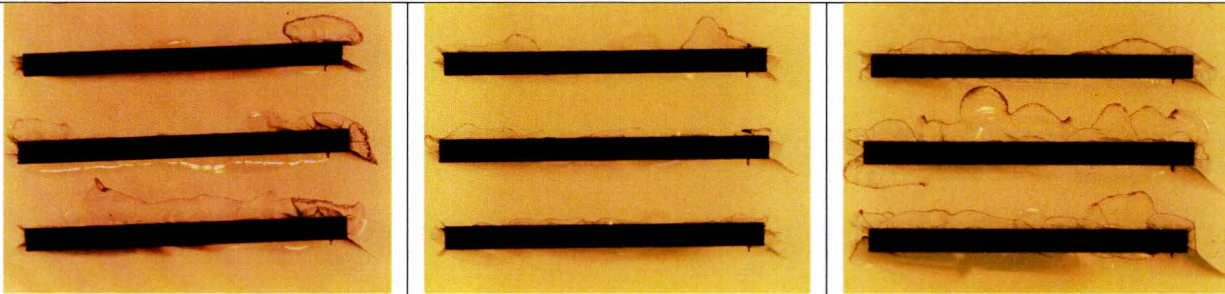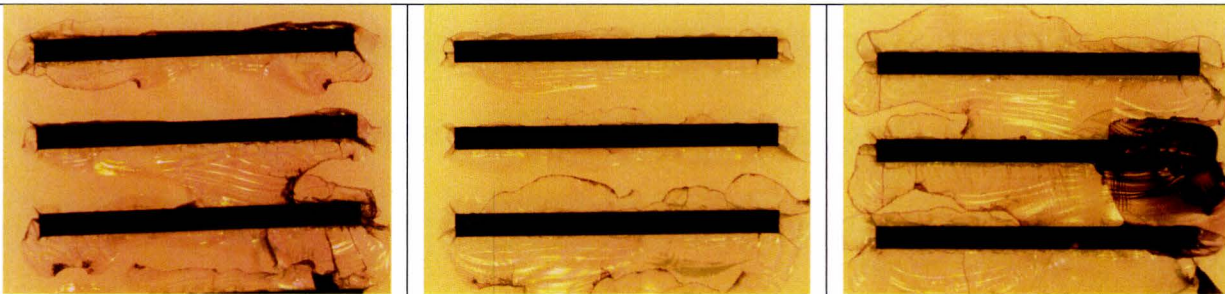
Group 5	Group 6	Group 7
n=1.25, from top to bottom a=10, a=20, a=30		
n=1.25, from top to bottom a=40, a=50, a=60		
n=1.2.5, from top to bottom a=10, a=20, a=30		
n=1.2.5, from top to bottom a=40, a=50, a=60		

Table F.2: Pictures optic microscope after irradiation.

Piece B, after irradiation

Group 5

a	b	c	d
	1 0,79		
	2 2,01	2 1,51	
	3 2,20	3 1,21	3 4,21
	4 1,58		4 3,59
	5 1,64		5 5,01
	6 1,30	6 0,86	6 4,36

Group 6

a	b	c	d
1 2,36	1 3,23		1 5,05
2 2,28	2 3,72		2 6,15
	3 3,22		
	4 2,24		
			5 6,34
			6 4,86

Group 7

a	b	c	d
1 1,77	1 2,69	1 2,02	1 5,79
2 1,72		2 1,85	2 8,01
	5 3,27		5 6,15
	6 2,70		6 5,65

Piece B, after 24 hour with 10% HF

Group 5

a	b	c	d
	1 0,96		
	2 2,43	2 1,70	
	3 2,75	3 1,37	3 6,62
	4 1,90		4 5,72
	5 2,14		5 6,02
	6 1,63	6 1,43	6 3,95

Group 6

a	b	c	d
1 2,60	1 3,08		1 17,52
2 2,59	2 3,88		2 4,70
	3 3,62		
	4 2,48		
			5 7,23
			6 11,60

Group 7

a	b	c	d
1 1,88	1 3,80	1 1,75	
2 1,95		2 1,85	
	5 2,38		
	6 6,53		

Piece B, after 24 hour with 10% HF and 7.22 hour with +50% HF

Group 5

a	b	c	d
	1 0,47		
	2 2,32	2 1,62	
	3 2,66	3 2,06	3 6,69
	4 1,64		4 5,68
	5 2,06		5 6,50
	6 1,44	6 1,54	6 2,80

Group 6

a	b	c	d
1 2,62	1 2,43		1 16,24
2 2,76	2 2,82		2 3,84
	3 3,39		
	4 2,74		
			5 15,11
			6 9,20

Group 7

a	b	c	d
1 1,76	1 3,80	1 1,62	
2 1,70		2 1,73	
	5 1,77		
	6 6,59		

Piece B, after 24 hour with 10% HF, 7.22 hour with +50% HF and 48 hours with 10% HF.

Group 5

a	b	c	d
	1 0,82		
	2 2,41	2 1,80	
	3 2,40	3 1,22	3 6,73
	4 1,71		4 5,49
	5 1,90		5 6,96
	6 1,46	6 1,58	6 2,80

Group 6

a	b	c	d
1 2,58	1 3,19		1 16,00
2 2,69	2 3,76		2 3,90
	3 3,66		
	4 2,56		
			5 15,11
			6 9,20

Group 7

a	b	c	d
1 1,79	1 2,40	1 1,55	
2 1,70		2 1,61	
	5 4,30		
	6 6,70		

Figure F.1: Etching depths of the structures.

Results substrate B

5A.
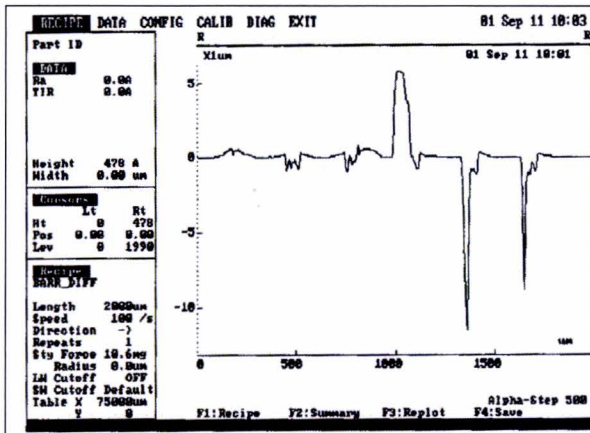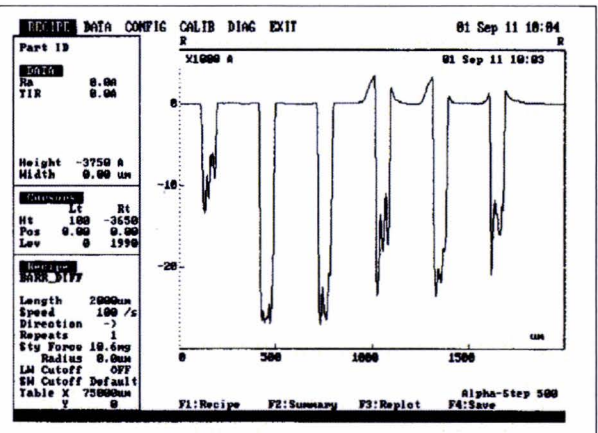
5B.
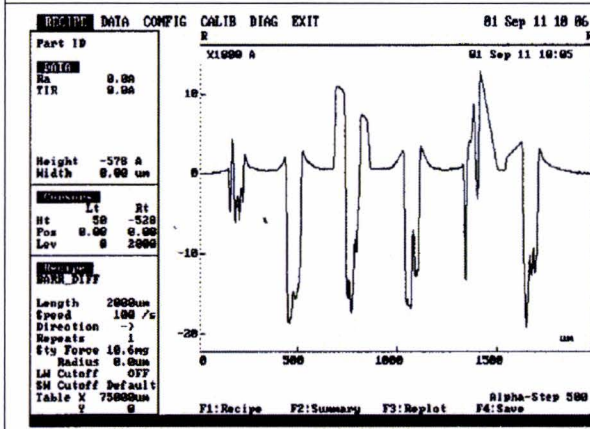
5C.
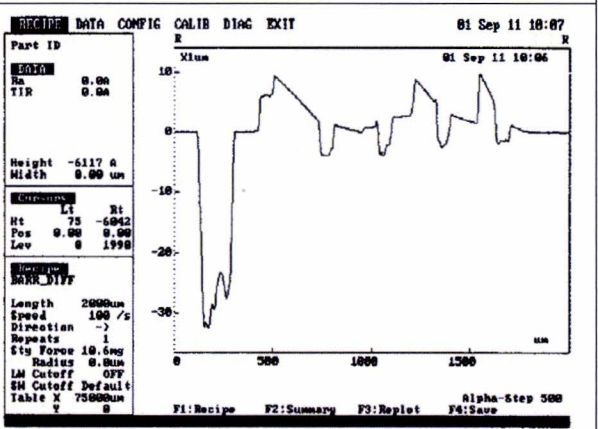
5D.
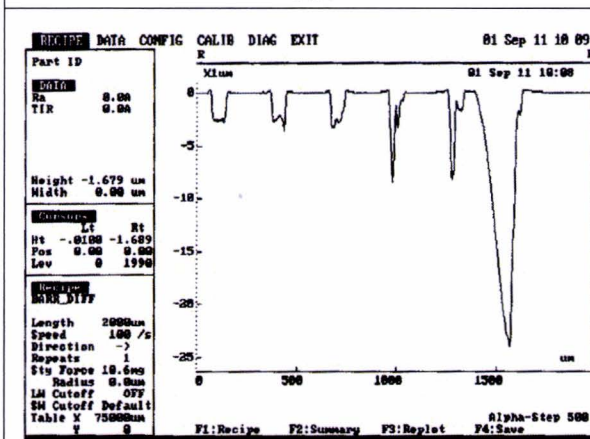
6A.
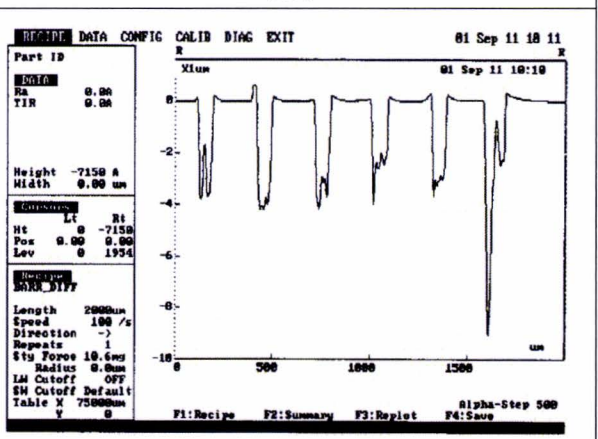
6B.

Table F.3: Alpha-step scans after 50% HF: the numbers correspond with the group (sub)numbers in previous table measured from 1 to 6.
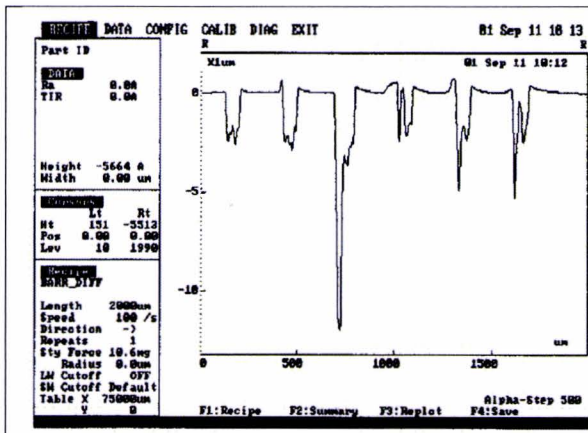
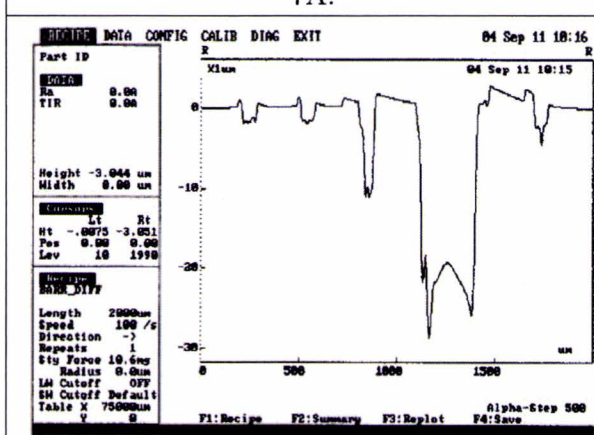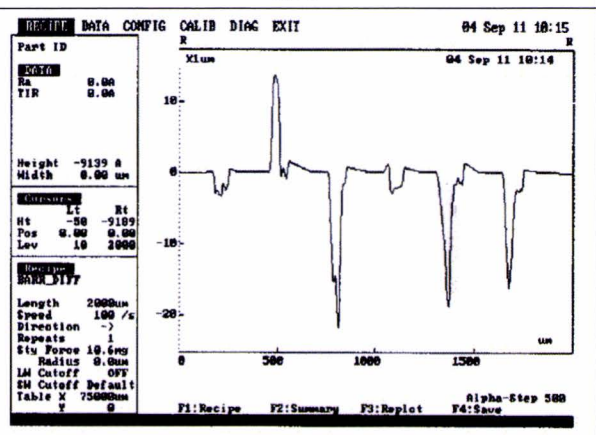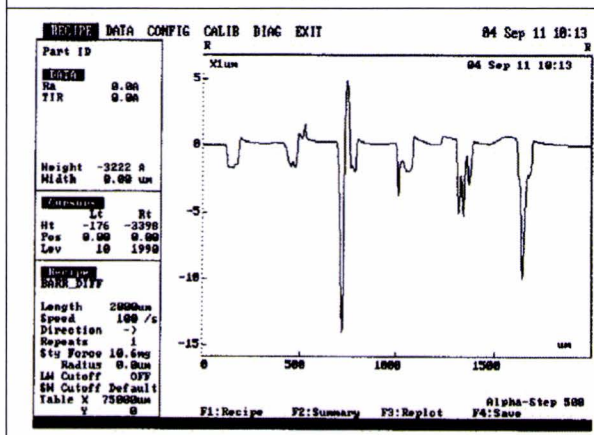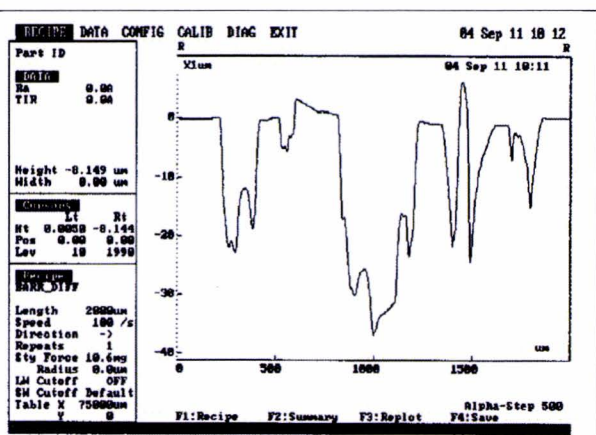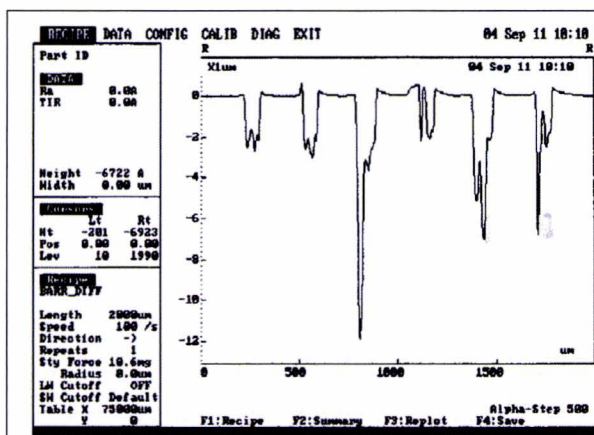6C.
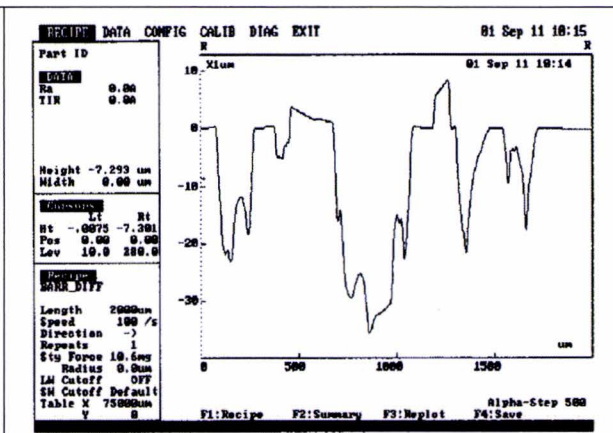
6D.
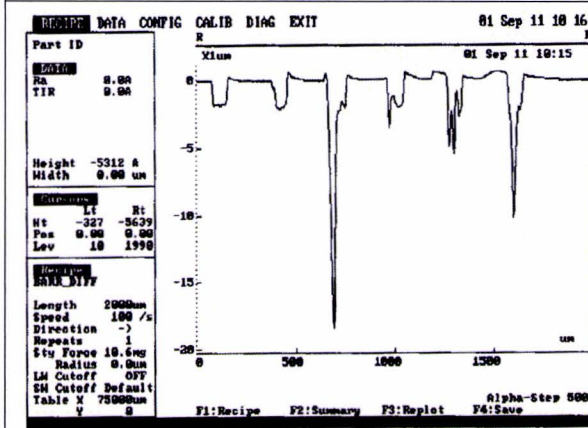
7A.
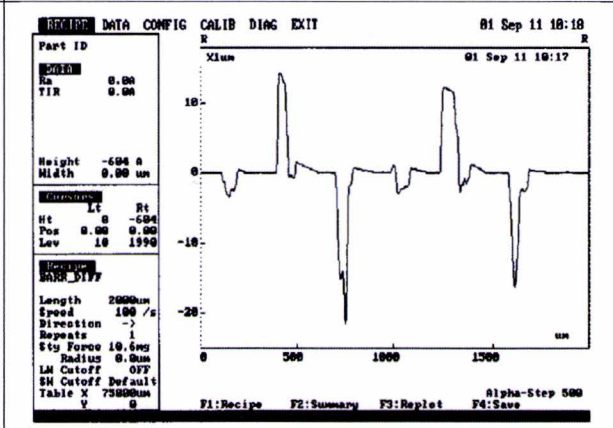
7B.
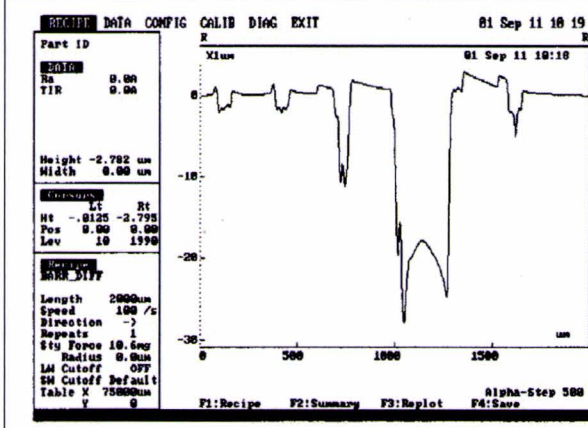
7C.
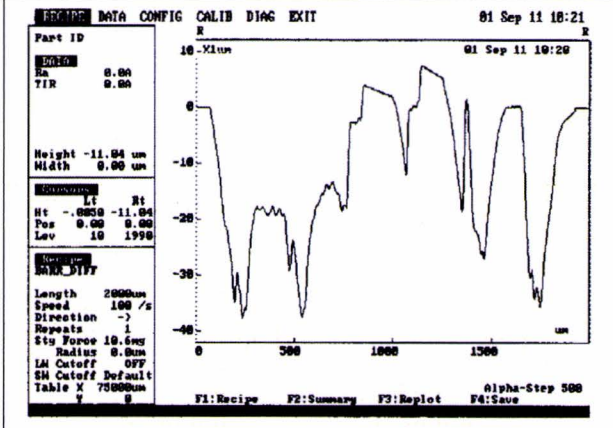
7D.

Table F.4: Alpha-step scans after 50% HF: the numbers correspond with the group (sub)numbers in previous table measured from 1 to 6.

5A.
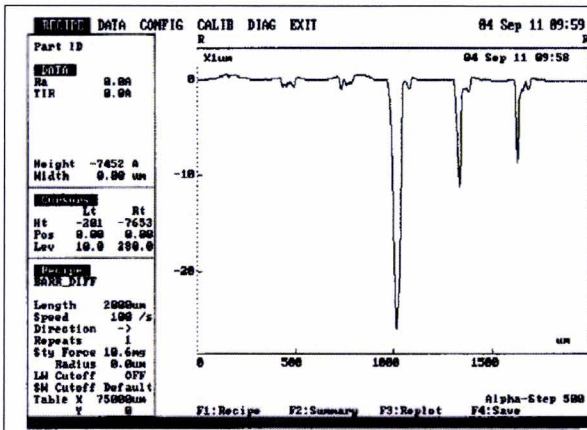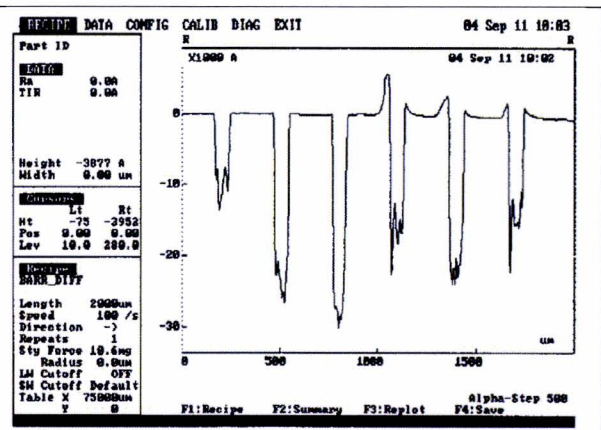
5B.
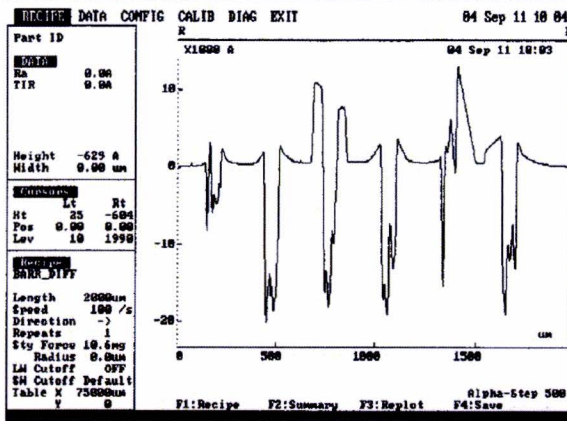
5C.
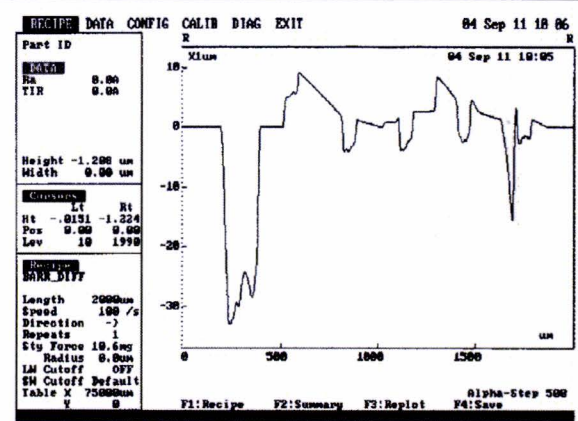
5D.
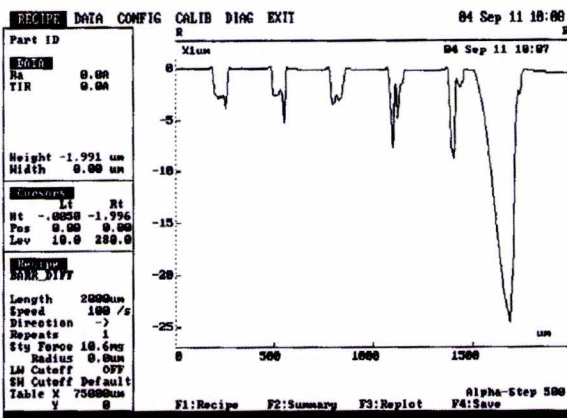
6A.
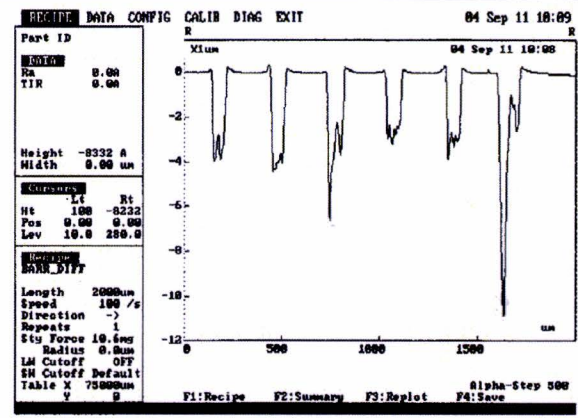
6B.

Table F.5: Alpha-step scans after 48 hours 10% HF: the numbers correspond with the group (sub)numbers in previous table measured from 1 to 6.
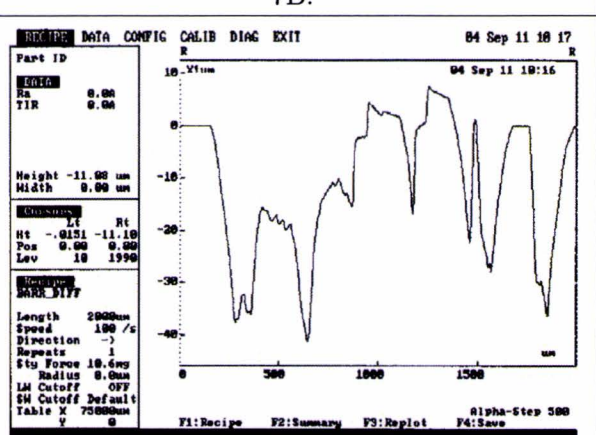
Table F.6: Alpha-step scans after 48 hours 10% HF: the numbers correspond with the group (sub)numbers in previous table measured from 1 to 6.

Results substrate C

Depths and comments, alpha-step 500 [GROUP 12], with Al etchant, room temperature

Parameters: n=1,66; z=6; Ep=150mW ; pol=0degrees ; 90degrees with scratch (before etching)

a	f(kHz)	V (mm/s)	1e D (um)	Edges	Edges	Bottom	Cracks	2e D (um)	Edges	Edges	Bottom	Cracks	3e D (um)	Edges	Edges	Bottom	Cracks	4e D (um)	Edges	Edges	Bottom	Cracks
10	100	16,6	1,865	High	High	Reas.	Few	1,231	Low	Low	R&decr.	Many	1,838	V low	V low	1e:R(1,5), 2e:reas(2,5)	None	0,848	V high	V high	R&decr.	Many
20	200	16,6	1,893	Low	High	Reas.	Few	0,934	High	High	R&mount.	Many	1,339	Low	Low	R but same height	Few	0,617	V high	V high	R,2e deep	Many
30	400	22,1	1,156	Low	Low	R&decr.	Many	0,976	High	High	R&decr.	Many	0,816	V high	V high	Rough & mountain	Many	0,763	V high	V high	Reas.	Many

Parameters: n=1,66; z=6; Ep=150mW ; pol=0degrees ; 90degrees with scratch (after 5 min etching)

a	f(kHz)	V (mm/s)	1e D (um)	Edges	Edges	Bottom	Cracks	2e D (um)	Edges	Edges	Bottom	Cracks	3e D (um)	Edges	Edges	Bottom	Cracks	4e D (um)	Edges	Edges	Bottom	Cracks
10	100	16,6	1,808	High	High	Reas.	Few	1,304	Low	Low	R&decr.	Many	1,805	Low	Low	2 plat, 1.1 & 1.5	None	1,075	V high	V high	R&decr.	Many
20	200	16,6	1,85	High	Low	Rough	Few	1,206	Low	Low	R&decr.	Many	1,412	Low	Low	Rough	Few	1,047	Low	V high	2plat, 0,7&2.5	Many
30	400	22,1	1,206	Low	Low	Ruw&decr.	Many	1,042	High	High	Very rough	Many	0,969	V High	V high	Rough 2e lower(1.5)	Many	0,932	Low	V high	Reas.	Many

Parameters: n=1,66; z=6; Ep=150mW ; pol=0degrees ; 90degrees with scratch (after 10 min etching)

a	f(kHz)	V (mm/s)	1e D (um)	Edges	Edges	Bottom	Cracks	2e D (um)	Edges	Edges	Bottom	Cracks	3e D (um)	Edges	Edges	Bottom	Cracks	4e D (um)	Edges	Edges	Bottom	Cracks
10	100	16,6	1,833	High	High	Reas.	Few	1,246	High	High	R&decr.	Many	1,79	V low	V low	2 plat. 1.5&2.5	None	1,08	Low	High	decr.	Many
20	200	16,6	1,984	Low	High	Reas.	Few	1,148	High	High	R&mount	Many	1,402	V low	V low	very rough	Few	1,067	Low	Low	2 plat. 0.8&1.5	Many
30	400	22,1	1,216	Low	Low	2 plat. 0.9&1.5	Many	1,171	Low	High	very Rough	Many	0,957	Low	High	2 plat. 0.7&1.8	Many	0,861	Low	V high	very high peak	Many

Parameters: n=1,66; z=6; Ep=150mW ; pol=0degrees ; 90degrees with scratch (after 30 min etching)

a	f(kHz)	V (mm/s)	1e D (um)	Edges	Edges	Bottom	Cracks	2e D (um)	Edges	Edges	Bottom	Cracks	3e D (um)	Edges	Edges	Bottom	Cracks	4e D (um)	Edges	Edges	Bottom	Cracks
10	100	16,6	1,989	med	med	Reas.	Few	1,508	low	low	R&decr.	Many	1,961	low	low	decr.	None	1,264	log	high	decr. 1^2	Many
20	200	16,6	2,01	low	low	Reas.	Few	1,413	low	low	R&mount	Many	1,528	low	low	good	Few	1,219	low	low	2 plat 1&1.6	Many
30	400	22,1	1,392	low	low	2 plat 1&1.7	Many	1,377	low	high	Very rough	Many	1,218	low	V high	2 plat 1&1.8	Many	1,113	low	v high	good	Many

Figure F.2: Depths before etching and after 5, 10 and 30 minutes.

Parameters: n=1,66; z=6; Ep=150mW ; pol=0degrees ; 90degrees with scratch (after 60 min etching)

a	f(kHz)	V (mm/s)	1e D(um)	Edges		Bottom	Cracks	2e D(um)	Edges		Bottom	Cracks	3e D(um)	Edges		Bottom	Cracks	4e D(um)	Edges		Bottom	Cracks
10	100	16,6	2,199	low	low	Reas.	Few	1,702	low	low	R&decr.	Many	2,067	low	low	2 plat 1.5&2.5	None	1,463	low	high	2 plat, 1.1^2.1	Many
20	200	16,6	2,228	low	high	Reas.	Few	1,576	low	low	R&mount	Many	1,651	low	low	reas	Few	1,619	low	low	2 plat 1.5&2.0	Many
30	400	22,1	1,611	low	low	2 plat 1.2&1.9	Many	1,558	low	V High	Very rough	Many	1,438	low	V high	moutain	Many	1,387	low	V high	reas	Many

Parameters: n=1,66; z=6; Ep=150mW ; pol=0degrees ; 90degrees with scratch (after 90 min etching)

a	f(kHz)	V (mm/s)	1e D(um)	Edges		Bottom	Cracks	2e D(um)	Edges		Bottom	Cracks	3e D(um)	Edges		Bottom	Cracks	4e D(um)	Edges		Bottom	Cracks
10	100	16,6	2,112	Med	Med	Reas.	Few	1,782	low	High	R&decr.	Many	2,062	low	low	2 plat 1.5&2.5	None	1,48	low	V high	2 plat, 1.1^2.1	Many
20	200	16,6	2,23	low	low	rough	Few	1,692	low	low	R&mount	Many	1,717	low	low	good	Few	1,73	low	V high	mountain	Many
30	400	22,1	1,546	low	VH	2 plat 1&2	Many	1,624	low	V H	Very rough	Many	1,601	low	B high	moutain	Many	1,322	High	V high	reas	Many

Parameters: n=1,66; z=6; Ep=150mW ; pol=0degrees ; 90degrees with scratch (after 150 min etching)

a	f(kHz)	V (mm/s)	1e D(um)	Edges	Bottom	Cracks	2e D(um)	Edges	Bottom	Cracks	3e D(um)	Edges	Bottom	Cracks	4e D(um)	Edges	Bottom	Cracks
10	100	16,6	2,203			Few	1,762			Many	2,142			None	1,531			Many
20	200	16,6	2,210			Few	1,772			Many	1,775			Few	1,780			Many
30	400	22,1	1,649			Many	1,641			Many	1,538			Many	1,485			Many

Parameters: n=1,66; z=6; Ep=150mW ; pol=0degrees ; 90degrees with scratch (after 270 min etching)

a	f(kHz)	V (mm/s)	1e D(um)	Edges	Bottom	Cracks	2e D(um)	Edges	Bottom	Cracks	3e D(um)	Edges	Bottom	Cracks	4e D(um)	Edges	Bottom	Cracks
10	100	16,6	2,115			Few	1,818			Many	2,130			None	1,480			Many
20	200	16,6	2,226			Few	1,599			Many	1,735			Few	1,830			Many
30	400	22,1	1,641			Many	1,606			Many	1,566			Many	1,490			Many

Figure F.3: Depths after 60, 90, 150 and 270 minutes.

Results substrate D

Comments, optic microscope (after irradiation)

Parameters: n=1,66; z=6; Ep=150mW ; pol=90degrees ; 90degrees with scratch

a	f(kHz)	V(mm/s)	1e	2e	3e	4e
10	100	16,6		Cracks/part under surf?	Cracks/part under surf?	Reasonable
20	200	16,6		Cracks/part under surf!(-)	Cracks/part under surf!(-)	Under surf. (-)
30	400	22,1	no sharp edge	Cracks/part under surf?		Under surf. (-)

Parameters: n=1,66; z=6; Ep=150mW ; pol=90degrees ; 0degrees with scratch

a	f(kHz)	V(mm/s)	1e	2e	3e	4e
10	100	16,6	Not compl.	Not compl./Part under surf!(-)	Not compl.	Cracks/part under surf?
20	200	16,6			Reasonable/Part under surf?	Not compl./Part under surf?
30	400	22,1		Part under surf!(-)		Cracks/Not compl./under surf!(-)

Parameters: n=1,66; z=6; Ep=150mW ; pol=0degrees ; 90degrees with scratch

a	f(kHz)	V(mm/s)	1e	2e	3e	4e
10	100	16,6			Missed a big spot	Not compl.
20	200	16,6				
30	400	22,1	Under surf!(-)	Under surf!(-)		

Parameters: n=1,66; z=6; Ep=150mW ; pol=0degrees ; 0degrees with scratch

a	f(kHz)	V(mm/s)	1e	2e	3e	4e
10	100	16,6				Not compl.
20	200	16,6				
30	400	22,1			Cracks/ under surf!(-)	Cracks/ under surf!(-)

Figure F.4: Comments on the surface viewed by optic microscope.

Depths and comments, alpha-step 500 - After irradiation

Parameters: n=1,66; z=6; Ep=150mW ; **pol=90degrees ; 90degrees with scratch**

a	f(kHz)	V (mm/s)	D (um)	1e	Fig	D (um)	2e	Fig	D (um)	3e	Fig	D (um)	4e	Fig
10	100	16,6	1,26		1	1,1			1,25			0,93		
20	200	16,6	0,98			0,56	H. Upr. Eg.	2	0,74	Decr. D=1,4>0,2		0,83	Very R.	
30	400	22,1	0,89	Incr. D=0,4>1,4		0,68	Bottom very R.		0,86	Very R.		X	Upr. Mat, no D	3

Parameters: n=1,66; z=6; Ep=150mW ; **pol=90degrees ; 0degrees with scratch**

a	f(kHz)	V (mm/s)	D (um)	1e	Fig	D (um)	2e	Fig	D (um)	3e	Fig	D (um)	4e	Fig
10	100	16,6	0,58	Very R.		0,1	Bad, no D., H upr. Eg.		0,4	Reas., L. Upr. Eg.,		0,3	L. Upr Eg, very R, P.ab.Surf
20	200	16,6	0,15	Not compl.	4	0,47	Very R. L. Upr. Eg.		0,36	L. Upr Eg, very R, P.ab.Surf		0,23	Bad, P.ab.Surf.
30	400	22,1	0,3	Very R., P. ab. Surf.	X		No D., P. ab. Surf.		0,37	L. Upr. Eg, very R, P.ab.Surf	X		U. Surf, no D.

Parameters: n=1,66; z=6; Ep=150mW ; **pol=0degrees ; 90degrees with scratch**

a	f(kHz)	V (mm/s)	D (um)	1e	Fig	D (um)	2e	Fig	D (um)	3e	Fig	D (um)	4e	Fig
10	100	16,6	0,51	L.Upr.Eg, very R, 2P.ab.Surf		0,43	L.Upr.Eg, very R, P.ab.Surf.		0,5			0,5	Big plat, L.Upr.Eg	
20	200	16,6	0,95	Incr. D=0,2>1,7		1,21		5	0,48			0,44	Very R, H.upr.Eg, 1P.ab.Surf	
30	400	22,1	0,55	SS(2), H.Upr.Eg,		0,57	SS(2), H.Upr.Eg, bottom reas.		0,6	Incr. D=0,5>1,0		0,37	H.upr.Eg, 1P.ab.Surf	

Parameters: n=1,66; z=6; Ep=150mW ; **pol=0degrees ; 0degrees with scratch**

a	f(kHz)	V (mm/s)	D (um)	1e	Fig	D (um)	2e	Fig	D (um)	3e	Fig	D (um)	4e	Fig
10	100	16,6	0,67	SS(6),very R, H.upr.Eg		0,62	SS(6),very R, H.upr.Eg		0,58	H.upr.Eg, 2P.ab.Surf		0,62	L.upr.Eg, 3P.ab.Surf	
20	200	16,6	0,75	H.Upr.Eg	6	0,76	SS(6),very R, H.upr.Eg, 1P.ab.Surf		0,66	H.upr.Eg		0,63	SS(6), 2P.ab.Surf	
30	400	22,1	0,61	SS(6),very R, H.upr.Eg		0,49	SS(6),very R, H.upr.Eg, 1P.ab.Surf		X	No D, U. Surf		X	Only peaks above Surf	

Reas.	Reasonable	H. Upr. Eg.	High upright Edges	Upr. Mat	Uprisinh material
Incr. D	Increasing depth	L. Upr. Eg.	Low upright Edges	no D.	no depth
Decr. D	Decreasing depth	Very R.	Very rough	SS(1)	Same shape as picture (1)
U. Surf.	Under surface	Not compl.	Not complete		
Big plat	Big plateau	P. ab. Surf.	Peaks above surface		

| | Depths and comments, alpha-step 500, After 5 min etching with HF, 84 graden celcius | | | | | | | | | | | | | |

Parameters: n=1,66; z=6; Ep=150mW ; pol=90degrees ; 90degrees with scratch

a	f(kHz)	V (mm/s)	D (um)	1e	Fig	D (um)	2e	Fig	D (um)	3e	Fig	D (um)	4e	Fig
10	100	16,6	1,49		7	1,39	1H.upr.Eg (R)		1,45	1H.upr.Eg(R)		1,19	1H.upr.Eg(R)	
20	200	16,6	1,49	SS(7)		1,06	H.upr.Eg, SS(2)		1,24	1H.upr.Eg(R)		1,28	H.upr.Eg, bottom R	
30	400	22,1	1,53		8	1,30	H.upr.Eg.		1,55		9	0,60	Figure 10(bad)	10

Parameters: n=1,66; z=6; Ep=150mW ; pol=90degrees ; 0degrees with scratch

a	f(kHz)	V (mm/s)	D (um)	1e	Fig	D (um)	2e	Fig	D (um)	3e	Fig	D (um)	4e	Fig
10	100	16,6	0,88	Still very Rough		0,44	Bad, 2P.ab.Surf, 1H.upr.Eg(R)		0,75	1H.upr.Eg(L)		0,67	Very R. 1P.ab.surf, 1H.upr.Eg(R)	
20	200	16,6	0,46	Not compl. Very R		0,88	Very R, L.upr.Eg, 1P.ab.Surf		0,80	H.upr.Eg, very R		0,72	H.upr.Eg, 1P.ab.Surf, very R	
30	400	22,1	0,95	Very R, 1L upr.Eg(R)		0,43	10um peak.ab.surf on edge		0,89	1P.ab.Surf(big)		0,46	4P.ab.Surf, bad, very R	

Parameters: n=1,66; z=6; Ep=150mW ; pol=0degrees ; 90degrees with scratch

a	f(kHz)	V (mm/s)	D (um)	1e	Fig	D (um)	2e	Fig	D (um)	3e	Fig	D (um)	4e	Fig
10	100	16,6	0,80	Rough bottom		0,69	Very R		0,82	Big plat, rest reas.		0,60	Big plat, very R	
20	200	16,6	1,37	Incr. D=0,5>1,8		1,48			0,72	Very R		0,72	Very R	
30	400	22,1	0,65	SS(2), H.upr.Eg		0,43	SS(2), H.upr.Eg, very R		1,30	Reas.		0,84	Very R	

Parameters: n=1,66; z=6; Ep=150mW ; pol=0degrees ; 0degrees with scratch

a	f(kHz)	V (mm/s)	D (um)	1e	Fig	D (um)	2e	Fig	D (um)	3e	Fig	D (um)	4e	Fig
10	100	16,6	1,05	Very R		0,94	Very R		0,96	1P.ab.Surf		0,99	1P.ab.surf	
20	200	16,6	1,25			1,10	Very R, 1P.ab.Surf		1,01	1big P.ab.surf		1,14	1P.ab.surf	
30	400	22,1	1,28	very R		1,16	1P.ab.Surf		0,68	2P.ab.surf, 1H.upr.Eg(R)		X	peaks above surface	

Reas.	Reasonable		H. Upr. Eg.	High upright Edges	Upr. Mat	Uprisinh material
Incr. D	Increasing depth		L. Upr. Eg.	Low upright Edges	no D.	no depth
Decr. D	Decreasing depth		Very R.	Very rough	SS(1)	Same shape as picture (1)
U. Surf.	Under surface		Not compl.	Not complete		
Big plat	Big plateau		P. ab. Surf.	Peaks above surface		

Figure F.6: Depths after 5 minutes etching with 50% HF.

| Depths and comments, alpha-step 500, After 10 min etching with HF, 84 graden celcius |||||||||||||||||

Parameters: n=1,66; z=6; Ep=150mW ; pol=90degrees ; 90degrees with scratch

a	f(kHz)	V (mm/s)	D (um)	1e	Fig	D (um)	2e	Fig	D (um)	3e	Fig	D (um)	4e	Fig
10	100	16,6	1,51	1H.upr.EG(L)		1,40	1H.upr.Eg(R)		1,48	1H.upr.Eg(R)		1,23	1P.ab.Surf	
20	200	16,6	1,37	Very R		1,06	H.upr.Eg(broad)		1,13	1H.upr.Eg(R), 1P.ab.Surf		1,32	H.upr.Eg, very rough	
30	400	22,1	1,59	Good	12	1,30	1H.upr.Eg(R), berg in het midden		1,55	Good, 1L.upr.Eg(R)		0,60	Bad!	

Parameters: n=1,66; z=6; Ep=150mW ; pol=90degrees ; 0degrees with scratch

a	f(kHz)	V (mm/s)	D (um)	1e	Fig	D (um)	2e	Fig	D (um)	3e	Fig	D (um)	4e	Fig
10	100	16,6	0,97	Very rough		0,43	Bad, 2P.ab.Surf, 1H.upr.Eg(R)		0,89	Not compl. Bad!		0,66	1H.upr.Eg(R)	
20	200	16,6	0,51	Not compl. Very R		0,95	Very R, L.upr.Eg, 1P.ab.Surf		0,76	1 P.ab.Surf, H.upr.Eg, very R		0,75	H.upr.Eg, very R	
30	400	22,1	1,01	Very R, 1L upr.Eg(R)		0,39	10um peak.ab.surf on edge		0,97	H.upr.Eg		0,49	verybad	

Parameters: n=1,66; z=6; Ep=150mW ; pol=0degrees ; 90degrees with scratch

a	f(kHz)	V (mm/s)	D (um)	1e	Fig	D (um)	2e	Fig	D (um)	3e	Fig	D (um)	4e	Fig
10	100	16,6	0,80	Very rough		0,66	very R, 2P.ab.Surf		0,85	Big plat, rest good		0,60	big plat, very R	
20	200	16,6	1,39	Incr D=0,6>1,9		1,50	Good		0,78	1H.upr.Eg(L)		0,77	very R	
30	400	22,1	1,03	H.upr.Eg, BAD		1,08	H.upr.Eg, very R		1,36	Incr D=1>2		0,87	very R	

Parameters: n=1,66; z=6; Ep=150mW ; pol=0degrees ; 0degrees with scratch

a	f(kHz)	V (mm/s)	D (um)	1e	Fig	D (um)	2e	Fig	D (um)	3e	Fig	D (um)	4e	Fig
10	100	16,6	1,04	very R, 1P.ab.surf		0,93	L.upr.Eg, very R		1,00	Very R		1,02	1P.ab.Surf, bad	
20	200	16,6	1,16	1 P.ab.surf		1,12	1H.upr.Eg(R), very R		1,11	1H.upr.Eg(L)		1,02	3P.ab.suf	
30	400	22,1	1,28	reasonable		1,28	Very R		0,89	1P.ab.Surf, 1H.upr.Eg(R)		X	Very bad	

Reas.	Reasonable		H. Upr. Eg.	High upright Edges	Upr. Mat	Uprisinh material
Incr. D	Increasing depth		L. Upr. Eg.	Low upright Edges	no D.	no depth
Decr. D	Decreasing depth		Very R.	Very rough	SS(1)	Same shape as picture (1)
U. Surf.	Under surface		Not compl.	Not complete		
Big plat	Big plateau		P. ab. Surf.	Peaks above surface		

Figure F.7: Depths after 10 minutes etching with 50% HF.

Depths and comments, alpha-step 500, After 30 min etching with HF, 84 graden celcius																
Parameters: n=1,66; z=6; Ep=150mW ; pol=90degrees ; 90degrees with scratch																
a	f(kHz)	V (mm/s)	D (um)	1e	Fig	D (um)	2e	Fig	D (um)	3e	Fig	D (um)	4e	Fig
10	100	16,6	1,61			1,38			1,46			1,18		
20	200	16,6	1,37						1,22					
30	400	22,1	1,59			1,34			1,54					

Parameters: n=1,66; z=6; Ep=150mW ; pol=90degrees ; 0degrees with scratch														
a	f(kHz)	V (mm/s)	D (um)	1e	Fig	D (um)	2e	Fig	D (um)	3e	Fig	D (um)	4e	Fig
10	100	16,6	1,00									0,67		
20	200	16,6				0,89			0,88			0,82		
30	400	22,1	1,01			0,41			1,03					

Parameters: n=1,66; z=6; Ep=150mW ; pol=0degrees ; 90degrees with scratch														
a	f(kHz)	V (mm/s)	D (um)	1e	Fig	D (um)	2e	Fig	D (um)	3e	Fig	D (um)	4e	Fig
10	100	16,6	0,80			0,69			0,93					
20	200	16,6	1,40			1,40			0,77			0,75		
30	400	22,1							1,36			0,87		

Parameters: n=1,66; z=6; Ep=150mW ; pol=0degrees ; 0degrees with scratch														
a	f(kHz)	V (mm/s)	D (um)	1e	Fig	D (um)	2e	Fig	D (um)	3e	Fig	D (um)	4e	Fig
10	100	16,6	1,02			1,21			1,02			1,13		
20	200	16,6	1,13			1,07			1,05			1,03		
30	400	22,1	1,30			1,19								

Reas.	Reasonable		H. Upr. Eg.	High upright Edges		Upr. Mat	Uprisinh material
Incr. D	Increasing depth		L. Upr. Eg.	Low upright Edges		no D.	no depth
Decr. D	Decreasing depth		Very R.	Very rough		SS(1)	Same shape as picture (1)
U. Surf.	Under surface		Not compl.	Not complete			
Big plat	Big plateau		P. ab. Surf.	Peaks above surface			

Figure F.8: Depths after 150 minutes etching with 50% HF.

Depths and comments, alpha-step 500, After 150 min etching with HF, 84 graden celcius

Parameters: n=1,66; z=6; Ep=150mW ; pol=90degrees ; 90degrees with scratch

a	f(kHz)	V (mm/s)	D (um)	1e	Fig	D (um)	2e	Fig	D (um)	3e	Fig	D (um)	4e	Fig
10	100	16,6	1,56			1,45			1,49			1,24		
20	200	16,6	1,40						1,23					
30	400	22,1	1,59			1,28			1,56					

Parameters: n=1,66; z=6; Ep=150mW ; pol=90degrees ; 0degrees with scratch

a	f(kHz)	V (mm/s)	D (um)	1e	Fig	D (um)	2e	Fig	D (um)	3e	Fig	D (um)	4e	Fig
10	100	16,6	0,93									0,71		
20	200	16,6										0,79		
30	400	22,1	1,02						1,01					

Parameters: n=1,66; z=6; Ep=150mW ; pol=0degrees ; 90degrees with scratch

a	f(kHz)	V (mm/s)	D (um)	1e	Fig	D (um)	2e	Fig	D (um)	3e	Fig	D (um)	4e	Fig
10	100	16,6	0,80			0,69			0,96					
20	200	16,6	1,39			1,50			0,72			0,78		
30	400	22,1							1,34			0,87		

Parameters: n=1,66; z=6; Ep=150mW ; pol=0degrees ; 0degrees with scratch

a	f(kHz)	V (mm/s)	D (um)	1e	Fig	D (um)	2e	Fig	D (um)	3e	Fig	D (um)	4e	Fig
10	100	16,6	1,06						0,93			1,05		
20	200	16,6	1,15			1,08			1,02			1,05		
30	400	22,1	1,26			1,15								

Reas.	Reasonable	H. Upr. Eg.	High upright Edges	Upr. Mat	Uprisinh material
Incr. D	Increasing depth	L. Upr. Eg.	Low upright Edges	no D.	no depth
Decr. D	Decreasing depth	Very R.	Very rough	SS(1)	Same shape as picture (1)
U. Surf.	Under surface	Not compl.	Not complete		
Big plat	Big plateau	P. ab. Surf.	Peaks above surface		

Figure F.9: Depths after 150 minutes etching with 50% HF.
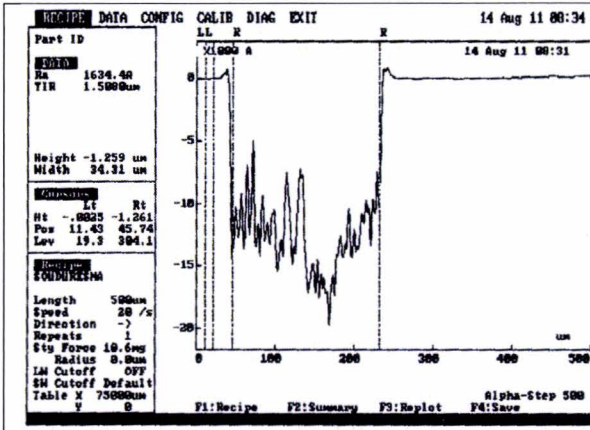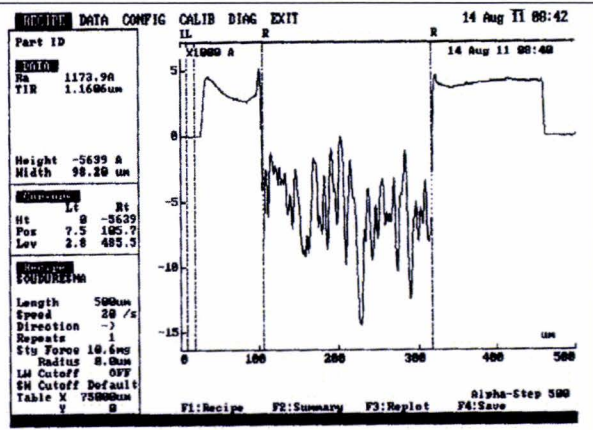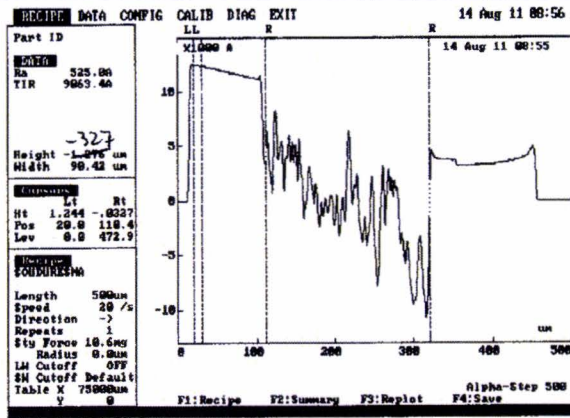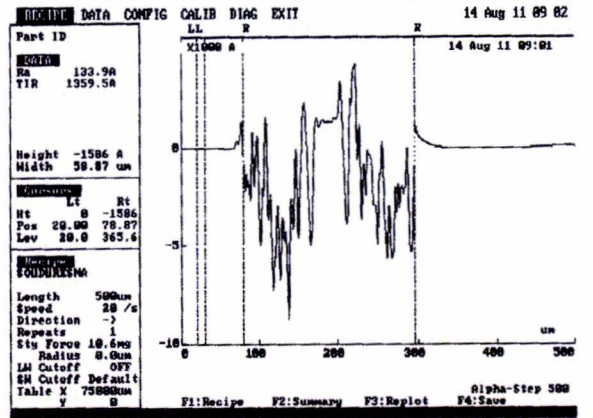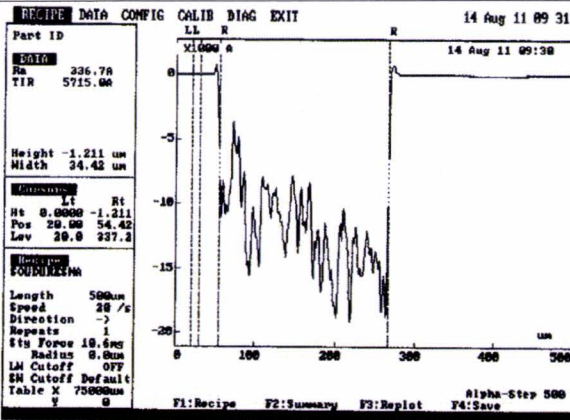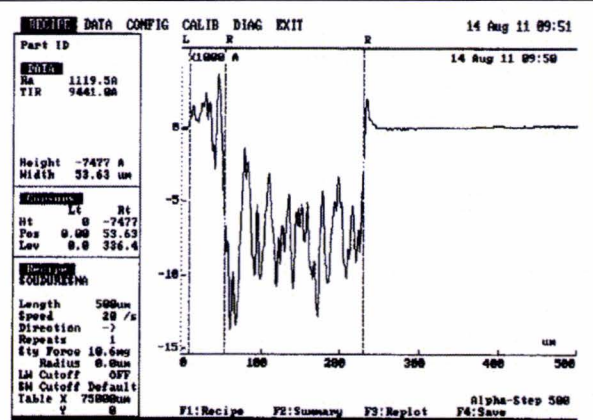
Table F.7: Alpha-step scans: the numbers correspond with the numbers in previous tables.
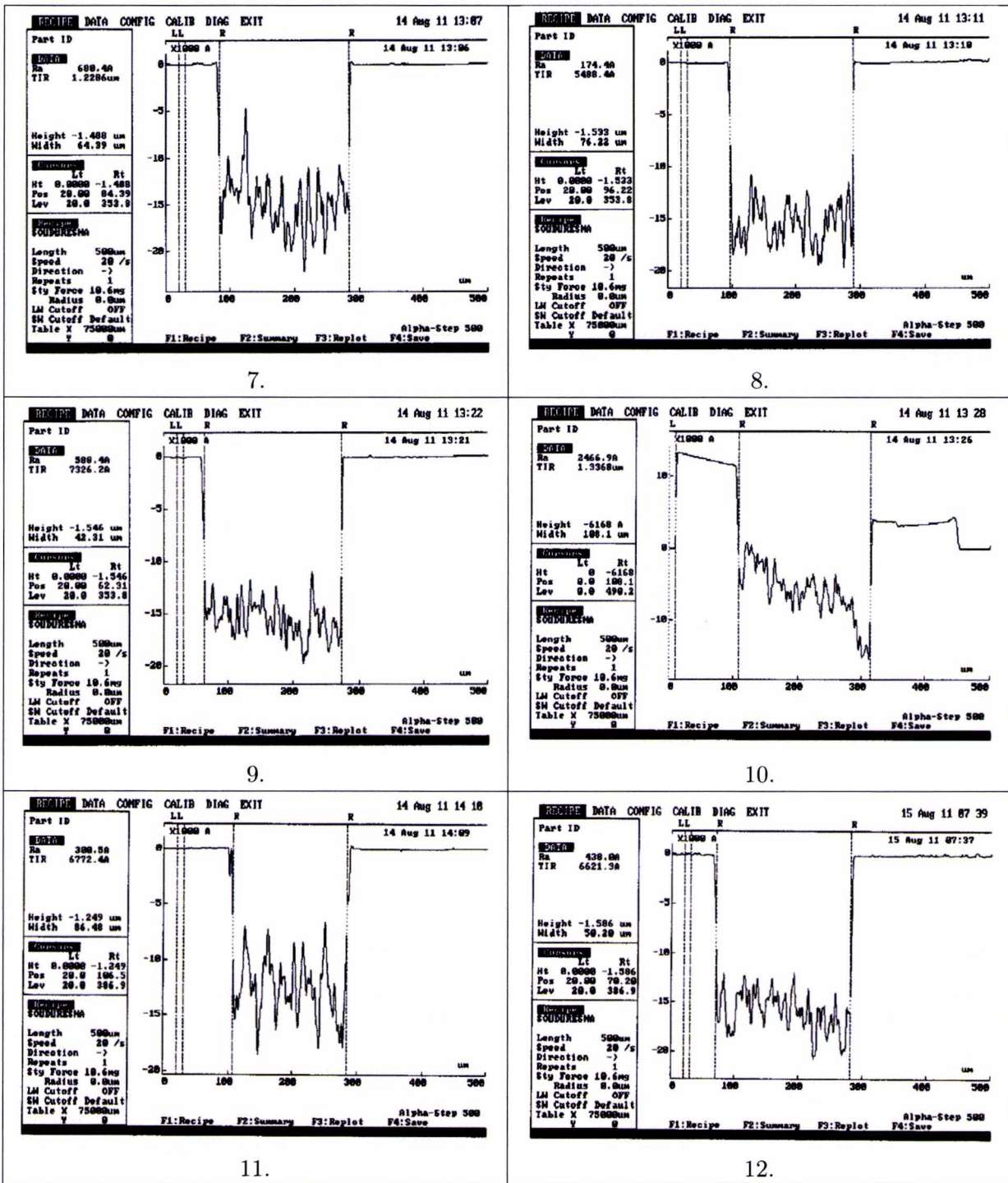
Table F.8: Alpha-step scans: the numbers correspond with the numbers in previous tables.

Appendix G

Ruby: results follow-up experiment
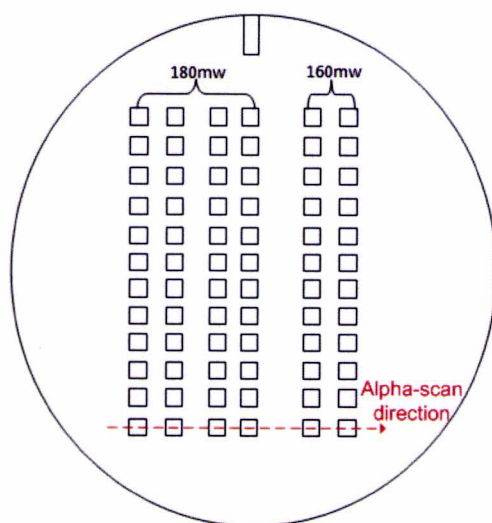
Figure G.1: Structures on the ruby substrate E.

Dephts, Ruby squares, after irradiation

Parameters: n=1,66; z=6; Ep=180mW/252nJ ; pol=0degrees ; 90degrees with scratch

a	f(kHz)	V(mm/s)	1e		2e		3e		4e		Average
10	100	16,6	1,42		1,76		1,54		1,35		1,52
20	200	16,6	1,74		1,95		1,31		1,77		1,69
30	400	22,1	1,85		1,57		1,31		1,8		1,63

Parameters: n=1,66; z=6; Ep=180mW/252nJ ; pol=0degrees ; 0degrees with scratch

a	f(kHz)	V(mm/s)	1e		2e		3e		4e		Average
10	100	16,6	1,14		0,93		1,57		1,62	(GRAPH A)	1,32
20	200	16,6	1,71		1,74		1,56		1,29		1,58
30	400	22,1	1,81		1,55		1,32		1,04		1,43

Parameters: n=1,66; z=6; Ep=180mW/252nJ ; pol=90degrees ; 90degrees with scratch

a	f(kHz)	V(mm/s)	1e		2e		3e		4e		Average
10	100	16,6	1,2		1,56		1,65		1,52		1,48
20	200	16,6	1,58		1,32		1,78		1,4		1,52
30	400	22,1	1,96		1,79		1,39		1,35		1,62

Parameters: n=1,66; z=6; Ep=180mW/252nJ ; pol=90degrees ; 0degrees with scratch

a	f(kHz)	V(mm/s)	1e		2e		3e		4e		Average
10	100	16,6	1,28		1,85		1,68		1,76		1,64
20	200	16,6	1,37	dal van 3um	2,06	GRAPH B	1,98		1,44		1,71
30	400	22,1	1,96	plat 2&0,5	1,51		1,8		1,4		1,67

Parameters: n=1,66; z=6; Ep=160mW; pol=0degrees ; 90degrees with scratch

a	f(kHz)	V(mm/s)	1e		2e		3e		4e		Average
10	100	16,6	1,04		1,13	plat van 2&1	1,29		1,04	(goede deel)	1,13
20	200	16,6	1,06		1,83		1,6		0,98		1,37
30	400	22,1	0,9	berg bov surf	1,72		1,15		0,98		1,19

Parameters: n=1,66; z=6; Ep=160mW ; pol=0degrees ; 0degrees with scratch

a	f(kHz)	V(mm/s)	1e		2e		3e		4e		Average
10	100	16,6	1,01		0,98	(berg bov surf)	1,26		1,09		1,09
20	200	16,6	1,18	dal 2.5um	1,8		1,1		1,05		1,28
30	400	22,1	1,37		1,17		1,3		1,02		1,22

Figure G.2: Depths after irradiation.

Dephts, Ruby squares, after 30min 50% HF etching

Parameters: n=1,66; z=6; Ep=180mW/252nJ ; **pol=0degrees ; 90degrees with scratch**										
a	f(kHz)	V(mm/s)		1e		2e	3e		4e	Average
10	100	16,6	1,55		1,92		1,66	1,47		1,65
20	200	16,6	2,12		2,2		1,51	1,84		1,92
30	400	22,1	2,23		1,91		1,6	2,14		1,97

Parameters: n=1,66; z=6; Ep=180mW/252nJ ; **pol=0degrees ; 0degrees with scratch**										
a	f(kHz)	V(mm/s)		1e		2e	3e		4e	Average
10	100	16,6	1,24		1,35		1,8	1,76	(GRAPH C)	1,54
20	200	16,6	1,98		1,98		1,89	1,54		1,85
30	400	22,1	2,11		1,77		1,66	1,44		1,75

Parameters: n=1,66; z=6; Ep=180mW/252nJ ; **pol=90degrees ; 90degrees with scratch**										
a	f(kHz)	V(mm/s)		1e		2e	3e		4e	Average
10	100	16,6	1,35		1,72		1,73	1,65		1,61
20	200	16,6	1,76		1,62		1,89	1,58		1,71
30	400	22,1	2,13		2,08		1,66	1,69		1,89

Parameters: n=1,66; z=6; Ep=180mW/252nJ ; **pol=90degrees ; 0degrees with scratch**										
a	f(kHz)	V(mm/s)		1e	2e		3e		4e	Average
10	100	16,6	1,5		1,86		1,82	1,88		1,77
20	200	16,6	1,68	(D)dal van 3um	2,24	GRAPH E	2,21	1,74		1,97
30	400	22,1	1,98	plat 2,5&1	1,84		2,01	1,62		1,86

Parameters: n=1,66; z=6; **Ep=160mW; pol=0degrees ; 90degrees with scratch**										
a	f(kHz)	V(mm/s)		1e		2e	3e		4e	Average
10	100	16,6	1,21		1,36	plat van 2&1	1,41	1,18	(goede deel)	1,29
20	200	16,6	1,32		2,04		1,73	1,25		1,59
30	400	22,1	1,19	berg WEG	1,92		1,55	1,24		1,48

Parameters: n=1,66; z=6; **Ep=160mW ; pol=0degrees ; 0degrees with scratch**										
a	f(kHz)	V(mm/s)		1e		2e	3e		4e	Average
10	100	16,6	1,15		1,13	(berg bov surf)	1,44	1,21		1,23
20	200	16,6	1,44	dal 2.5um	2,03		1,35	1,28		1,53
30	400	22,1	1,54		1,45		1,63	1,32		1,49

Figure G.3: Depths after 30 minutes etching with 50% HF.

Dephts, Ruby squares, after 150 min 50% HF etching

Parameters: n=1,66; z=6; Ep=180mW/252nJ ; **pol=0degrees ; 90degrees with scratch**									
a	f(kHz)	V(mm/s)		1e		2e	3e		4e	Average
10	100	16,6	1,96		1,97		1,68	1,51		1,78
20	200	16,6	2,04		2,24		1,56	1,82		1,92
30	400	22,1	2,23		1,88		1,62	1,62		1,84

Parameters: n=1,66; z=6; Ep=180mW/252nJ ; **pol=0degrees ; 0degrees with scratch**									
a	f(kHz)	V(mm/s)		1e		2e	3e		4e	Average
10	100	16,6	1,29		1,39		1,80	1,76	(GRAPH F)	1,56
20	200	16,6	2,00		2,00		1,96	1,46		1,86
30	400	22,1	2,19		1,80		1,67	1,67		1,83

Parameters: n=1,66; z=6; Ep=180mW/252nJ ; **pol=90degrees ; 90degrees with scratch**									
a	f(kHz)	V(mm/s)		1e		2e	3e		4e	Average
10	100	16,6	1,37		1,54		1,74	1,67		1,58
20	200	16,6	1,78		1,52		1,90	1,57		1,69
30	400	22,1	2,13		2,02		1,69	1,73		1,89

Parameters: n=1,66; z=6; Ep=180mW/252nJ ; **pol=90degrees ; 0degrees with scratch**									
a	f(kHz)	V(mm/s)		1e	2e		3e		4e	Average
10	100	16,6	1,47		1,82		1,96	1,94		1,80
20	200	16,6	1,64	(D)dal van 3um	2,32	GRAPH G	2,23	1,68		1,97
30	400	22,1	1,86	plat 2,5&1	1,79		2,14	1,65		1,86

Parameters: n=1,66; z=6; **Ep=160mW; pol=0degrees ; 90degrees with scratch**									
a	f(kHz)	V(mm/s)		1e		2e	3e		4e	Average
10	100	16,6	1,24		1,35	plat van 2&1	1,45	1,08	(goede deel)	1,28
20	200	16,6	1,27		2,10		1,80	1,27		1,61
30	400	22,1	1,19		1,94		1,51	1,23		1,47

Parameters: n=1,66; z=6; **Ep=160mW ; pol=0degrees ; 0degrees with scratch**									
a	f(kHz)	V(mm/s)		1e		2e	3e		4e	Average
10	100	16,6	1,14		1,15	(berg bov surf)	1,50	1,27		1,27
20	200	16,6	1,45	dal 2.5um	1,94		1,40	1,28		1,52
30	400	22,1	1,65		1,49		1,56	1,37		1,52

Figure G.4: Depths after 150 minutes etching with 50% HF.
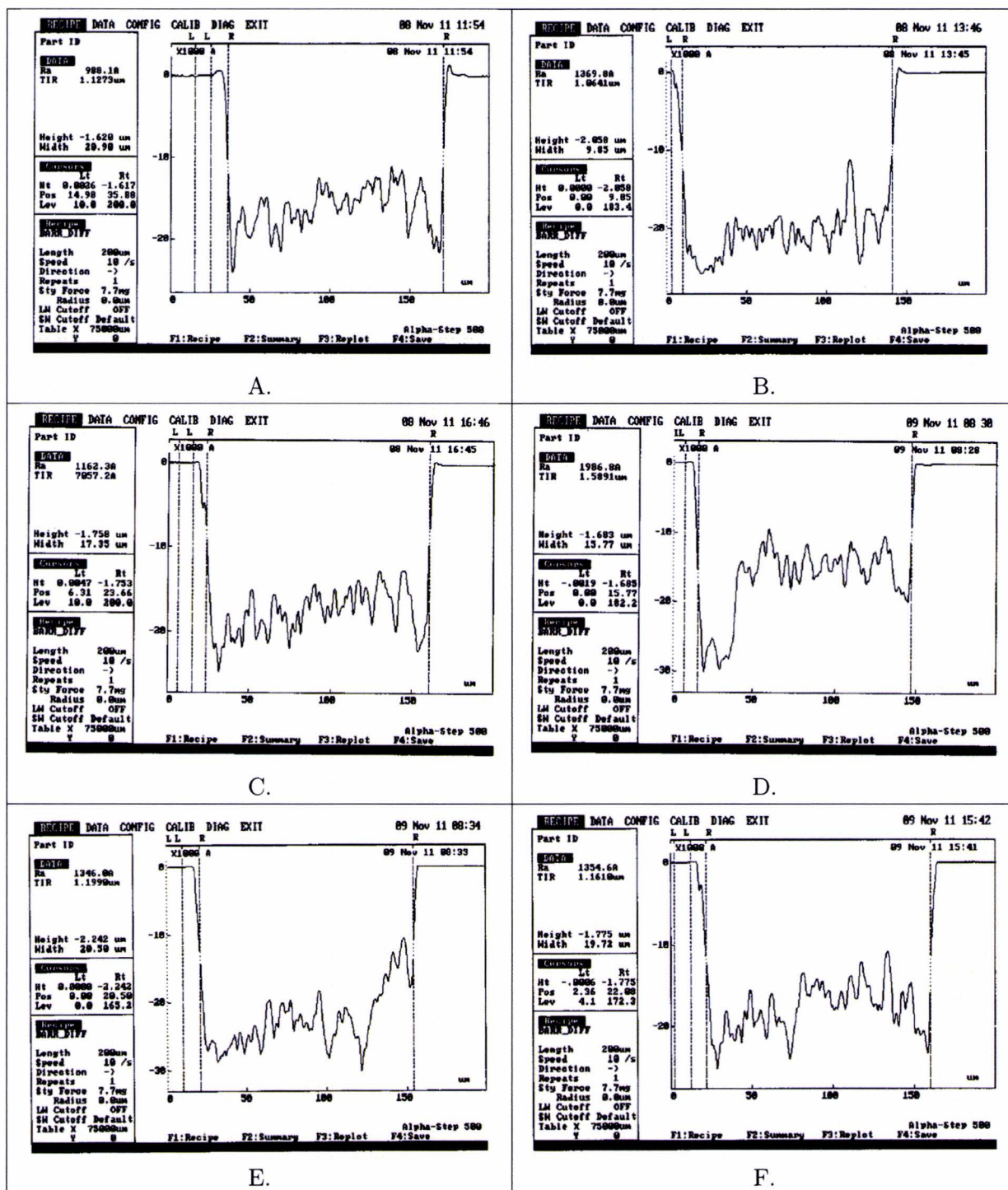
Table G.1: Alpha-step scans: the letters correspond with the letters in previous tables.
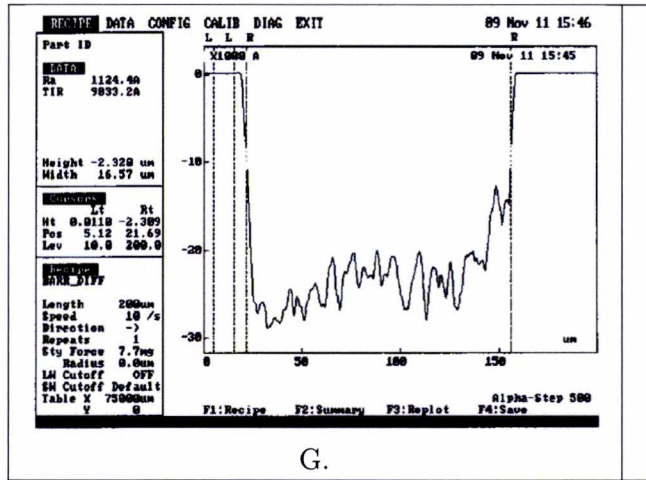
Table G.2: Alpha-step scans: the letter correspond with the letter in previous tables.
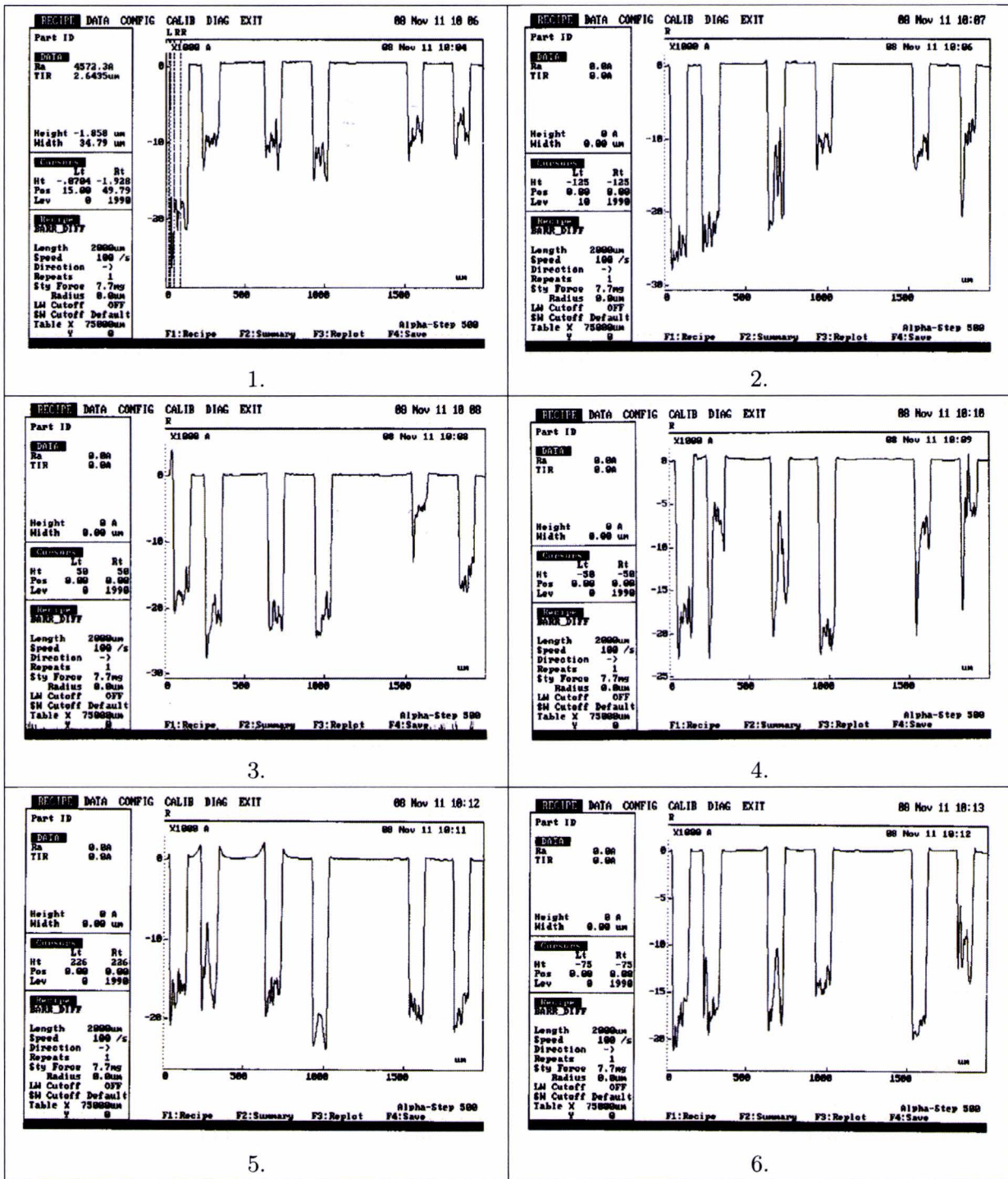
Table G.3: Alpha-step scans after irradiation: the numbers correspond with the number of the row from bottom to top in picture G.1.
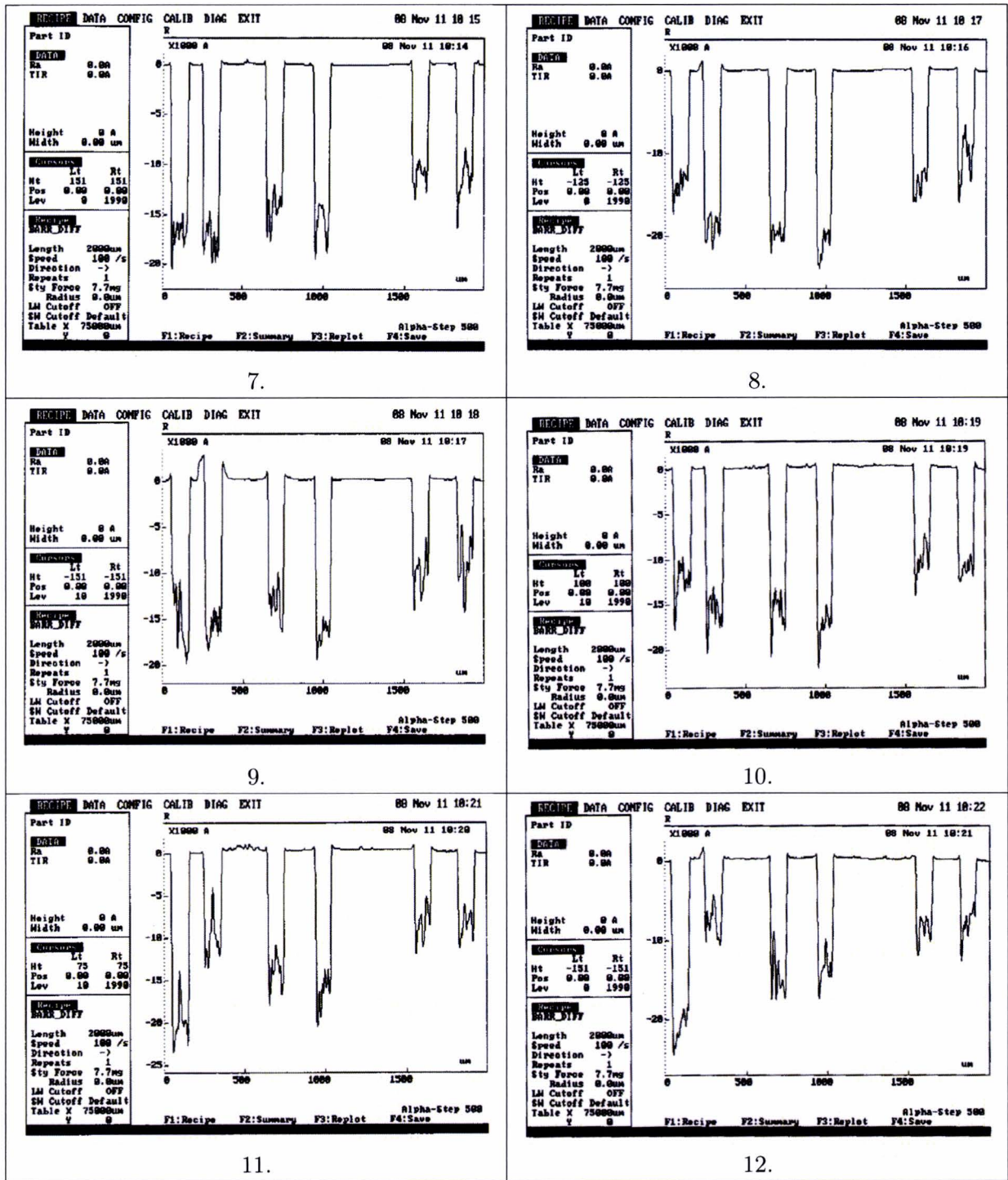
Table G.4: Alpha-step scans after irradiation: the numbers correspond with the number of the row from bottom to top in picture G.1.
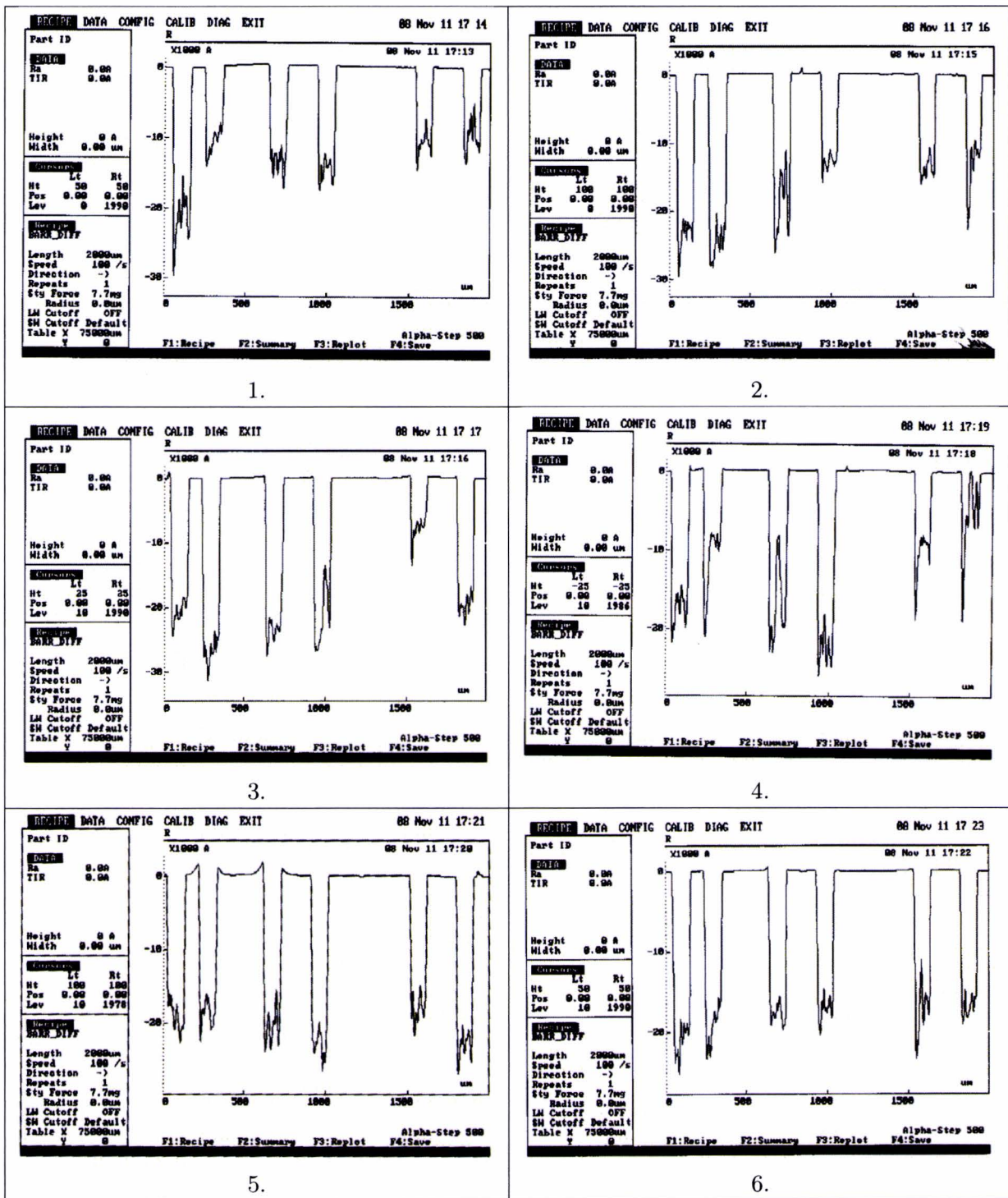
Table G.5: Alpha-step scans 30 minutes of etching with 50% HF: the numbers correspond with the number of the row from bottom to top in picture G.1.
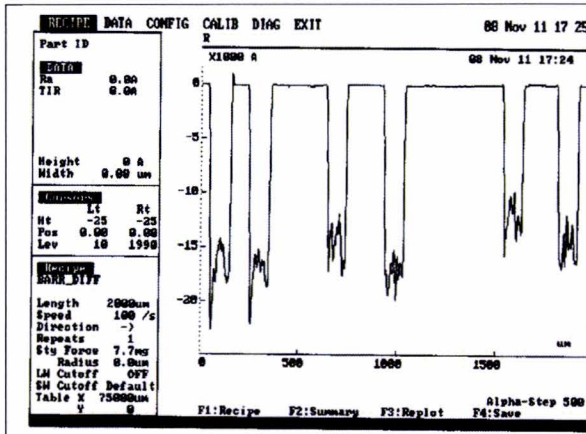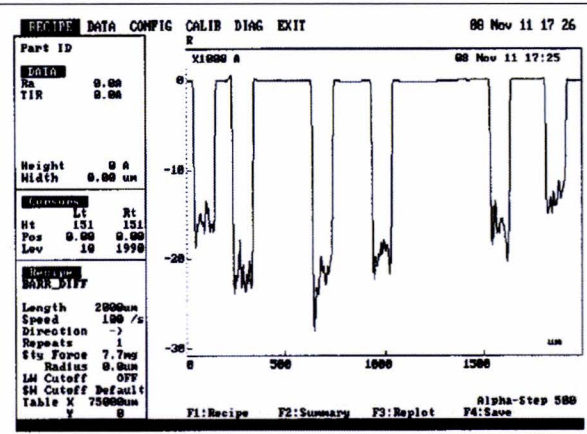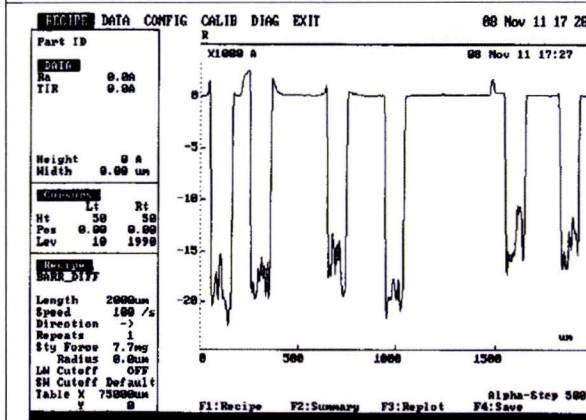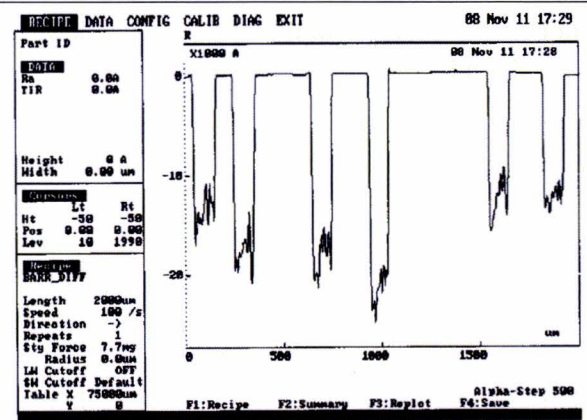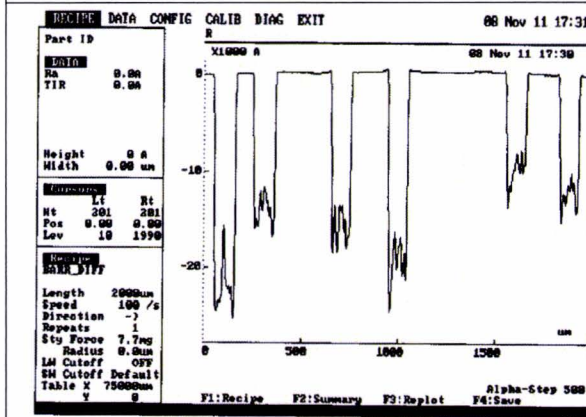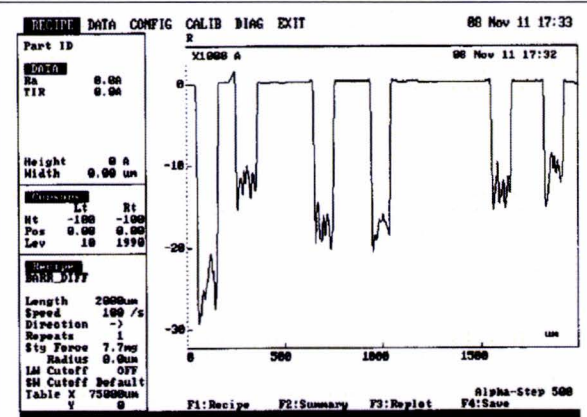
Table G.6: Alpha-step scans 30 minutes of etching with 50% HF: the numbers correspond with the number of the row from bottom to top in picture G.1.
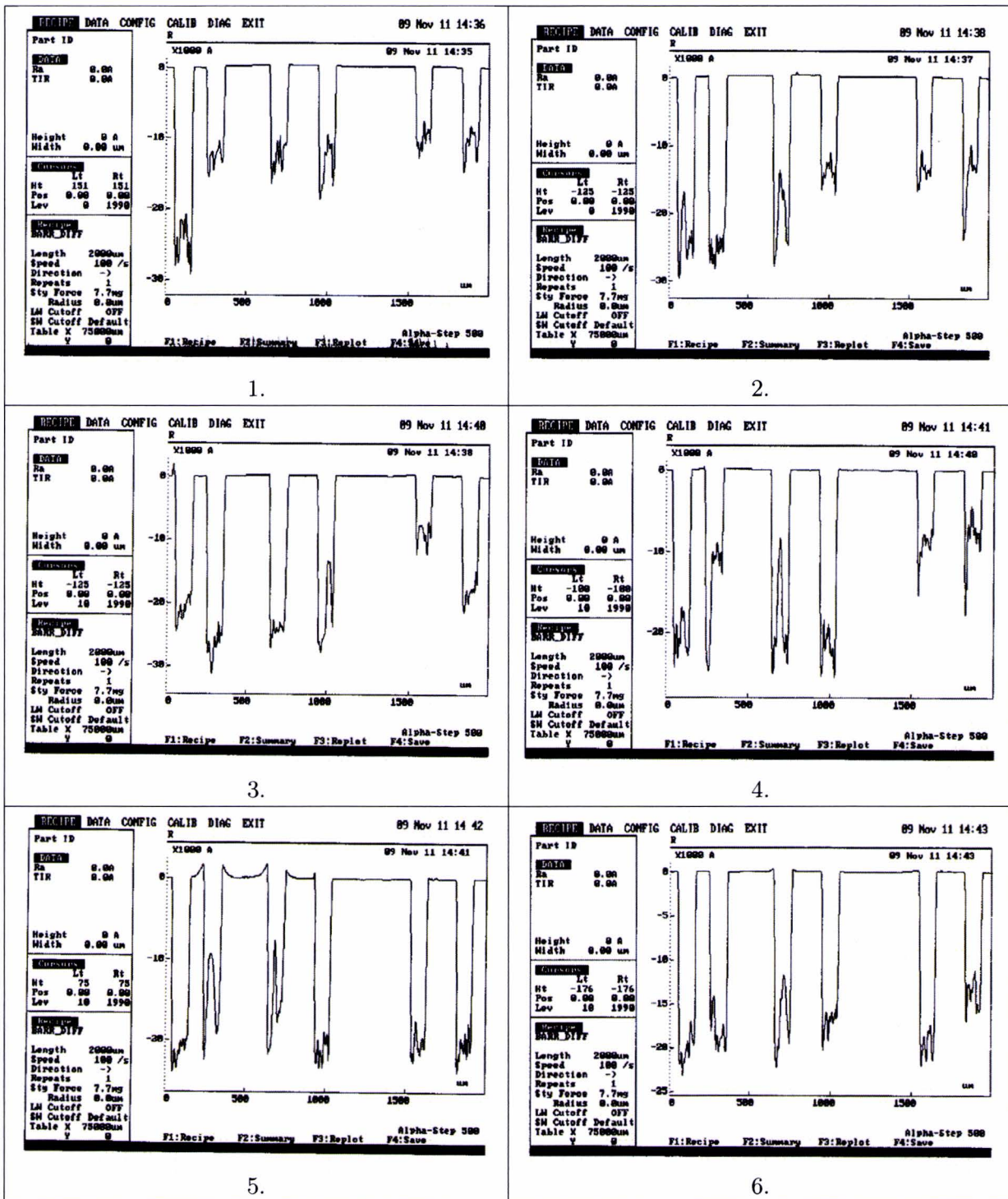
Table G.7: Alpha-step scans 150 minutes of etching with 50% HF: the numbers correspond with the number of the row from bottom to top in picture G.1.
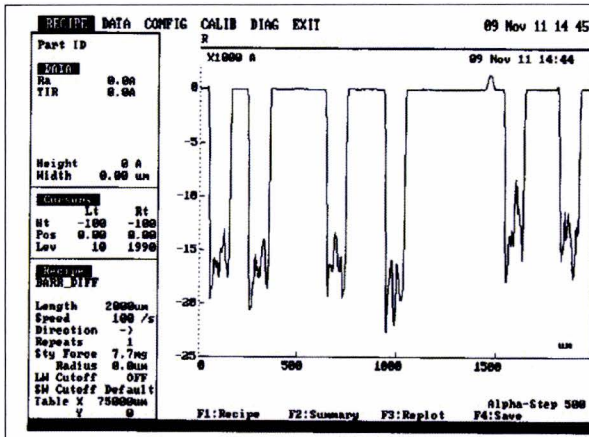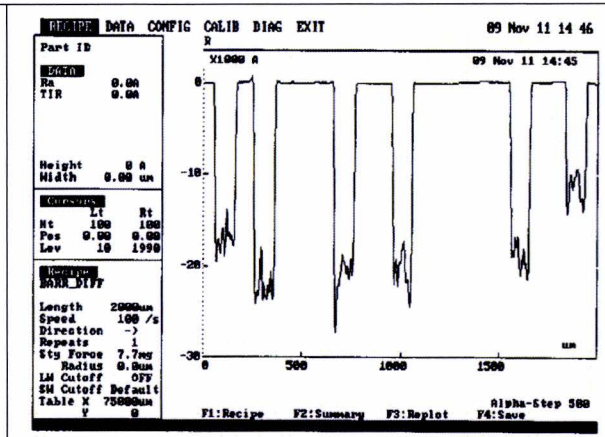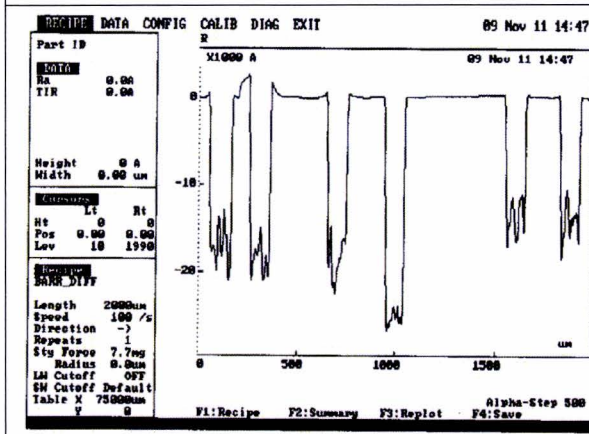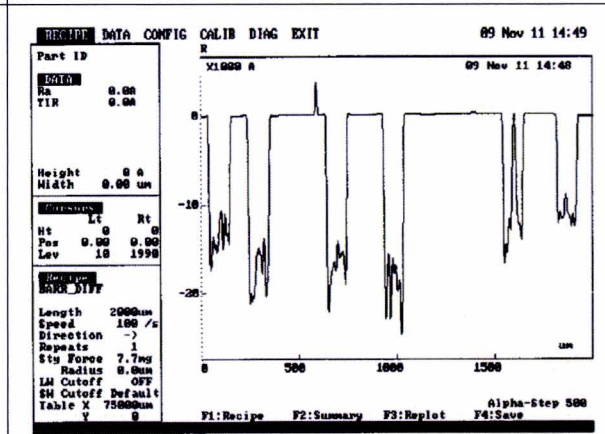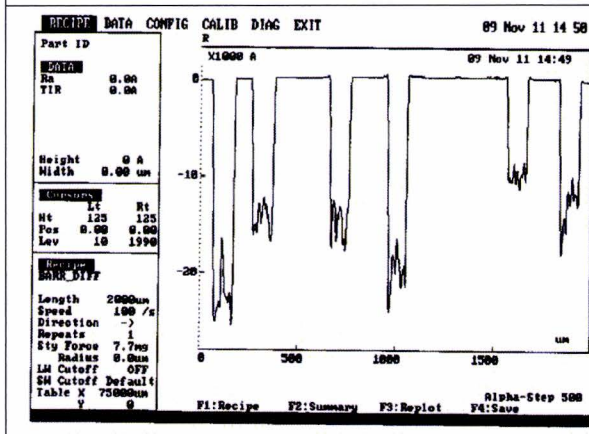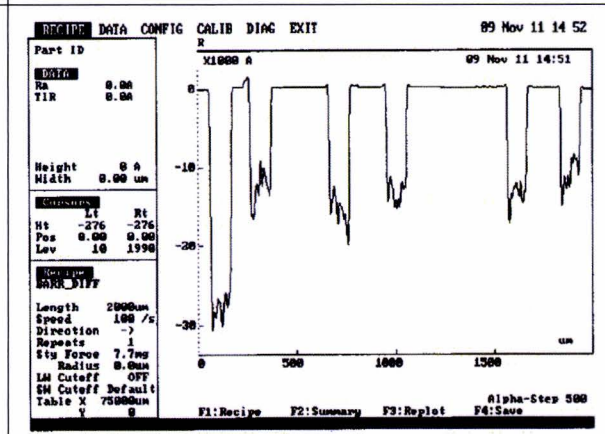
Table G.8: Alpha-step scans 150 minutes of etching with 50% HF: the numbers correspond with the number of the row from bottom to top in picture G.1.

Appendix H

Ruby: results last experiments
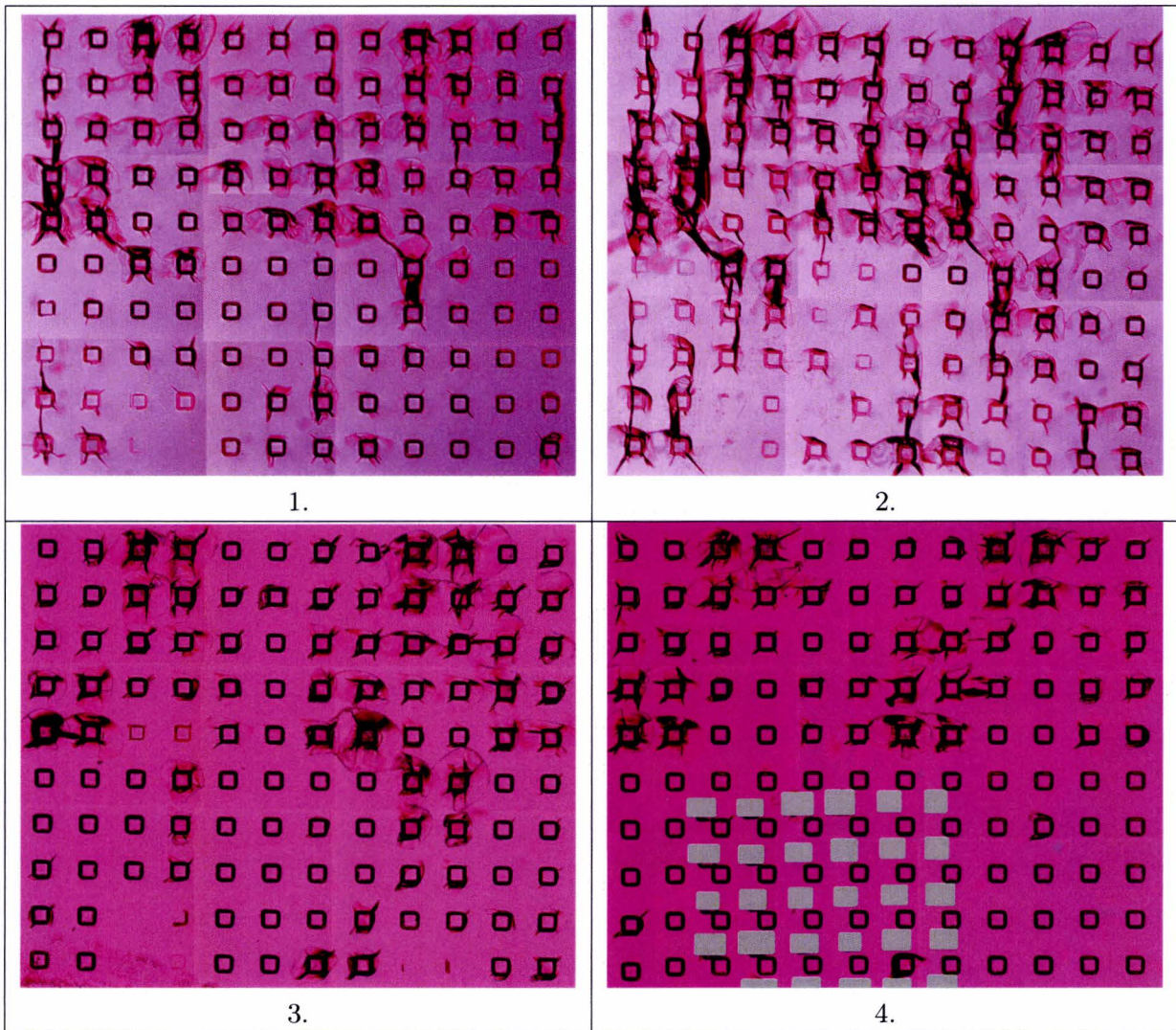
Table H.1: Pictures optic microscope after irradiation.

Appendix I

M-file: analytical approximations

Analytical model with Castigliano's Theorem.

```
%% Shock absorber

clear all;
close all;

% Startimg Geometry
R = 0.618e-3;                        %[m] measurered radius of the bar
w = 0.053e-3;                        %[m] measurered width of the bar
h = 0.15e-3;                         %[m] measurered heigth of the bar
L = pi*R/2;                          % half Length of the curvature

% New Geometry
R = 0.58e-3;                         %[m] new radius
%w = [0.03:0.001:0.06]*10^-3;         %[m] new range of widths
%h = [0.12:0.01:0.20]*10^-3;          %[m] new range of heights
w = 0.06e-3
h = 0.19e-3
%%%%%%%%%%%%%%%%%%%%%%%%%%%%%%%%%%%%%%%%%%%%%%%%%%%%%%%%%%%%%%%%%%%%%%%%%%%
% Material properties for LIGA
%E = 207e9;                           %[GPa] Young's Modulus
%v = 0.31;                            %[-]   poisson's ratio
%G = 79*10^9;                         %[GPA] Shear Modulus

% Material properties for Ruby
%E = 320e9;                           %[GPa] Young's Modulus
%v = 0.340;                           %[-]   poisson's ratio
%G = 119e9;                           %[GPA] Shear Modulus

% Material properties for Sapphire
%E = ((462.6+426.4)/2)*1e9;           %[GPa] Young's Modulus
%v = 0.309;                           %[-]   poisson's ratio
%G = ((144.3+162.9)/2)*1e9;           %[GPA] Shear Modulus

% Material properties for Fused Silica
E = 78e9;                            %[GPa] Young's Modulus
v = 0.17;                            %[-]   poisson's ratio
G = 3.33e10;                         %[GPA] Shear Modulus
%%%%%%%%%%%%%%%%%%%%%%%%%%%%%%%%%%%%%%%%%%%%%%%%%%%%%%%%%%%%%%%%%%%%%%%%%%%

% Initial conditions looping
```

```
Q  = length(w);
Q2 = length(h);
Xdis = zeros(Q2,Q);
Ydis = zeros(Q2,Q);
Zdis = zeros(Q2,Q);
n=1;
m=1;

% Loop with variation of the width and heigth
while m <= Q2;
    for j = h(:,m);
        while n <= Q;
            for i = w(:,n);

                % Moment of inertia
                I  =  (j*(i^3)) / 12;
                Ip =  (i*(j^3)) / 12;

                % Force in three directions
                H =  (17*10^-3)*9.81;              % Horizontal Force
                V =  (0*10^-3)*9.81;               % Vertical Force
                Pz = (17*10^-3)*9.81;              % Perpendicular Force

                % Rotate force for the different springs:
                % spring1
                H1 =    (1/3)*H;
                V1 =    (1/3)*V;
                % spring2
                Hx2 = -H1*sind(30)  +  V1*cosd(30);
                Vy2 = -V1*sind(30)  -  H1*cosd(30);
                % spring3
                Hx3 = -H1*sind(30)  -  V1*cosd(30);
                Vy3 =  H1*cosd(30)  -  V1*sind(30);

                % XY1-diplacement formulas in mm
                d_x1 = ((R^3)./(E.*I) * (   2*V1 + 3*H1*pi/2))  *10^3;
                d_y1 = ((R^3)./(E.*I) * (   V1*pi/2 + 2*H1)  )  *10^3;

                % XY2-displacement formulas in mm
                d_x2 = ((R^3)./(E.*I) * (   2*Vy2 + 3*Hx2*pi/2)) *10^3;
                d_y2 = ((R^3)./(E.*I) * (   Vy2*pi/2 + 2*Hx2)  ) *10^3;

                % XY3-displacement formulas in mm
                d_x3 = ((R^3)./(E.*I) * (   2*Vy3 + 3*Hx3*pi/2)) *10^3;
                d_y3 = ((R^3)./(E.*I) * (   Vy3*pi/2 + 2*Hx3)  ) *10^3;

                % Using the rotation matrix the X and Y displacements can
                % be calulated in the new axis
                d_x1_new = d_x1;     % already in the right axes
                d_y1_new = d_y1;     % already in the right axes
                d_x2_new = d_x2*cosd(240)  + d_y2*sind(240);
                d_y2_new = d_x2*-sind(240) + d_y2*cosd(240);
                d_x3_new = d_x3*cosd(120)  + d_y3*sind(120);
                d_y3_new = d_x3*-sind(120) + d_y3*cosd(120);

                % The average of the displacements
```

```
                delta_x = [(d_x1_new + d_x2_new + d_x3_new) / 3 ]
                delta_y = [(d_y1_new + d_y2_new + d_y3_new) / 3 ]

                % Z-displacement formula
                delta_z  =(1/3)*((Pz*(L^4)/(E.*I))+Pz*(L^3)/(G.*Ip))*(10^3);

                Xdis(m,n) = delta_x;
                Ydis(m,n) = delta_y;
                Zdis(m,n) = delta_z;

                n=n+1;
            end
        end
        m = m+1;
        n = 1;
    end
end

X_meas = Xdis * 0.24;             %correcting factors icw LIGA measurement
Y_meas = Ydis * 0.24;             %correcting factors icw LIGA measurement
Z_meas = Zdis;                    %correcting factors icw LIGA measurement

Displacement = [X_meas;Y_meas;Z_meas]

%Figures
% figure
% subplot(2,3,1);
% [C,f]=contourf(w*10^3,h*10^3,X_meas);
% clabel(C,f);
% xlabel('Width of the spring [mm]');
% ylabel('Height of the spring [mm]');
% title('Xdisplacement [mm]');
%
% subplot(2,3,2);
% [C,f]=contourf(w*10^3,h*10^3,Y_meas);
% clabel(C,f);
% xlabel('Width of the spring [mm]');
% ylabel('Height of the spring [mm]');
% title('Ydisplacement [mm]');
%
% subplot(2,3,3);
% [C,f]=contourf(w*10^3,h*10^3,Z_meas);
% clabel(C,f);
% xlabel('Width of the spring [mm]');
% ylabel('Height of the spring [mm]');
% title('Zdisplacement [mm]');
%
% subplot(2,3,4);
% [C,f]=contourf(w*10^3,h*10^3,H./X_meas);
% clabel(C,f);
% xlabel('Width of the spring [mm]');
% ylabel('Height of the spring [mm]');
% title('Spring Constant in X [N/mm]');
%
% subplot(2,3,5);
% [C,f]=contourf(w*10^3,h*10^3,V./Y_meas);
```

```
% clabel(C,f);
% xlabel('Width of the spring [mm]');
% ylabel('Height of the spring [mm]');
% title('Spring Constant in Y [N/mm]');
%
% subplot(2,3,6);
% [C,f]=contourf(w*10^3,h*10^3,Pz./Z_meas);
% clabel(C,f);
% xlabel('Width of the spring [mm]');
% ylabel('Height of the spring [mm]');
% title('Spring Constant in Z [N/mm]');
```

Analytical model using Compliance and Stiffness matrices

```
%% Shock absorber helix paper

clear all;
close all;

syms theta %G J E Iz Iy phi r A y

% Material properties for LIGA
E = 207e9;                          %[GPa] Young's Modulus
G = 79*10^9;                        %[GPA] Shear Modulus

% Material properties for Ruby
%E = 320e9;                         %[GPa] Young's Modulus
%G = 119e9;                         %[GPA] Shear Modulus

% Material properties for Fused Silica
%E = 78e9;                          %[GPa] Young's Modulus
%G = 3.33e10;                       %[GPA] Shear Modulus

w = 0.053e-3;
h = 0.15e-3;
r = 0.618e-3;
y = r;
p = 0;
A = w*h;

Iy   =  (h*(w^3)) / 12;
Iz   =  (w*(h^3)) / 12;
J    =  (h*(w^3)) / 3 ;

c0 = [1/(G*J) 0             0          0        0        0 ;
      0       1/(E*Iz)      0          0        0        0 ;
      0       0             1/(E*Iy)   0        0        0 ;
      0       0             0          1/(E*A)  0        0 ;
      0       0             0          0        0        0 ;
      0       0             0          0        0        0 ];

R = [ -r/y          0     -p/(2*pi*y)  ;
      0             1      0                 ;
      p/(2*pi*y)    0     -r/y              ];

T = [0   0  r ;
     0   0  0 ;
    -r   0  0 ];

null = [0 0 0 ;
        0 0 0 ;
        0 0 0 ];

H_inv = [R null ; T*R R];
c = H_inv * c0 * H_inv.';

% Rotation matrix around Z
R1 = [ cos(theta) -sin(theta) 0 ;
       sin(theta) cos(theta)  0 ;
```

```
                0                0                1   ];

T1 = [0                          (−p∗theta)/(2∗pi)   0  ;
        (p∗theta)/(2∗pi)    0                         0  ;
        0                         0                    0  ];

H1_inv = [R1 null  ; T1∗R1 R1];
C1 = H1_inv ∗ c ∗ H1_inv.';
C1 = C1∗r;
C = int(C1,theta,0,13∗(pi/12));
K1 = inv(C);
K1_vpa = VPA(K1,2)

% Spring 2
phi_2 = (2∗pi)/3;
R2 = [ cos(phi_2) −sin(phi_2) 0  ;
        sin(phi_2) cos(phi_2)  0  ;
        0               0             1  ];
H2_inv = [R2 null  ; null R2];
C2 = H2_inv ∗ C ∗ H2_inv.';
K2 = inv(C2);
K2_vpa = VPA(K2,2)

% Spring 3
phi_3 = −(2∗pi)/3;
R3 = [ cos(phi_3) −sin(phi_3) 0  ;
        sin(phi_3) cos(phi_3)  0  ;
        0               0             1  ];
H3_inv = [R3 null  ; null R3];
C3 = H3_inv ∗ C ∗ H3_inv.';
K3 = inv(C3);
K3_vpa = VPA(K3,2)

% Total Spring
K = K1 + K2 + K3  ;
K = VPA(K,2)

% Displacement
displ = 0.17./K.∗10^3;
d = VPA(displ,2)
```

Appendix J

Stiffness matrices

$$
C_1 = \begin{bmatrix}
\frac{X_{11}}{EI_z} + \frac{X_{12}}{GJ} & \frac{X_{21}}{EI_z} - \frac{X_{21}}{GJ} & 0 & 0 & 0 & \frac{X_{61}}{GJ} \\
\frac{X_{21}}{EI_z} - \frac{X_{21}}{GJ} & \frac{X_{12}}{EI_z} + \frac{X_{11}}{GJ} & 0 & 0 & 0 & \frac{X_{26}}{GJ} \\
0 & 0 & \frac{X_{33}}{EI_y} & -\frac{X_{61}}{EI_y} & \frac{X_{26}}{EI_y} & 0 \\
0 & 0 & -\frac{X_{61}}{EI_y} & \frac{X_{11}r^2}{EI_y} + \frac{X_{12}}{AE} & -\frac{X_{21}r}{EI_y} - \frac{X_{21}}{AE} & 0 \\
0 & 0 & \frac{X_{26}}{EI_y} & -\frac{X_{21}r}{EI_y} - \frac{X_{21}}{AE} & \frac{X_{12}r^2}{EI_y} + \frac{X_{11}}{AE} & 0 \\
\frac{X_{61}}{GJ} & -\frac{X_{26}}{GJ} & 0 & 0 & 0 & \frac{X_{33}r^2}{GJ}
\end{bmatrix}
\tag{J.1}
$$

where

$$
X_{11} = r(\frac{13\pi}{24} - \frac{1}{8})
$$
$$
X_{12} = r(\frac{13\pi}{24} + \frac{1}{8})
$$
$$
X_{21} = r(\frac{\sqrt{3} - 2}{8})
$$
$$
X_{33} = \frac{13\pi r}{12}
$$
$$
X_{26} = \frac{r^2(\sqrt{2} + \sqrt{6} + 4)}{4}
$$
$$
X_{61} = \frac{\sqrt{2}r^2\sqrt{3} - 1}{4}
$$

$$
K = \begin{bmatrix}
2.5e-3 & 9.8e-13 & 0 & 0 & 0 & -2.3e-10 \\
5.7e-14 & 2.5e-3 & 0 & 0 & 0 & 0 \\
0 & 0 & 2.1e-3 & 0 & 1.2e-10 & 0 \\
0 & 0 & 6.4e-10 & 7.2e3 & 1.4e-6 & 0 \\
0 & 0 & 0 & 0 & 7.2e3 & 0 \\
0 & 5.8e-11 & 0 & 0 & 0 & 5.5e3
\end{bmatrix}
\tag{J.2}
$$

Appendix K

Schematic overview models
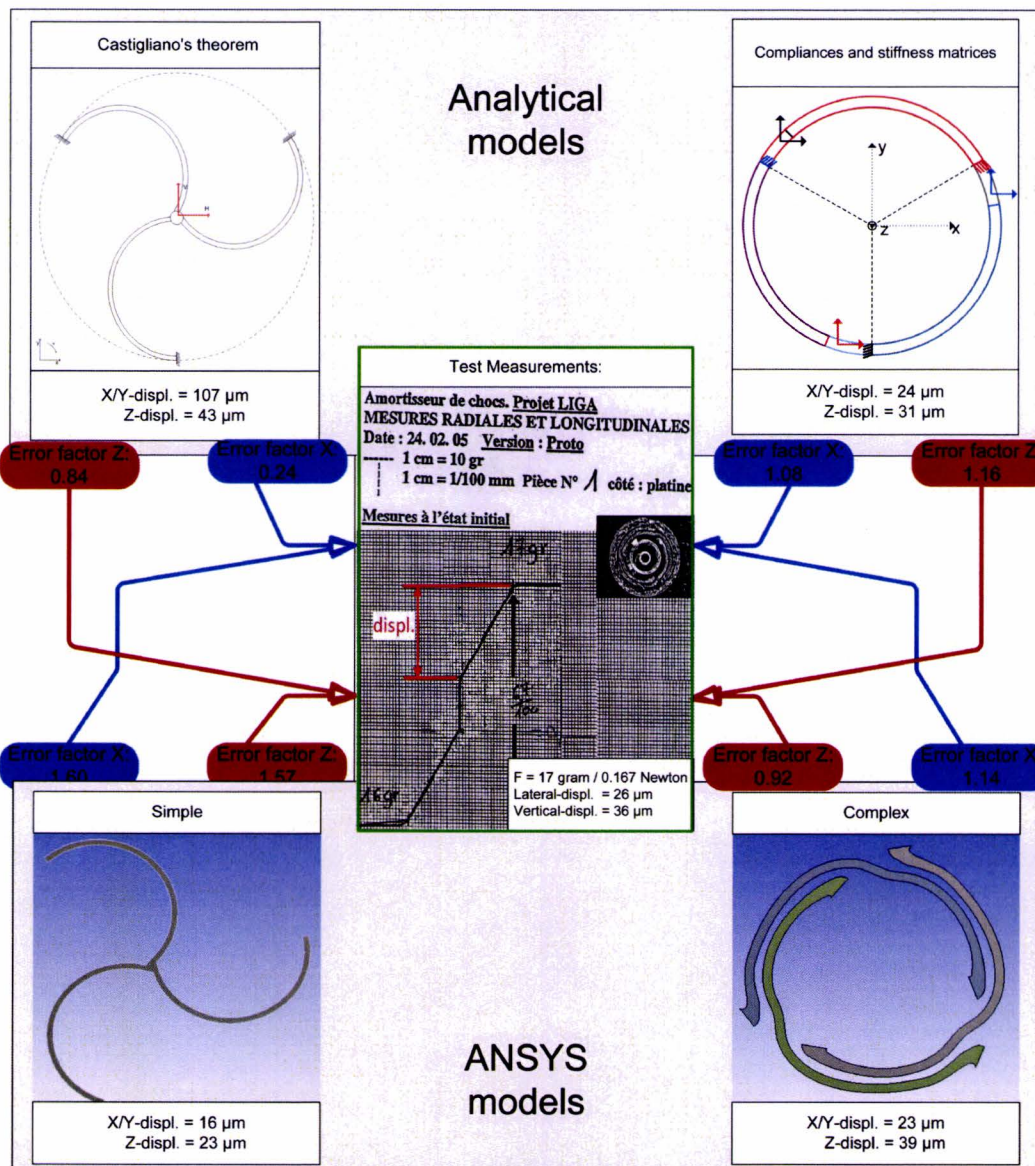
Figure K.1: Overview of the different models.

Appendix L

ANSYS simulations results

Dimensions[mm]			Displacements[μm]		Max princp. Stress[GPA]	
Radius	Width	Height	XY-direction	Z-direction	XY-direction	Z-direction
0.55	0.03	0.15	37.0	57.6	1117	1806
		0.17	29.1	47.4	904	1592
		0.18	26.0	43.4	817	1504
		0.19	23.2	40.0	740	1424
		0.20	20.9	36.9	672	1353
		0.21	18.8	34.3	612	1288
		0.24	14.0	27.9	468	1124
0.55	0.04	0.11	30.3	47.3	796	1049
		0.12	27.0	40.3	725	954
		0.13	24.1	34.8	664	875
		0.15	19.6	27.1	566	753
0.55	0.05	0.08	25.4	59.1	851	1265
		0.09	22.3	46.1	754	1089
		0.10	19.8	37.2	676	955
		0.15	12.1	17.0	441	590
0.06	0.04	0.14	27.8	39.5	689	780
		0.15	25.0	35.0	637	727
		0.16	22.7	31.3	592	681
0.60	0.05	0.09	28.7	59.5	849	1012
		0.10	25.4	48.0	761	885
		0.11	22.7	39.7	689	793
		0.12	20.5	33.4	629	719
		0.14	16.9	24.9	534	608
		0.15	15.5	21.9	496	565
0.618	0.04	0.14	30.5	43.5	670	875
		0.15	27.5	38.6	619	815
		0.16	24.9	34.6	575	763
		0.17	22.7	31.2	536	717
		0.19	18.9	26.0	469	641
		0.20	17.3	23.9	441	609

Table L.1: Crystalline Ruby Simulations 1 of 2.

Dimensions[mm]			Displacements[μm]		Max princp. Stress[GPA]	
Radius	Width	Height	XY-direction	Z-direction	XY-direction	Z-direction
0.618	0.05	0.09	31.4	65.2	831	1158
		0.10	27.8	52.6	745	1014
		0.11	24.9	43.5	674	903
		0.12	22.4	36.7	615	813
		0.13	20.3	31.5	565	740
		0.14	18.5	27.4	522	682
		0.15	17.0	24.1	484	633
0.650	0.04	0.15	31.9	45.1	645	840
		0.16	28.9	40.4	599	787
		0.17	26.3	36.5	558	741
		0.18	23.9	33.2	521	700
		0.21	18.4	25.9	432	601
0.650	0.05	0.10	32.3	61.2	775	1041
		0.11	28.9	50.6	701	926
		0.12	26.0	42.7	640	834
		0.13	23.6	36.7	588	763
		0.14	21.5	31.9	543	704
		0.15	19.7	28.1	503	654
		0.16	18.0	25.0	469	610
0.700	0.04	0.15	39.6	56.3	681	867
		0.17	32.5	45.7	588	765
		0.18	29.6	41.6	550	724
		0.19	27.0	38.1	515	687
		0.20	24.7	35.1	483	654
		0.21	22.7	32.5	454	624
		0.22	20.9	30.2	428	596
		0.24	17.7	26.3	382	549
0.700	0.05	0.13	29.2	45.7	619	789
		0.14	26.6	39.8	571	728
		0.15	24.3	35.1	530	677
		0.16	22.3	31.2	493	632
		0.17	20.6	28.0	461	593
		0.18	19.0	25.4	432	559

Table L.2: Crystalline Ruby Simulations 2 of 2.

Dimensions[mm]			Displacements[μm]		Max princp. Stress[GPA]	
Radius	Width	Height	XY-direction	Z-direction	XY-direction	Z-direction
0.550	0.05	0.15	48.5	63.7	439	553
		0.20	32.2	37.8	318	401
		0.21	29.9	34.7	300	381
		0.22	27.8	31.9	284	362
		0.23	25.9	29.6	270	345
		0.25	22.5	25.6	244	316
0.550	0.06	0.14	34.1	50.6	386	478
		0.15	31.4	44.2	359	441
		0.16	29.0	39.0	335	409
		0.17	26.9	34.7	313	381
		0.18	25.0	31.2	294	357
0.580	0.05	0.15	56.4	74.8	459	571
		0.20	37.4	44.5	332	421
		0.23	29.9	34.9	281	363
		0.24	27.9	32.4	267	347
		0.25	26.1	30.2	254	333
0.580	0.06	0.15	36.5	51.9	372	467
		0.18	29.1	36.6	306	379
		0.19	27.1	33.1	288	358
		0.20	25.3	30.1	272	339
0.600	0.05	0.15	62.0	82.3	494	526
		0.20	41.0	49.0	357	390
		0.25	28.6	33.3	274	310
		0.26	26.7	31.2	261	298
0.600	0.06	0.15	40.1	57.0	401	423
		0.19	29.7	36.4	310	329
		0.20	27.7	33.1	293	312
0.618	0.05	0.13	82.0	118.2	564	694
		0.14	74.5	102.7	520	636
		0.17	57.2	71.9	419	517
		0.20	45.0	53.9	348	436
		0.25	31.4	36.8	266	345
		0.26	29.4	34.4	254	331
		0.27	27.5	32.3	242	318
		0.28	25.8	30.3	231	307
0.618	0.06	0.15	44.0	62.6	390	481
		0.20	30.5	36.5	285	349
		0.21	28.5	33.4	270	331
		0.22	26.7	30.7	256	315

Table L.3: Fused Silica Simulations 1 of 2.

Dimensions[mm]			Displacements[μm]		Max princp. Stress[GPA]	
Radius	Width	Height	XY-direction	Z-direction	XY-direction	Z-direction
0.650	0.050	0.15	78.9	105.3	502	609
		0.20	52.2	63.0	361	451
		0.25	36.4	43.1	276	358
		0.27	31.9	37.9	251	331
		0.28	29.9	35.6	239	319
		0.29	28.0	33.6	229	307
		0.30	26.3	31.8	219	297
0.650	0.060	0.15	51.1	72.9	405	494
		0.20	35.3	42.6	296	361
		0.23	29.0	33.1	253	312
		0.24	27.3	30.7	240	298
		0.25	25.7	28.6	229	286
0.670	0.050	0.15	85.9	115.3	512	616
		0.20	56.8	69.1	369	456
		0.25	39.6	47.3	281	363
		0.30	28.6	35.0	222	302
		0.31	26.9	33.1	213	292
0.670	0.060	0.15	55.7	79.8	414	498
		0.20	38.5	46.7	302	366
		0.24	29.7	33.7	245	303
		0.25	28.0	31.4	234	290
0.700	0.05	0.15	97.7	131.4	528	630
		0.20	64.6	78.9	380	467
		0.25	45.0	54.2	289	373
		0.30	32.4	40.1	229	310
		0.32	28.7	36.1	210	291
		0.33	27.0	34.3	201	282
		0.34	25.5	32.7	193	273
		0.35	24.1	31.2	185	265
0.700	0.06	0.15	63.3	91.0	424	509
		0.20	43.7	53.3	309	375
		0.25	31.8	35.9	239	300
		0.26	30.0	33.5	228	286
		0.27	28.3	31.4	218	275

Table L.4: Fused Silica Simulations 2 of 2.

Dimensions[mm]			Displacements[μm]		Percentage[%]	
Radius	Width	Height	XY-direction	Z-direction	XY-direction	Z-direction
0.600	0.036	0.135	0.0369	0.0536	42	49
		0.150	0.0312	0.0449	20	25
		0.165	0.0265	0.0384	2	7
0.600	0.040	0.135	0.0293	0.0421	13	17
		0.150	0.0250	0.0350	4	3
		0.165	0.0216	0.0298	17	17
0.600	0.044	0.135	0.0234	0.0341	10	5
		0.150	0.0202	0.0282	22	22
		0.165	0.0176	0.0238	32	34
0.650	0.036	0.153	0.0385	0.0560	48	56
		0.170	0.0322	0.0472	24	31
		0.187	0.0272	0.0406	5	13
0.650	0.040	0.153	0.0310	0.0436	19	21
		0.170	0.0263	0.0365	1	1
		0.187	0.0225	0.0312	14	13
0.650	0.044	0.153	0.0251	0.0350	4	3
		0.170	0.0215	0.0291	17	19
		0.187	0.0186	0.0248	29	31

Table L.5: Crystalline Ruby Variations.

Dimensions[mm]			Displacements[μm]		Percentage[%]	
Radius	Width	Height	XY-direction	Z-direction	XY-direction	Z-direction
0.600	0.045	0.225	41.6	51.5	60	43
		0.250	34.4	43.2	32	20
		0.275	28.7	36.9	11	2
0.600	0.050	0.225	34.1	49.9	31	11
		0.250	28.6	33.3	10	7
		0.275	24.2	28.3	7	21
0.600	0.055	0.225	27.8	31.7	7	12
		0.250	23.6	26.4	9	27
		0.275	20.2	22.3	22	38
0.65	0.054	0.207	42.9	50.9	65	41
		0.230	36.6	42.4	41	18
		0.253	31.6	36.0	22	0
0.65	0.060	0.207	33.7	40.0	30	11
		0.230	29.1	33.6	12	7
		0.253	24.7	27.2	5	24
0.65	0.066	0.207	26.7	32.4	3	10
		0.230	23.2	26.7	11	26
		0.253	20.4	22.4	22	38

Table L.6: Fused Silica Variations.

Appendix M

M-file: Control of PI-stages and flexure

Analytical model with Castigliano's Theorem.

```
(* :: Package :: *)

%% Control of PI and Flexures
%%% Input XY Array %%%
close all;

% Initial Conditions
resolution = 6000;          %[-]    Points within one flexure domain
Xframe = 100000;            %[nm]   X-length of the flexure domain
Yframe = 100000;            %[nm]   Y-length of the flexure domain

% Initial Conditions for loop:
n=1;                        % Counting points of lengths XY
p=0;                        % Counting points within flexure domain
f=1;                        % Counting number of flexure domains
Xmin = XY(n,1);             % Starting point is Xmin
Xmax = XY(n,1);             % Starting point is Xmax
Ymin = XY(n,2);             % Starting point is Ymin
Ymax = XY(n,2);             % Starting point is Ymax
Curve = [XY(n,1) XY(n,2)]/1000;  % Curve starts with starting point
Midpoints = [;];
L=length(XY);


while n < L-1
    Xmin_t = min(Xmin,XY(n+1,1));
    Xmax_t = max(Xmax,XY(n+1,1));
    Ymin_t = min(Ymin,XY(n+1,2));
    Ymax_t = max(Ymax,XY(n+1,2));

        if Xmax_t - Xmin_t <= Xframe & Ymax_t - Ymin_t <= Yframe & p<=resolution;
        n=n+1;       % Counting length XY
        p=p+1;       % Counting length resolution
        Xmin = Xmin_t;
        Xmax = Xmax_t;
        Ymin = Ymin_t;
        Ymax = Ymax_t;
        Curve = [Curve; XY(n+1,1) XY(n+1,2)];
        else
        Xpi = ((Xmax+Xmin)/2)/1000; % in um
```

```matlab
            Ypi = ((Ymax+Ymin)/2)/1000; % in um
            Center = [Xpi Ypi];
            Midpoints = [Midpoints ; Xpi Ypi];
            % disp(['Position PI-stage is ',num2str(Center)])
            % disp(['Laser on'])
            % disp(['Move flexure along curve:'])
            Xtrans = Xpi-50000;
            Ytrans = Ypi-50000;
            Curve_for_flexure=[Curve(:,1)-Xtrans Curve(:,2)-Ytrans]
            disp(['Laser off'])
            Xmin = XY(n,1);
            Xmax = XY(n,1);
            Ymin = XY(n,2);
            Ymax = XY(n,2);
            Curve = [];
            p=0;
            end
end

% Last points outside last domain.
Xpi = ((Xmax+Xmin)/2)/1000; % in um;
Ypi = ((Ymax+Ymin)/2)/1000; % in um;
Center = [Xpi Ypi];
% disp(['Position PI-stage is ',num2str(Center)])
% disp(['Laser on'])
% disp(['Move flexure along curve:'])
Xtrans = Xpi-50000;
Ytrans = Ypi-50000;
Curve_for_flexure=[Curve(:,1)-Xtrans Curve(:,2)-Ytrans]
% disp(['Laser off'])

%% Plot laserpattern
X_range =XY(:,1);
Y_range =XY(:,2);
% figure;
hold on;
plot(X_range/1000, Y_range/1000,'b'); grid;
hold on;
plot(X_range/1000,Y_range/1000,'ro');
xlabel('x-axis [um]');
ylabel('y-axis [um]');

%% Plot Rectangles
Midpoints = [Midpoints ; Center];
N_of_Midpoints = length(Midpoints);
X_mid =Midpoints(:,1);
Y_mid =Midpoints(:,2);
plot(X_mid,Y_mid,'o');
xlabel('x-axis [um]');
ylabel('y-axis [um]');
title(['Laserpath with ',num2str(N_of_Midpoints),' flexure domains - Framesize = ',
for q=1:N_of_Midpoints;
rectangle('position',[X_mid(q,1)-50 Y_mid(q,1)-50 100 100]);
end
```

Appendix N

Pictures of the fs-prototype

Fs-prototype 1 | After irradiation | After 24 hours etching

Fs-prototype 2 | After irradiation

Fs-prototype 3		
After irradiation	After 2 hours etching	After 6 hours etching

Fs-prototype 4		
After irradiation	After 6 hours etching	After 20 hours etching

Fs-prototype 5		
After irradiation	After 6 hours etching	After 20 hours etching

Fs-prototype 6	
Frontside after irradiation	Backside after irradiation

Fs-prototype 7
After 24 hours etching

List of Tables

List of Figures